TURUN YLIOPISTON JULKAISUJA
ANNALES UNIVERSITATIS TURKUENSIS

SARJA - SER. D OSA - TOM. 862

MEDICA - ODONTOLOGICA

NONALCOHOLIC FATTY LIVER DISEASE IN OBESITY AND TYPE 2 DIABETES

Studies using ^{1}H MRS and PET

by

Ronald J.H. Borra

TURUN YLIOPISTO
UNIVERSITY OF TURKU
Turku 2009

From
Department of Diagnostic Radiology, University of Turku,
and the Medical Imaging Centre of Southwest Finland,
Turku University Hospital — Turku, Finland

Turku PET Centre, and the Department of Medicine,
University of Turku — Turku, Finland

Supervised by
Docent Riitta Parkkola, MD, PhD
Department of Diagnostic Radiology, University of Turku,
and the Medical Imaging Centre of Southwest Finland, Turku University Hospital
Turku, Finland

Professor Pirjo Nuutila, MD, PhD
Turku PET Centre and the Department of Medicine
University of Turku
Turku, Finland

Reviewed by
Professor Leena Kivisaari, MD, PhD
Helsinki Medical Imaging Center
University Hospital of Helsinki
Helsinki, Finland

Professor Tommy Olsson, MD, PhD
Department of Medicine
Umeå University Hospital
Umeå, Sweden

Dissertation opponent
Professor Johannes A. Romijn, MD, PhD
Department of Endocrinology and Metabolism
Leiden University Medical Center
Leiden, the Netherlands

ISBN 978-951-29-3983-1 (PRINT)
ISBN 978-951-29-3984-8 (PDF)
ISSN 0355-9483
Painosalama Oy — Turku, Finland 2009

To those affected by NAFLD
and its complications

Ὁ βίος βραχὺς, ἡ δὲ τέχνη μακρὴ, ὁ δὲ καιρὸς ὀξὺς,
ἡ δὲ πεῖρα σφαλερὴ, ἡ δὲ κρίσις χαλεπή

Ἱπποκράτης

Ars longa, vita brevis, occasio praeceps,
experimentum periculosum, iudicium difficile

Hippocrates

1. ABSTRACT

Ronald J.H. Borra

NONALCOHOLIC FATTY LIVER DISEASE IN OBESITY AND TYPE 2 DIABETES
Studies using ^{1}H MRS and PET

Medical Imaging Centre of Southwest Finland and Turku PET Centre;
Department of Diagnostic Radiology, University of Turku, Finland
Annales Universitatis Turkuensis, Painosalama Oy, Turku, Finland 2009

In the healthy state excess fat is deposited at appropriate sites, such as subcutaneous fat depots. When fat begins to accumulate outside these regular depots, within the liver and other organs, it is named ectopic fat. To discriminate hepatic ectopic fat from fatty liver due to alcohol abuse, the condition is termed nonalcoholic fatty liver disease (NAFLD). The exact pathophysiology of NAFLD is unclear, but the deposition of ectopic fat within the liver is increased in both type 2 diabetes (T2DM) and obesity. Accumulation of ectopic fat severely impairs hepatic metabolism and without appropriate intervention NAFLD may lead to nonalcoholic steatohepatitis (NASH) and eventually to liver cirrhosis. Resulting from the dramatic increase in patients with T2DM and obesity worldwide, cirrhosis due to nonalcoholic fatty liver disease has been predicted to become the main cause for liver transplantation by the year 2020. This poses a great need for (1) a better understanding of the effects of ectopic liver fat on liver metabolism, (2) new pharmacological treatment options for NAFLD and (3) new affordable and rapid methods for early detection of liver fat accumulation in patients at high risk for NAFLD. In the current study liver fat content and glucose uptake were studied non-invasively using proton magnetic resonance spectroscopy (^{1}H MRS) and positron emission tomography (PET) in patients with T2DM, patients with obesity and healthy volunteers. Liver fat content was found to be inversely associated with liver glucose uptake in patients with T2DM and also to be associated with impaired myocardial metabolism in these patients. In addition our data indicate that liver fat content might be significantly reduced by one month Trimetazidine treatment in obese patients. Finally, we were able to develop a new rapid method, using in-and-out-of-phase MR imaging, for the non-invasive assessment of liver fat content.

Keywords: nonalcoholic fatty liver disease, NAFLD, liver, proton magnetic resonance spectroscopy, ^{1}H MRS, positron emission tomography, PET, diabetes, obesity, rosiglitazone, trimetazidine, magnetic resonance imaging, MRI

1. TIIVISTELMÄ

Ronald J.H. Borra

EI-ALKOHOLIPERÄINEN RASVAMAKSA LIHAVILLA JA TYYPIN 2 DIABEETIKOILLA
Protoni-magneettispektroskopia ja PET-tutkimus

Varsinais-Suomen Kuvantamiskeskus sekä Valtakunnallinen PET-keskus;
Diagnostinen Radiologia,Turun yliopisto
Annales Universitatis Turkuensis, Painosalama Oy, Turku, Finland 2009

Ravinnosta saatu ylimääräinen energia varastoituu ihmiselimistöön rasvana. Pääosa rasvasta kertyy ihon alle, mutta sitä kertyy myös maksaan ja muihin elimiin sekä vatsaontelon sisään. Tätä muualle kuin ihonalaiskudoksiin kertyvää rasvaa nimitetään ektooppiseksi rasvaksi. Maksa saattaa rasvoittua myös muista syistä kuin ravinnosta saadusta ylimääräisestä energiasta, esimerkiksi alkoholinkäytön seurauksena. Maksan rasvoittumista, joka ei liity lisääntyneeseen alkoholinkäyttöön, on englanninkielisessä kirjallisuudessa alettu kutsua termillä nonalcoholic fatty liver disease (NAFLD) eli ei-alkoholiperäinen rasvamaksa. Taudin tarkkaa syntymekanismia ei tunneta, mutta sen tiedetään liittyvän sekä tyypin 2 diabetekseen että lihavuuteen. Ektooppisen rasvan kertyminen maksaan häiritsee vakavasti maksan aineenvaihduntaa ja voi johtaa hoitamattomana ei-alkoholiperäisen rasvamaksan tulehtumiseen (nonalcoholic steatohepatitis, NASH) ja lopulta maksakirroosiin. Liikalihavuus ja tyypin 2 diabetes lisääntyvät maailmanlaajuisesti räjähdysmäisesti. On jopa ennustettu, että vuonna 2020 ei-alkoholiperäinen rasvamaksa aiheuttaa suurimman osan tarpeesta maksan elinsiirtoihin. Ongelman yleisyyden ja kansanterveydellisen merkityksen vuoksi onkin erittäin tärkeä selvittää tarkasti ektooppisen rasvan vaikutus maksan aineenvaihduntaan. Oleellista on selvittää, miten rasvan kertymistä maksaan voidaan nopeasti, luotettavasti ja edullisesti mitata sekä miten tautitilaa voidaan hoitaa. Tässä tutkimuksessa maksan rasvapitoisuutta ja sokerinkäyttöä tutkittiin kajoamattomasti protoni-magneettis-pektroskopialla (^{1}H MRS) ja positroniemissiotomografialla (PET) terveillä verrokeilla, diabeetikoilla ja lihavilla potilailla. Tutkimuksessa todettiin, että diabeetikoilla korkea maksan rasvapitoisuus liittyy maksan alentuneeseen sokerinkäyttöön sekä huonoon sydänlihasfunktioon. Lisäksi havaittiin, että trimetatsidiini-lääkitys alensi merkitsevästi maksan rasvan määrää lihavilla potilailla. Tässä työssä kehitettiin myös uusi, nopea ja kajoamaton magneettikuvaukseen perustuva menetelmä (in-and-out-of-phase MR imaging) maksan rasvapitoisuuden määrittämiseen.

Avainsanat: ei-alkoholiperäinen rasvamaksa, NAFLD, maksa, protoni-magneetti-spektroskopia, ^{1}H MRS, positroniemissiotomografia, PET, diabetes, lihavuus, rosiglitatsoni, trimetatsidiini, magneettikuvaus, MRI

2. TABLE OF CONTENTS

3. ABBREVIATIONS

AMARES	Advanced Method for Accurate, Robust, and Efficient Spectral fitting
B_0	Magnetic Field (Static)
BMI	Body Mass Index
CHD	Coronary Heart Disease
CRP	C-Reactive Protein
hsCRP	high sensitivity C-Reactive Protein
CT	Computed Tomography
CVD	Cardiovascular Disease
DNL	De-Novo Lipogenesis
ETL	Echo Train Length
[^{18}F]FDG	[^{18}F]-2-fluoro-2-deoxy-D-glucose
f_0	Larmor frequency
FFA	Free Fatty Acid
FFE	Fast Field Echo
FFT	Fast Fourier Transform
FSPGR	Fast Spoiled Gradient Echo
γ	Gyromagnetic ratio
^{1}H MRS	Proton Magnetic Resonance Spectroscopy
HGP	Hepatic Glucose Production
HGU	Hepatic Glucose Uptake
HSL	Hormone-Sensitive Lipase
HU	Hounsfield Units
HLSVD	Hankel Lanczos Singular Values Decomposition
jMRUI	java Magnetic Resonance User Interface
LC	Lumped Constant
LDL	Low-Density Lipoprotein
LFC	Liver Fat Content
LPL	Lipoprotein Lipase
M_0	Net magnetization
MBA	Multiple Breath-hold Averaging
MHz	Megahertz
MR	Magnetic Resonance
MRE	Magnetic Resonance Elastography
MRI	Magnetic Resonance Imaging
MRS	Magnetic Resonance Spectroscopy
NAFLD	Nonalcoholic Fatty Liver Disease
NASH	Nonalcoholic Steatohepatitis
NEFA	Non-Esterified Fatty Acids
NEX	Number of Exitations
NMR	Nuclear Magnetic Resonance
NOS	Number of Scans
NS	Nonsignificant
[^{15}O]H_2O	[^{15}O]-water

PE	Polyethylene
PPAR-γ	Peroxisome Proliferator-Activated Receptor gamma
PRESS	Point Resolved Spectroscopy
PROBE	Proton Based Examination
RF	Radio Frequency
ROI	Region Of Interest
SAS	Statistical Analysis System
SD	Standard Deviation
SI	Signal Intensity
SV	Single Voxel
T	Tesla
T_1	Spin-lattice (longitudinal) relaxation time
T_2	Spin-spin (transverse) relaxation time
T2DM	Type 2 Diabetes Mellitus
T1W	T1-Weighted
TAG	Triacylglycerol
TE	Echo Time
TR	Time of Repetition
US	Ultrasonography
VLCD	Very Low Calorie Diet
VLDL	Very-Low-Density Lipoprotein

4. LIST OF ORIGINAL PUBLICATIONS

This thesis is based on the following original publications, which are referred to in the text by roman numerals I-IV. Additional unpublished data is also presented.

I Lautamäki R, **Borra R**, Iozzo P, Komu M, Lehtimäki T, Salmi M, Jalkanen S, Airaksinen KE, Knuuti J, Parkkola R, Nuutila P: Liver steatosis coexists with myocardial insulin resistance and coronary dysfunction in patients with type 2 diabetes. *Am J Physiol Endocrinol Metab* 291:E282-E290, 2006 (© APS, 2006)

II **Borra R**, Lautamäki R, Parkkola R, Komu M, Sijens PE, Hällsten K, Bergman J, Iozzo P, Nuutila P: Association between liver fat content and hepatic glucose uptake in patients with type 2 diabetes. *Metabolism* 57(10):1445–1451, 2008 (© Elsevier Inc., 2008)

III **Borra R**, Maggio R, Bucci M, Tuunanen H, Kankaanpää M, Knuuti J, Parkkola R, Nuutila P, Iozzo P: Effects of Trimetazidine on liver fat content: a pilot study in humans *(Submitted)*

IV **Borra RJ**, Salo S, Dean K, Lautamäki R, Nuutila P, Komu M, Parkkola R: Nonalcoholic fatty liver disease: rapid evaluation of liver fat content with in-phase and out-of-phase MR imaging. *Radiology* 250:130-136, 2009 (© RSNA, 2008)

5. INTRODUCTION

The liver is a central organ and performs multiple metabolic functions for the entire body. Because of its unique location, most blood of the gastrointestinal tract is drained first to the liver, and this organ has a key role in filtering all nutrients that enter the body. Furthermore, the liver responds to different hormones which are released in response to food intake and reacts to agents released by the intra-abdominal (visceral) fat depots. In case of an excess of food intake, the bloodstream to the liver will contain an unusually high concentration of lipids.

The liver has an amazing capacity to transform, store and release nutrients, according to the needs of the body. Interestingly, the interplay between the different nutrients and the hormonal and neuronal signals the liver receives affects the fate of individual nutrients. In concert with this, the liver is able to switch rapidly between different modes, e.g. from glucose storage to glucose production.

Disturbances in the delicate metabolic equilibrium of the liver can result in a wide range of whole body disease and vice versa. The occurrence of the metabolic disease type 2 diabetes mellitus has experienced an extremely rapid increase, affecting currently over 190 million people worldwide. The number of patients is expected to rise to 300 million in 2025 (Zimmet et al., 2003). Type 2 diabetes is a highly invalidating disease, especially when taking into account its severe long term complications: cardiovascular disease, blindness, kidney failure and impotence.

The highly accelerated incidence of type 2 diabetes has been fuelled by a tremendous increase in obesity worldwide, resulting from excess calorie intake and lack of physical exercise. Such a highly anabolic state of the body results in an accumulation of fat in both (normal) adipose tissue and (abnormal) locations as the liver, visceral fat depots and muscle, also named *ectopic* fat accumulation. Thus, when the energy intake exceeds the storage capacity of adipose tissue, this leads to an energy overflow to ectopic sites (Shulman, 2000).

Ectopic fat accumulation in the liver can have several negative effects on the normal metabolic functions of the liver. To separate this form of ectopic lipid accumulation in the liver from alcohol induced liver lipid accumulation, the term *nonalcoholic fatty liver disease* (NAFLD) is used. Together with an inflammatory reaction, the fat accumulated in the liver can progress to a condition known as nonalcoholic steatohepatitis (NASH), a highly under-diagnosed condition in patients with type 2 diabetes. Since NASH can progress to (irreversible) liver fibrosis, it has been predicted that nonalcoholic fatty liver disease will be the major cause of liver transplantation in 2020 (Charlton, 2004).

Taking into account the above, investigation and monitoring of the liver metabolic function and early detection of liver lipid accumulation is of great importance. Unfortunately, the liver is not easily accessible and liver biopsy is currently considered the gold-standard to assess possible liver inflammation and degree of ectopic fat

accumulation. However, liver biopsy has several drawbacks, the main problem being a considerable risk of complications associated with the procedure. Furthermore, the highly small biopsy sample size often does not allow for reliable fat content measurement in case of heterogeneous fat distribution. The issues above cause liver biopsy to be an inappropriate tool for routine human clinical screening.

Magnetic resonance imaging (MRI) is an imaging technique allowing for high resolution imaging of the liver without the use of ionizing radiation. In combination with magnetic resonance spectroscopy (^{1}H MRS), this technique offers possibilities to assess liver anatomy and fat content non-invasively in vivo. Despite being a relatively new technique, ^{1}H MRS has been rapidly gaining ground as a safe alternative for liver biopsy for the assessment of liver fat content alone.

Positron emission tomography (PET) is a second non-invasive technique, relying on short-lived positron emitting isotopes (tracers), to allow for quantification of tissue metabolic processes in vivo with a high degree of sensitivity and resolution. The most commonly used tracer is fluorine labeled glucose, [^{18}F]-2-fluoro-2-deoxy-D-glucose ([^{18}F]FDG). This technique has been successfully used to quantify liver glucose metabolism in vivo (Iozzo et al., 2003a).

Recent research using ^{1}H MRS, MRI and PET has shown the implications of ectopic liver fat accumulation in patients with type 2 diabetes as a marker for whole body insulin resistance, and in particular myocardial insulin resistance and coronary function (Lautamaki et al., 2006a). After the observation that liver fat content is a potentially highly useful marker also for disease outside of the liver, this study investigated the local effects of ectopic liver fat accumulation on liver insulin resistance and glucose metabolism in patients with type 2 diabetes. In addition, the effects of the oral antidiabetic drug Rosiglitazone on liver metabolism were studied.

Inspired by the results of these studies, a substudy with the anti-anginal drug Trimetazidine was conducted. Trimetazidine inhibits fatty acid oxidation and the goal of this substudy was to investigate possible beneficial effects of Trimetazidine on ectopic fat accumulation in the liver. In the last part of this study a rapid imaging-based method, suitable for routine screening, was developed and validated. The goal of this substudy was to develop a non-invasive method to rapidly assess if liver fat content is normal or increased in patients with type 2 diabetes.

6. REVIEW OF THE LITERATURE

6.1 THE LIVER

The liver is a central and essential organ and performs several important functions. The most important function in view of the current work is the liver's buffer function between the gut and the systemic circulation (Souhami and Moxham, 1997). This allows the liver to maintain glucose, fat and amino acid homeostasis. Due to its anatomical location, the liver is a rather inaccessible organ for conventional (non-imaging) techniques.

6.1.1 Liver anatomy

The liver is positioned in the upper right part of the abdomen, right beneath the thoracic diaphragm. The organ is highly vascular and has a double blood supply: approximately 75% of the blood is supplied by the portal vein (Figure 1) and approximately 25% by the hepatic artery. Both vessels run in the free edge of the lesser omentum and enter the liver at the hilus. The portal vein mainly drains nutrients and hormones from the splanchnic area directly into to liver, having an important influence on liver metabolic processes. The hepatic artery mainly supplies the liver with oxygen rich blood (Guyton and Hall, 1996). The human liver is divided into eight functionally independent segments which are organized in four anatomic lobes: left lobe (segment 2 and 3), right lobe (segment 5, 6, 7, and 8), caudate lobe (segment 1) and quadrate lobe (segment 4a and 4b). Lobes are again subdivided in smaller lobules which form the actual functional units of the liver. Each lobule is approximately 1.0-2.5mm in size and consists of hepatic cells, has its own central vein, and a peripheral portal triad, including a portal vein, bile duct and hepatic artery.

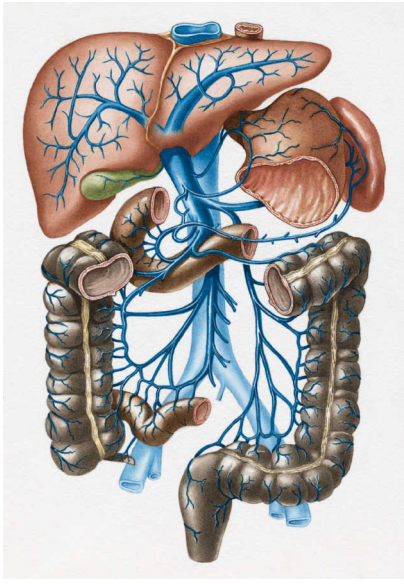

Figure 1. Liver anatomy and venous blood supply. The main blood supply comes from the portal vein, draining nutrients and hormones from the splanchnic area directly into to liver. © Dorling Kindersley

The liver is also innervated by nerves which accompany the vessels and ducts into the lobulus: parasympathetic innervation through the left vagus nerve and also sympathetic innervation (Guyton and Hall, 1996).

6.1.2 Liver fat metabolism

Free fatty acids (FFAs) are delivered to the liver mainly by the portal route. FFAs are derived both from ingested meals as well as released from abdominal (visceral) fat depots. A third source of liver FFA are the triglycerides stored within the liver. After a meal (postprandially) FFA are mainly stored in the liver as triglycerides, whereas during fasting they are mainly oxidized. During oxidation of FFA acetyl-CoA is formed, which can be used as a substrate for gluconeogenesis.

Effects of (increased) supply of FFA to the liver are not entirely clear. It seems that FFA in general increases hepatic gluconeogenesis and that the hepatic autoregulation prevents the hepatic glucose production (HGP) from actually increasing in the healthy individual with normal liver insulin sensitivity (Seppala-Lindroos et al., 2002). However, in patients with type 2 diabetes hepatic autoregulation seems to be defective, resulting in an increased HGP.

6.1.2.1 Triacylglycerol (TAG)

Fat in the form of triacylglycerol (TAG) is the most concentrated form of energy that is available for biological tissues (Gibbons et al., 2000). The high energy content of TAG is strikingly illustrated by the fact that the first unaided crossing of the polar icecap was possible due to the very high *butter-fat* content of the expedition's 220 kg food reserves. The food reserves were transported on man-powered sledges, and the weight of the similar amount of energy in carbohydrate form would have made the expedition impossible (Stroud, 1993).

Triacylglycerols are made of a backbone of glycerol to which three fatty acids are attached (Figure 2), demonstrating the property of TAG to store free fatty acids in a compound with low biological toxicity, compared to fatty acids by themselves. Furthermore, high levels of TAG for a short or medium period of time are very well tolerated, and therefore TAG provides a safe way to store and transport fatty acids. For the fatty acids to become available and mobilized, TAGs have to undergo lipolysis. In humans the main storage pool for TAG in the entire body is the subcutaneous tissue, which exports part of its storage as fatty acids. In addition, the liver has a vast capability of storing TAG which are exported in the form of very-low-density lipoprotein (VLDL) and ketone bodies.

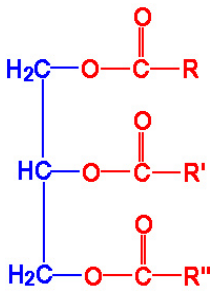

Figure 2. Basic structure of Triacylglycerol (TAG) consisting of a glycerol backbone (in blue) and three chains of fatty acids (in red, R-groups).

There is a fine balance between the adipose tissue and the liver, which together constitute a metabolic cycle: VLDL TAG fatty acids produced by the liver can be incorporated into the adipose tissue by the action of lipoprotein lipase (LPL). In turn, due to hormone-sensitive lipase (HSL), fatty acids are released by the adipose tissue, which can be used for liver VLDL synthesis.

HSL is expressed mainly in adipose tissue and not in the liver and promotes actively the release of TAG stored in cytosolic droplets in the adipocyte. Insulin and catecholamines and their mutual balance regulate the activity of HSL, depending on the nutritional status of the body (Holm et al., 1997). Insulin and catecholamines work antagonistically, with insulin inhibiting the activation of HSL and adrenalin promoting the activation of HSL, resulting in a release of fatty acids. The liver of a normal human adult has a TAG concentration of about 5 micromol/g fresh weight (Cairns and Peters, 1984), but the normal range has been considered to extend as high as 45 micromol/g fresh weight. The hepatic storage capacity of a normal adult (liver weight 1.5 kg) would, therefore, range from 7.5 to 67.5 mmol (6.7-60.7 g).

Due to its ability to store high amounts of TAG the liver works as a buffer, taking up excess of (cytotoxic) fatty acids and storing them as TAG or VLDL. In this way the liver protects the body from fatty acid lipotoxicity (Unger and Orci, 2002;Unger, 2002). There are three potential sources for fatty acids which enter the hepatic TAG pool: FFAs in the plasma (originating mainly from adipose tissue), de-novo lipogenesis and remnant lipoproteins. Animal experiments with perfused rat livers have shown that in the normal state the main contribution to the liver TAG synthesis is the plasma FFA level. Most likely plasma FFA levels are also the main contributor to liver TAG synthesis in humans. Measurement of de-novo lipogenesis is problematic but recently great advances have been made using stable isotope labeling techniques (Parks and Hellerstein, 2006). Studies using the aforementioned stable isotope techniques have shown that the extent of dietary fatty acid recycling via serum FFA and VLDL-TAG is determined by the rate of delivery of dietary fat to the intestine (Barrows et al., 2005).

6.2 NONALCOHOLIC FATTY LIVER DISEASE

The condition of liver lipid accumulation, resembling alcohol-induced injury but occurring in patients who do not use alcohol (or maximum 2-3 glasses/day), is called nonalcoholic fatty liver disease (NAFLD) (Neuschwander-Tetri and Caldwell, 2003). Several (often incorrectly used) synonyms for the same disease are diabetes hepatitis, fatty-liver hepatitis, alcohol-like liver disease, Laennec's disease and nonalcoholic steatohepatitis (NASH) (Angulo, 2002). NAFLD disease is an increasingly recognized condition, fuelled by the increasing prevalence of obesity, and is very rapidly becoming a major health problem world-wide (Browning et al., 2004;Angulo, 2007).

NAFLD in the early stage is usually asymptomatic (Adams and Lindor, 2007), but it is by itself a risk factor for hepatocellular carcinoma (HCC) and is also part of the natural (progressive) history of NASH, which can lead to cryptogenic fibrosis (Bugianesi, 2007). Due to this risk of progression to more severe liver disease through the

consequences of its fibro-inflammatory risk, NAFLD has been predicted to be the major cause of liver transplantation in 2020 (Charlton, 2004) stressing the great need for early detection of the disease.

6.2.1 Epidemiology of NAFLD

The prevalence of nonalcoholic fatty liver, NAFLD, is clearly increased in many obesity-related disorders. It has been shown that there is an increased relative risk for NALFD of 4.6 in obese persons with a body-mass index (BMI) of a least 30 kg/m^2 (Bellentani et al., 2000). Truncal obesity is an important risk factor for NAFLD, also in patients with a normal BMI (Ruderman et al., 1998). Type 2 diabetes increases not only the risk of NAFLD but also the severity of the disease *regardless of BMI* (Silverman et al., 1990;Wanless and Lentz, 1990). A prevalence of NAFLD in T2DM of approximately 50% in the US has been observed (Angulo, 2002). In patients with T2DM and severe obesity 100 percent had at least mild steatosis, 50 percent had steatohepatitis and 19 percent had cirrhosis (Silverman et al., 1989). Insulin resistance and hyperinsulinemia are associated with NAFLD also in subjects without T2DM (Marchesini et al., 1999). Furthermore, patients with a history of T2DM are at increased risk to develop NASH. Hypertriglyceridemia, but not hypercholesterolemia, is also an important risk factor for NAFLD. An ultrasound study by Assy et al. detected fatty infiltration of the liver in 50% of the patients with hypergtriglyceridemia (Assy et al., 2000).

The first important problem in determining the prevalence of NAFLD, is that the observed prevalence greatly depends on the sensitivity of the instrument used to measure liver fat content (LFC). Liver biopsy and also Magnetic Resonance Spectroscopy (MRS) are currently considered to be the two most sensitive techniques for measuring LFC (Adams and Lindor, 2007). The second problem is that NAFLD is poorly detected by measurement of liver enzymes in blood samples, since these enzymes are normal in up to 78% of the patients with NAFLD (Browning et al., 2004).

The fact that metabolic imbalance at the level of the liver can be detected at an early stage, was shown in a study by Machann et al. showing LFC to vary from 0.5% to as high as 39.3% in healthy subjects, with impaired glucose tolerance, overweight and a family history of type 2 diabetes (Machann et al., 2006). This might explain the occasional observed high values of LFC in subjects described as “healthy” volunteers.

The large impact of NAFLD on patient survival was recently emphasized in a study showing that NAFLD accompanied by elevated liver enzymes is associated with a clinically significant risk of developing end-stage liver disease, resulting in a lower survival in patients with NASH. Furthermore, this study showed that most patients with NAFLD will develop diabetes or impaired glucose tolerance in the long term and that progression of liver fibrosis is associated with more severe insulin resistance and weight gain (Ekstedt et al., 2006). These findings stress the need for methods to detect (and treat) NAFLD at an early stage.

6.2.2 Etiology of NAFLD

Since the first description of the disease in 1980 by Ludwig et al. (Ludwig et al., 1980) the pathogenesis of NAFLD has remained to be poorly understood. It is evident that an accumulation of triglycerides within the hepatocytes takes place, but the mechanism by which this happens is very unclear.

A popular hypothesis for the development of NAFLD is the "Second hit hypothesis" which was first described in 1998 (Day and James, 1998) and has continued to be used to described possible phases of NAFLD and NASH (Figure 3)

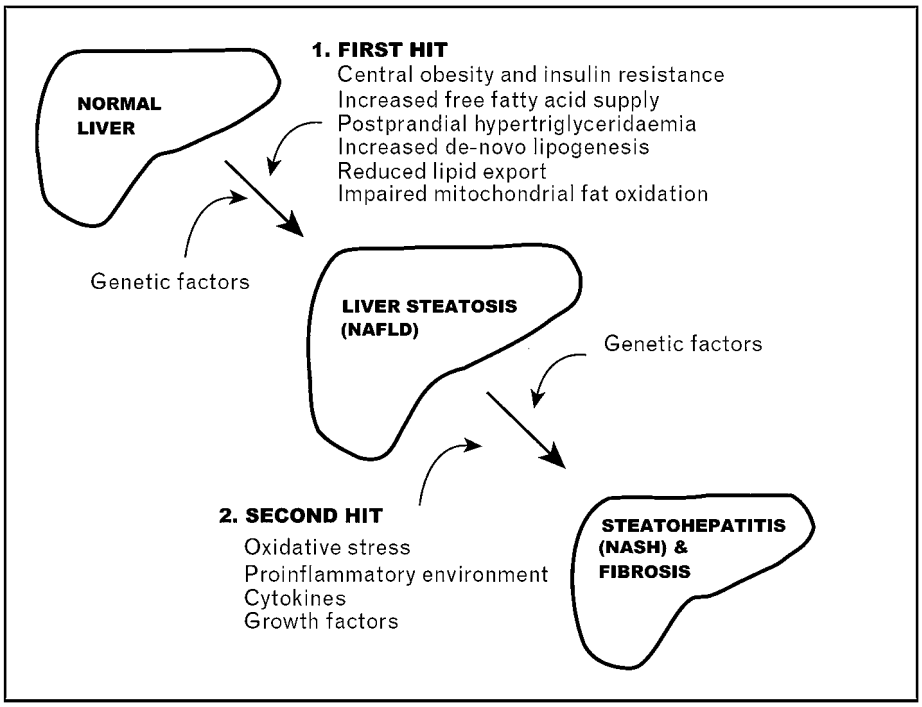

Figure 3. Recent version of the "Second hit hypothesis" for the development of fatty liver. Modified from "the trials and tribulations of the treatment of nonalcoholic fatty-liver disease" (Gan et al., 2008).

This hypothesis explains lipotoxicity as the reverse sequence in which the relative contribution of liver fat may be amplified in patients with overt steatosis (Sastre et al., 2007). In NAFLD the liver is not only receiving more lipid from outside, but also de-novo lipogenesis contributes to the accumulation of hepatic and lipoprotein fat in NAFLD (Donnelly et al., 2005). These observations together with the increasing awareness of the molecular interplay between lipid and carbohydrate metabolism, have led to a "lipocentric" view of the pathogenesis of insulin resistance and T2DM (Savage et al., 2007).

Certain studies using ^{1}H MRS in obese individuals have shown NAFLD to develop easier in obesity (Thomas et al., 2005) and a correlation between LFC and BMI has been observed (Schonfeld et al., 2003). However, the relation between liver fat content

and BMI is not completely straightforward depending on the study population (Seppala-Lindroos et al., 2002).

Currently the visceral fat mass in healthy subjects is regarded to be directly related to LFC, possibly by providing FFAs to the liver through the portal blood flow (Thamer et al., 2004). In contrast, the amount of (abdominal) subcutaneous adipose tissue seems not to be related to LFC (Hoyumpa, Jr. et al., 1975).

It has been hypothesized that, even though insulin resistance may lead to hepatic steatosis, the presence of hepatic fat may in turn worsen hepatic insulin resistance and could initiate a vicious cycle (Samuel et al., 2004). This hypothesis is supported by a study showing that the development of obesity leads to elevated liver enzymes, which in turn lead to glucose intolerance (Suzuki et al., 2005). Although hepatic insulin resistance has been postulated as a main cause for increased LFC, at present no evidence has been found for a direct relationship between LFC and reduced insulin stimulated uptake of glucose by the liver.

Interestingly, heart and liver share common mechanisms of lipotoxicity, although the resulting damage is different. In the heart, triglycerides are not toxic in a direct sense, but ceramide accumulation, formed via de-novo synthesis from FFA, plays a central role in apoptosis of cardiomyocytes (Bugianesi, 2008).

In summary, NAFLD is a very common disease with yet unknown exact pathology. To enhance our knowledge of NAFLD and its pathogenesis, there is a great need for mechanistic studies in patients at high risk for developing NAFLD, such as patients with T2DM and/or obesity.

6.2.3 Diagnosis of NAFLD

Traditionally measurements of transaminase levels and a good clinical history are regarded essential in diagnosing the underlying cause and treatment selection of fatty liver. However, in practice transaminase elevations are unspecific, lack diagnostic utility and are therefore of limited value (Rosman and Lieber, 1994;Limdi and Hyde, 2003). This poses a need for sensitive and specific methods for the diagnosis of fatty liver.

The current gold standard for liver fat content estimation is liver biopsy, although an accurate fat quantification using this invasive procedure is complicated for several practical reasons (see: 6.3). One of the main problems of liver biopsy is the sampling variability, a confounding factor which is often overlooked but should be considered especially when interpreting repeated biopsies within the same patient. High variability in degree of fibrosis observed in repeated biopsies, performed in order to assess the progression of nonalcoholic fatty liver disease, has been attributed tot the fact that histological NASH lesions can be unevenly distributed throughout the liver parenchyma. (Ratziu et al., 2005).

The difficulties described above pose a great need for other (non-invasive) methods for the diagnosis of NAFLD, also taking into account the vast expanding patient group at risk for developing this disease.

6.2.4 Treatment of NAFLD

Current evidence shows the greatest biochemical and histological benefits in NAFLD with weight-loss measures and thiazolidinediones, but further trials are needed to characterize the benefits and risks of the latter agents and currently there is insufficient data to recommend any other strategies for treating NAFLD (Gan et al., 2008).

In nondiabetic subjects a short (2 week) low-fat diet causes a decrease in LFC by 20±9% and a high-fat diet causes an increase in LFC by 35±21% (Westerbacka et al., 2005). Furthermore, a longer period (6 weeks) of very-low-calorie diet (VLCD) does not only reduces LFC by 43% but also causes a reduction of liver volume by 14.7% (Lewis et al., 2006). Intuitively logical, but nevertheless highly interesting, is the fact that in the aforementioned study the change in liver volume was predicted by the change in liver fat ($r=0.61$, $P=0.012$).

6.2.5 Effects of Trimetazidine on the fatty liver in vitro

As stated previously, liver steatosis fuelled by the epidemic of obesity and T2DM is expected to be the primary reason for liver transplantation in the next decade. In addition, the expanding number of patients with fatty liver disease limits the number of livers available for transplantation, because of the increased susceptibility of fatty livers to ischemia-reperfusion damage (Imber et al., 2002). However, the growing number of patients awaiting liver transplantation and the limited pool of donor organs have led to the acceptance of marginal livers for transplantation. Efforts have been made to improve preservation solutions, (Ben, I et al., 2006) in order to reduce graft dysfunction associated with the ischemic preservation of steatotic livers.

Several recent studies, focused on the *ex-vivo* preservation of donor organs, have demonstrated that addition of the anti-angina medication Trimetazidine to the preservation solution has a positive effect, especially in steatotic livers. The addition of Trimetazidine reduces transaminase release by perfused livers and promotes hepatocyte integrity through a reduction of oxidative stress and hepatic vascular resistance. (Ben, I et al., 2006;Ben, I et al., 2007). The cytoprotective effects of Trimetazidine have been attributed to decreased utilization of fatty acids for energy production - by inhibition of the beta-oxidation enzyme 3-keto-acyl-CoA dehydrogenase (Reaven et al., 1988;Kantor et al., 2000;Cano et al., 2003) - balanced by an increased synthesis of structural lipids.

Animal studies have shown that Trimetazidine directly shifts the incorporation of glycerol from triglycerides to phospholipids in the liver (Sentex et al., 2001). In humans, the administration of Trimetazidine decreases the levels of beta-hydroxybutyrate (Monti et al., 2006) which is a specific marker of hepatic fatty acid oxidation. However, at current there are no *in vivo* studies available on the effects of Trimetazidine on LFC in patients with NAFLD.

6.3 ASSESSMENT OF LIVER FAT CONTENT AND METABOLISM

The current gold standard for assessment of LFC is liver biopsy. However, this is an invasive procedure associated with (post) procedural pain, high costs and above all a significant amount of potential complications, such as bleeding, infection and biliary leakage. A recent study on percutaneous liver biopsy in patients with nonalcoholic steatohepatitis reported an overall complication rate of 10%, with 1–3% of post-biopsy patients requiring hospitalization, and an overall mortality rate of 0.01% (Gaidos et al., 2008). A second study, reviewing complications of percutaneous liver biopsy in general, reported even higher values: 13.6% minor complications, 1.0% major complications and a 0.25% risk of death (van der Poorten et al., 2006). In addition liver biopsy is subject to the aforementioned sampling error, since only approximately 1/50000th part of the liver becomes available for histological analysis (Maharaj et al., 1986) and liver fat deposition can, in some cases, be heterogeneous (Arun et al., 2007). Finally, lipid quantification or grading in histological biopsy samples is traditionally based on a subjective estimation by a pathologist, not on an objective (chemical) analysis, which also deceases the accuracy of liver biopsy in estimating exact LFC (Petersen et al., 1996;Hussain et al., 2005;Thomas et al., 2005). This problem was emphasized by a study comparing a computerized stereological point counting method versus pathologist visual estimation of lipid content in histological samples: (objective) point counting was shown to have a much higher reproducibility and therefore it is the preferred method when assessing LFC (Franzen et al., 2005).

In summary, liver biopsy for evaluation of LFC in the vast expanding (mainly asymptomatic) patient population suspected of having NAFLD (see 6.2.1) is a suboptimal method. Therefore, there has been a highly increasing focus on *non-invasive* methods to asses liver fat content.

6.3.1 Overview of non-invasive methods

Several *non-invasive* (radiological) methods are being used to asses liver fat content in vivo: transabdominal ultrasonography (US), computed tomography (CT), and magnetic resonance imaging (MRI) and spectroscopy (MRS). (Kwiterovich, Jr. et al., 1970;Davies et al., 1991;Joseph et al., 1991;Longo et al., 1995;Ricci et al., 1997;Mendler et al., 1998;Saadeh et al., 2002). All of these methods have their own specific performance, advances and drawbacks which are discussed below.

6.3.1.1 Transabdominal ultrasonography (US)

US is the most common imaging modality used to study the liver in general and also to assess LFC. US is characterized by very wide availability and low examination cost (Valls et al., 2006). Since fat accumulation in the liver increases scattering of the US beam, the fatty liver appears brighter than a non-fatty liver. This increased brightness has been shown to be characteristic in some studies (Mathiesen et al., 2002), but other studies have shown that other conditions, such as fibrosis, my have similar sonographic appearance in some patients (Konno et al., 2001). For these reasons, the brightness of the liver has to be compared to other abdominal organs (spleen or kidneys) which are

known to have low-fat content. Using these methods, a sensitivity and specificity for detection of increased LFC in the general population is 60%–95 % and 84%–100% (Charatcharoenwitthaya and Lindor, 2007).

The main weakness of US is that the measurement can be easily affected by practical issues inherent to the method, such as attenuation of the beam by large subcutaneous tissue and the inability to reliably detect (relatively) low levels of liver fat content: one study reported a sensitivity of 55% in patients with histologically shown LFC of less than 20% (Needleman et al., 1986). This results in the sensitivity and specificity of US for the detection of increased LFC to be only 49.1% and 75% (Mottin et al., 2004). In addition to these low values for sensitivity and specificity, the US method is also highly operator dependent resulting in low reproducibility. Furthermore, US lacks an objective classification method for the observed brightness, resulting in an subjective interpretation of the brightness into crude classes (such as mild, moderate or severe steatosis): this results in changes of LFC as large as 50% to remain undetected in some patients (Fishbein et al., 2005).

In summary, despite high availability and low costs, US is a poor method for measurement of LFC, especially in the obese patient population at risk for NAFLD.

6.3.1.2 Computed Tomography (CT)

CT relies on ionizing radiation and measures tissue density as a function of attenuation: less dense tissue (such as fat) appears darker on CT images (Piekarski et al., 1980). Based on this principle, unenhanced CT has been used quite widely for the evaluation of LFC in adults.

In theory, a major advantage of CT over US is that the liver attenuation can be objectively measured in Hounsfield Units (HU). However, in practice most CT scanners lack appropriate calibration for this purpose (Charatcharoenwitthaya and Lindor, 2007). For this reason, in analogy to US, measured liver HU are usually compared to HU measured from an organ with known low fat content (spleen) allowing for calculation of the liver-to-spleen ratio (Ricci et al., 1997). Using these methods, CT has been reported to have a sensitivity and specificity for the detection of moderate to severe increased LFC (over 30% by histological analysis) of 73%–100% and 95%–100%, respectively (Charatcharoenwitthaya and Lindor, 2007).

The main weakness of CT for the measurement of LFC is its inability to detect low levels of LFC, as observed in NAFLD. In addition, several other conditions and factors may interfere with the observed liver densities, such as edema. These issues, combined with the dependence on ionizing radiation, render unenhanced CT for the quantitative assessment a clinically unacceptable method (Park et al., 2006). Additionally, in the context of a rapidly increasing (obese) pediatric patient population at risk for NAFLD, there is a great need for non-invasive methods to measure LFC that are not dependent on ionizing radiation.

6.3.1.3 Magnetic Resonance Imaging (MRI)

Magnetic Resonance (MR), including both its imaging and more advanced applications such as Magnetic Resonance Spectroscopy (see: 6.3.1.4), is generally regarded as the best radiologic modality for the assessment of liver fat content and also provides excellent soft tissue contrast. However, MR is associated with high examination cost due to significant equipment prices and complex implementation.

MR of the (fatty) liver is based on the observation of signals from protons in both water and fat which contribute together to the observed MR signal, but precess at a different frequency (difference approximately 220 Hz at 1.5T). Different MR techniques can be used to decompose the original signal into its water and fat component. MRI uses the signal to construct an anatomical image and tissue contrast, but with an appropriate sequence such as in-phase and out-of-phase imaging (see: 6.3.2.3) the frequency difference can be used to obtain water and fat weighted images.

The main advantage of MR is that it performs clearly better than other imaging modalities in the detection of low levels of liver fat, when compared to US and CT. In the histological range of liver fat content of 5-10%, sensitivities of greater than 85% and specificity of almost 100% have been reported. Despite this relative superior performance, which is achieved without the use of ionizing radiation, MRI is not as widely used as one would expect. The main reasons are the aforementioned high costs per examination, the dependence on full patient cooperation, and some contraindications for the examinations such as a pacemaker implant or patient claustrophobia.

6.3.1.4 Magnetic Resonance Spectroscopy (MRS)

In contrast to MRI, MR spectroscopy resolves the observed signal into a frequency spectrum, providing biochemical information (Mehta et al., 2008). Proton magnetic resonance spectroscopy (^{1}H MRS) is currently by far the most promising and most sensitive non-invasive method to assess LFC (Adams and Lindor, 2007).

The MR spectrum describes the intensity of MR signal as a function of precession frequency. Using a high-field MR scanner, the water peak can be identified at 4.7 ppm and the main fat peak (of –(CH2)n–) at 1.2 ppm. In the non-fatty liver the spectrum is dominated by the large water peak. In the fatty liver, both the water and the fat peak(s) can be easily identified and analyzed. Using the MR spectroscopy method, the fat-water spectrum within a single volume (voxel) of liver tissue is measured.

The main advantage of ^{1}H MRS is its extremely high sensitivity also at very low LFC. In an optimal setup even LFC as low as 0.5 % can be reliably detected (Machann et al., 2006). Since the method does not rely on ionizing radiation and thus is safe for the patient, it is a potentially ideal tool for screening patients at risk for for NAFLD. Nevertheless, ^{1}H MRS is mainly used in academic institutions for research purposes because a great deal of expertise and experience is required for practical implementation of the method and reliable data analysis.

6.3.2 Basics concepts of MR Imaging and Spectroscopy

Magnetic resonance has revolutionized field of radiology during the past decades. High soft tissue contrast and image quality, no need for use of ionizing radiation and a virtually unlimited versatility are some of the key issues which have been thriving the development of this technique.

6.3.2.1 History and discovery of Magnetic Resonance

In 1924 Wolfgang Pauli proposed that nuclei possess a nuclear spin (Pauli, 1924). Already in 1936 C.J. Gorter, a Dutchman teaching at the University of Groningen at that time, unsuccessfully attempted to detect nuclear spins (Gorter, 1936).

In 1942, Gorter together with L.J.F Broer, both inspired by the molecular beam experiments by Rabi et al., attempted to measure the phenomenon of magnetic resonance again, unfortunately also this time without any success (Gorter and Broer, 1942). In retrospect, it can be concluded that Gorter's measurements were mainly unsuccessful due to the unfortunate choice of the examined substance - LiCl and KF. These substances have very long relaxation times which make the signal hard to measure. Gorter also conducted his experiments at very low temperatures which, ironically, make a possible signal even harder to observe.

The first successful magnetic resonance measurements were conducted in 1945 by E.M. Purcell et al. at the Massachusetts Institute of Technology, Cambridge Massachusetts (Purcell et al., 1946) and almost simultaneously by F. Bloch et al. at Stanford University, California (Bloch et al., 1946). Purcell et al, in contradiction to Gorter, was fortunate to study a good substance (paraffin) and to use a strong enough magnetic field to obtain a resonance signal. The *absorption* peak was observed by varying the current in the coils and thus the strength of the magnetic field.

Bloch used the method of nuclear *induction* to detect the nuclear resonance signal (Bloch, 1946) in contrary to Purcell who used the absorption method. The method of nuclear induction proved most useful and is still used today in NMR and MRI. Bloch introduced (described) the terms *longitudinal relaxation time (T_1)* and *transversal relaxation time (T_2)* in his theoretical analysis of his nuclear induction experiment (Bloch, 1946). These terms were previously used to describe paramagnetic relaxation but have thereafter been used in both NMR and currently in MRI. Bloch received the Nobel price for his theoretical analysis and practical description of his experiments. Purcell also received the Nobel price for his description of nuclear magnetic resonance relaxation effects in his absorption experiments (Bloembergen et al., 1948), including the proposition of the well-known Bloembergen-Purcell-Pound formula within the same publication.

An important step in research of magnetic resonance was made by the discovery of Spin Echoes by E. L. Hahn in 1950 (Hahn, 1950). Spin Echoes offered opportunities to directly measure relaxation times and would later facilitate the development of MRI. The Nobel Price winner R.R. Ernst made a very important step towards practical

applications of magnetic resonance by applying Fourier transform spectroscopy to magnetic resonance (Ernst and Anderson, 1966).

The first "MRI images" were produced only in by 1973 P.C. Lauterbur, who called his technique "zeugmatography" (Lauterbur, 1973) and received the Nobel price for his discovery in 2003, together with Sir. P. Mansfield who received credit in particular for the development of the rapid "echo-planar" imaging technique (Vlaardingerbroek and Boer, 2003).

6.3.2.2 Physics of Magnetic Resonance

Nuclei with an odd atomic weight (even number of protons and odd number of neutrons, or vice versa) possess a nuclear spin or intrinsic nuclear angular momentum. A nuclear spin with a positive charge produces a magnetic field that is oriented in the direction of rotation.

The nucleus of the atom of highest interest in MRI and also MRS is ^{1}H (proton) so the displayed positive nucleus in the following images can be thought of as a ^{1}H nucleus. Other nuclei besides ^{1}H that are of interest and can be observed with MRS are ^{13}C, ^{19}F, ^{23}Na and ^{31}P.

In an arbitrary volume of tissue, e.g. liver tissue, the spins within this tissue are randomly oriented in all directions. When vectors of all the spins are added together this produces a zero sum, resulting in no net magnetization to be observed. However, when the tissue is placed in a strong magnetic field B_0, more spins will be aligned along the magnetic field (low energy state) than against the magnetic field (high energy state). In this case the vector sum of all spins, the net magnetization M_0, is *not* equal to zero and is oriented in the direction of B_0 (Figure 4)

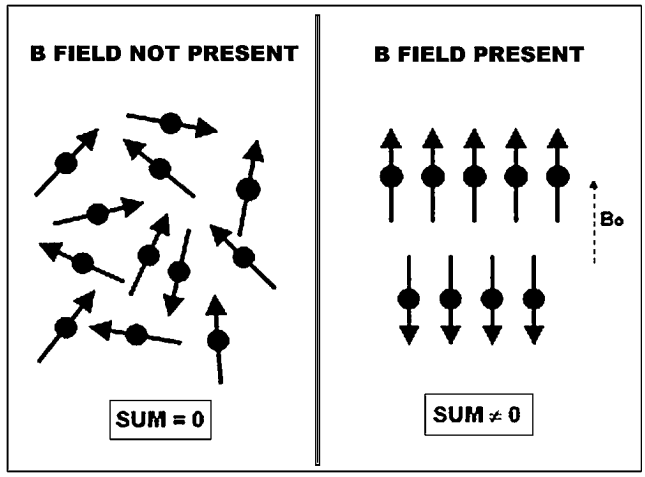

Figure 4 Effect of the magnetic B field on spin alignment.

Shortly said, the volume of tissue in the presence of the magnetic field B_0 becomes magnetized with a value of M_0.

Because of the interaction of the magnetic field with the moving positive nucleus the individual spins will start to precess (rotate) about the magnetic field. The rate of precession is proportional to the strength of the magnetic field and is expressed by the *Larmor* equation:

$$f_0 = \frac{\gamma B_0}{2\pi}$$

Where f_0 is the Larmor frequency in hertz (Hz), B_0 the magnetic field strength in Tesla (T) and γ a constant known as the *gyromagnetic ratio* ($s^{-1}T^{-1}$) which is specific for each nucleus. For example, the Larmor frequency for protons at 1.5 Tesla is 63.8646 MHz.

Figure 5 shows a graphical representation of a nucleus with spin processing around the magnetic field and its x, y and z components. B_0 is by convention defined to be in the z direction in a Cartesian coordinate system and so the nucleus with spin processes around the z axis in this representation.

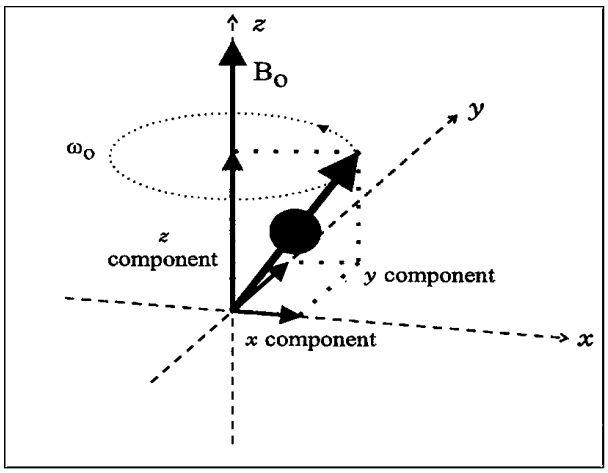

Figure 5. Graphical representation of spin procession around the B_0 field. Modified from "Clinical MR Spectroscopy" (Salibi and Brown, 1998).

Although the z *component* of the nuclear spin vector has the same direction as B_0, it is essential to note that the spinning nucleus as a whole is precessing *at an angle* to B_0. The basis of all applications of magnetic *resonance,* including magnetic resonance spectroscopy, is that the above described precessing spins can be disturbed by a radio frequency (RF) pulse of exactly (or very close to) the Larmor frequency.

The spins *resonate* (hence the name *magnetic resonance*) while absorbing the energy of the adequate RF pulse. As a result the net magnetization vector M_0 moves ("flips") towards the x,y plane. Figure 6 shows this process viewed in a coordinate system rotating at the Larmor frequency f_0. In this image the RF electromagnetic field is indicated by B_1.

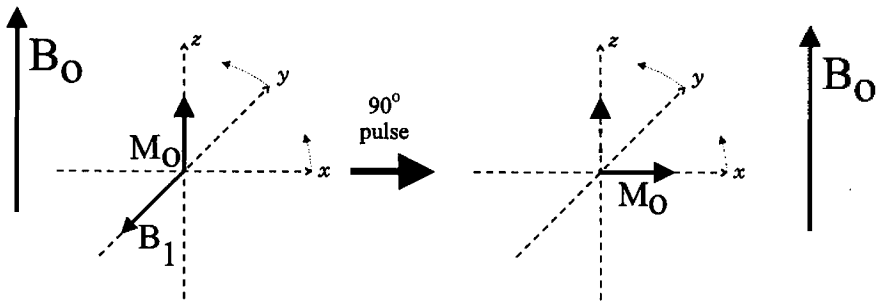

Figure 6. Spins flipped in the xy plane by radiofrequency field B_1. Modified from "Clinical MR Spectroscopy" (Salibi and Brown, 1998).

After application of the RF pulse two important effects occur, on which all techniques using magnetic resonance, including MRI and MRS are based:

1. The spins flipped by the RF pulse are in phase. This means they all are at the same point of their cycle at the same time. Due to interactions between the spins and inhomogeneity of the magnetic field this phase coherence diminishes. This process is called *spin-spin relaxation* and described by the transversal relaxation time (T_2).

2. All spins flipped by the RF pulse return to the direction of the static magnetic field B_0. This process is called *spin-lattice relaxation* and is described by the longitudinal relaxation time (T_1). The signal observed by an MR device at a certain location in a certain tissue depends on the T_1 and T_2 values in that specific location. Because different tissues have different T_1 and T_2 values, they can be differentiated and this information is translated in, for example, an MR-image.

If, for example, a whole human being in a strong external magnetic field B_0 is subjected to a RF pulse equal to the resonance frequency (Larmor frequency) for protons at B_0, then a large signal could be received. However, the information of this signal would be not very useful because the signal originates from all protons subjected to both the B_0 and the RF field in the human body.

Therefore MRI and MRS use variable magnetic fields superimposed on B_0 in both the x, y and z direction called *gradients*. With the help of gradients the magnetic field can be modified in such a manner that only in a certain area of tissue the magnetic field experienced by the protons satisfies the condition for magnetic resonance, called localization. The signal from these protons can be used to reconstruct an MR image of this area or slice.

MRS uses an even more demanding localization technique with three intersecting "slices" in order to allow a small, theoretically rectangular, region of interest to be examined. Therefore in MRS one does not speak of a pixel but of a voxel, which is a 3-dimensional pixel (Figure 7)

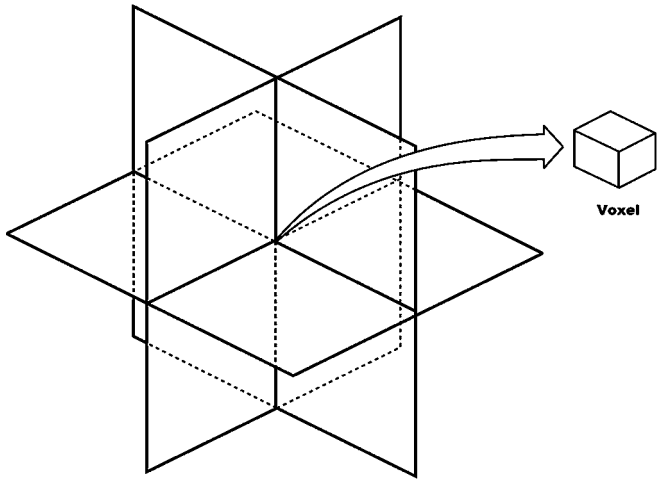

Figure 7. Three slices intersect to produce one voxel. (Adapted from: Kohler S, Signa Advantage PROBE/SV: Single-voxel Proton Brain Exam Applications Guide, Vol 5, General Electric Medical Systems, 1993)

6.3.2.3 In-phase and out-of-phase MR imaging

MR of the (fatty) liver is based on the observation of signals from protons in both water and fat which contribute together to the observed MR signal, but precess at a different frequency. The frequency difference between the main fat peak (methylene) and the water peak is approximately 220 Hz at 1.5T. Different MR techniques can be used to decompose the original signal into its water and fat components, such as in-phase and out-of-phase imaging.

The in-and-out-of-phase MR-sequence is based on different chemical shifts of water and fat and can be used to find fat accumulation in liver tissue (Dixon, 1984;Heiken et al., 1985;Buxton et al., 1986). Two echo's are obtained, one at approximately 2.1-2.3 ms at 1.5T magnetic field, when the water and fat signal are in opposed phase, and one at approximately 4.4 ms when the water and fat signal have the same phase (Prorok and Sawyer, 1992). Reconstruction of the data of this individual echo times results in two differently weighed images, with the intensity difference between the in-phase and out-phase image indicating the degree of LFC.

In a study by Levenson et al. this sequence exhibited good correlation with visually estimated histological sampling (Levenson et al., 1991). Mitchell et al. showed in phantom, animal and in vivo studies that in-and-out-of-phase imaging, using the Dixon method, can be used for estimation of liver fat content (Mitchell et al., 1991). However, Westphalen et al. have recently shown that iron accumulation is a potential pitfall in the determination of liver fat accumulation, since it alters the signal intensity of in-and-out-of-phase images (Westphalen et al., 2007). In particular, the value of in-and-out-of-phase imaging for the estimation of LFC in patients with type 2 diabetes is currently unclear.

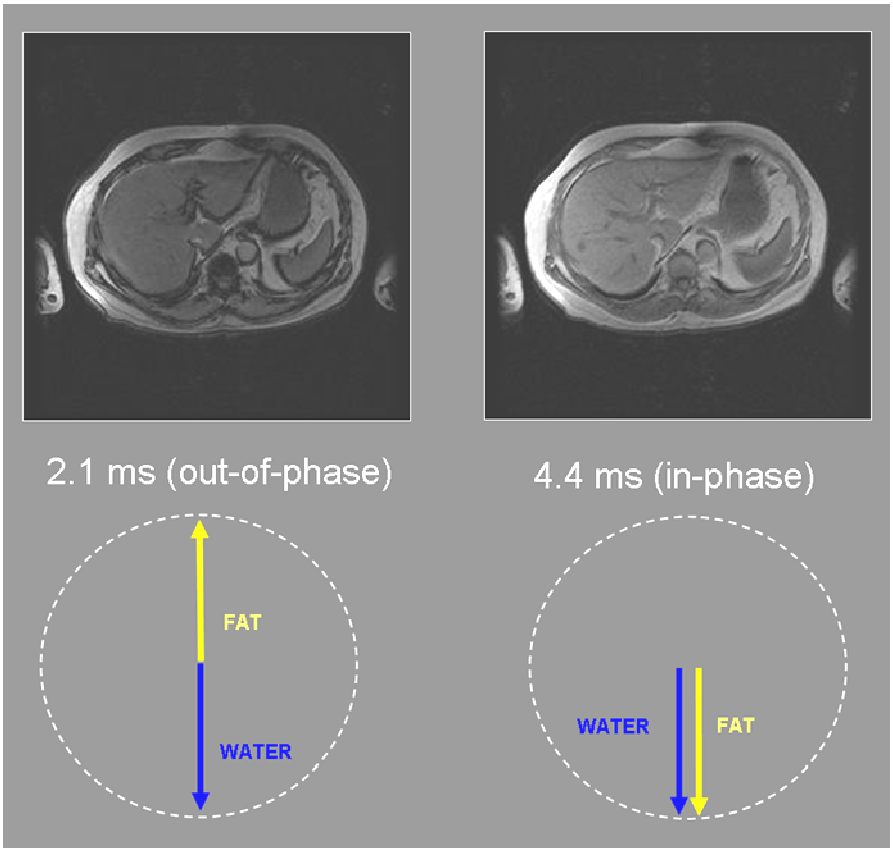

Figure 8. Basics of SI in in-phase and out-of- phase imaging. The colored arrows indicate the direction of the fat and water signal at each individual echo time, resulting in either addition or subtraction of the water and fat signal and corresponding MR-images.

6.3.2.4 Other MR imaging methods of the liver

A preliminary study using superparamagnetic iron oxide-enhanced magnetic resonance imaging (SPIO-enhanced MRI) has shown a significant relationship of imaging findings with histological NAFLD activity scores (Tomita et al., 2008). The method was able to predict NASH with moderate specificity (66.7%) but very high sensitivity (99.9%) and might therefore be helpful in identifying NASH patients among patients suspected of having NAFLD.

Recent advances in MR imaging have shown that MR-diffusion imaging might be useful in imaging of liver cirrhosis (Luciani et al., 2008). One of the most recent advanced MR applications is Magnetic Resonance Elastography (MRE), a technique visualizing the propagation of externally applied pressure waves within the liver (Huwart and van Beers, 2008). MRE also holds great promise for accurate non-invasive assessment of hepatic fibrosis.

6.3.3 Positron Emission Tomography (PET)

Positron emission tomography is a computerized tomographic method which uses short-lived radioactive isotopes. In brief, PET is based on introducing a positron emitting tracer into the body which can then be detected. Detection is based on the emitted positron combining with a local electron in the tissue, a process called annihilation. The result of this annihilation is two photons leaving the tissue in exactly opposite directions. These photons (coincidence events) are then detected by the PET scanner, allowing for determination of the site of annihilation and thus the positron tracer within the tissue (Saha, 2005).

PET allows for quantitative measurements of regional substrate metabolism, and by using fluorine labeled glucose ([^{18}F]-2-fluoro-2-deoxy-D-glucose, [^{18}F]FDG), can provide information on liver glucose metabolism non-invasively (Iozzo et al., 2003a). The high degree of sensitivity of the PET technique provides for an accurate method and allows for small sample sizes of study subjects. The PET tracer and glucose analogue [^{18}F]FDG is transported across the cell membrane and accumulates intracellularly in proportion to its phosphorylation, because the outflow of out of the cell is assumed to be relatively very slow (Sokoloff et al., 1977). [^{18}F]FDG remains trapped in the cell in the form of 6-phosphate-fluoro-deoxyglucose because it cannot be metabolized through the glycolytic pathway. These processes, leading to an accumulation of an intravenous administered bolus of [^{18}F]FDG, promote a high quality imaging of the organ.

6.3.3.1 Hepatic glucose uptake

Since it is virtually impossible to access the human liver by means of cannulation, traditional methods cannot be used to directly measure hepatic glucose uptake (HGU) in vivo. However, in validations studies at the Turku PET Centre, using a pig model, we have shown that [^{18}F]FDG-PET derived parameters provide accurate quantification of HGU (Iozzo et al., 2007).

In order to quantify the liver glucose uptake by its analogue [^{18}F]FDG, a conversion term named lumped constant, is used. The lumped constant in general represents the ratio of the metabolic rates of the tracer and the trace, in this case [^{18}F]FDG and glucose. The aforementioned validation study to measure HGU in pigs using [^{18}F]FDG showed that the average lumped constant for hyperinsulinemic and fasting condition has a value of 1.0 (Iozzo et al., 2007). The graphical analysis developed by Patlak and Blasberg can be successfully used to determine the liver's fractional [^{18}F]FDG uptake constant and, consequently, glucose uptake in absolute terms (Patlak and Blasberg, 1985). This makes [^{18}F]FDG PET and ideal method for non-invasive measurement of liver glucose uptake.

7. AIMS OF THE STUDY

I To investigate the role of nonalcoholic fatty liver disease as an indirect marker for cardiovascular risk factors, myocardial metabolism and blood flow in patients with type 2 diabetes and coronary artery disease.

II To study (1) the mutual relationship between liver fat content and hepatic glucose uptake in patients with type 2 diabetes and (2) the relationship between changes in liver fat content and hepatic glucose uptake induced by Rosiglitazone in these patients.

III To investigate the effects of treatment with Trimetazidine on liver fat content, hepatic enzymes and fibro-inflammatory score in obese patients.

IV To evaluate whether in-and-out-of-phase MR-imaging can reliably estimate liver fat content in patients with nonalcoholic fatty liver disease, using ^{1}H MRS as a reference standard.

8. SUBJECTS AND STUDY DESIGN

In total 55 patients with T2DM and ischemic coronary artery disease, 9 patients with obesity and 8 healthy subjects took part in the current study.

Characteristics of all patients and healthy subjects in studies I-IV are shown in Table 1

Table 1. Study subjects: general characteristics.

Study	Study group	N (M/F)	Age (yrs)	BMI average (kg/m^2)	BMI range (kg/m^2)	Intervention	fP-glucose (mmol/L)	HbA1c (%)
I	T2DM	55 (40/15)	64±7	30±4	20-40	Cross-sectional	7.5±1.9	7.1±0.9
II	T2DM Rosiglitazone	27 (19/8)	64±8	30±5	24-40	Rosiglitazone	7.3±2.0	7.3±0.9
	T2DM Placebo	27 (19/8)	63±7	30±3	20-37	Placebo	7.7±1.7	7.1±0.9
	Healthy subjects	8 (8/0)	54±10	26±3	23-30		5.2±0.3	5.2±0.3
III	Obese Trimetazidine	9 (4/5)	54±3	30±3	27-38	Trimetazidine	5.2±0.1	5.6±0.1
IV	T2DM	33 (23/10)	63±8	30±4	24-40	Cross-sectional	7.2±2.0	7.2±1.0

8.1 STUDY SUBJECTS

For the studies I and II in total 62 patients with T2DM and ischemic coronary artery disease were recruited. For the definition of T2DM the WHO criteria were used (Alberti and Zimmet, 1998). Patients were recruited through advertisements in a local newspaper and additionally from out-patient clinics in the district of Southwest-Finland. Treatment of T2DM with diet or with metformin and/or sulphonylurea and good or moderate glycemic control (HbA1c<8.5%) was required. All subjects were on stable medical therapy and had past or present angina pectoris symptoms under stress but no unstable angina pectoris. Patients with diabetes treated with thiazolidinediones, chronic insulin therapy, alcohol or drug abuse were excluded. Also patients with clinical signs of heart failure were not admitted to the study.

To minimize the effects of underweight or severe obesity, an additional exclusion criterion of BMI under $19 kg/m^2$ or over 40 kg/m^2 was used. This resulted in inclusion of 55 patients in study I.

In study II, all patients completing the 16 weeks intervention period with Rosiglitazone (n=58) were included. However, three patients were withdrawn during the intervention: one patient due to a kidney tumor (detected on abdominal MRI), one patient due to hepatopathy and one due to suspected sick sinus syndrome. Additionally, one patient withdrew consent. This resulted in a total of 54 patients to be included in study II.

For study III, nine non-diabetic, obese subjects were recruited, by means of local advertisement. Inclusion criteria were a body mass index (BMI) $\geq$ 27 kg/m^2 and $\leq$ 38 kg/m^2, age between 20 and 75 years, a normal physical examination and a stable weight and diet for the past three months. Exclusion criteria were regular medication, the presence of chronic diseases and alcohol or drug abuse.

Study IV included a subgroup of 33 patients of the total 62 recruited patients with T2DM and and ischemic coronary heart disease (CHD). Liver fat content was measured twice in 28 patients and once in 5 patients, resulting in a total of 61 full liver ^{1}H MRS and in-and-out-of-phase MRI examinations.

All patients and healthy subjects included in the studies above (I-IV) gave written informed consent before their participation. The studies were conducted according to the guidelines of the Declaration of Helsinki and furthermore the study protocol was approved by the Ethics Committee of the Hospital District of Southwest Finland.

8.2 STUDY DESIGN

8.2.1 Design of substudies I-II and IV

All subjects with T2DM underwent a screening visit before inclusion in the study. In addition an exercise-rest SPECT perfusion study was performed to select patients with a partially or completely reversible deficit in myocardial perfusion. Coronary angiography was performed to determine the stenotic vessels. The patients having met the aforementioned inclusion and exclusion criteria entered a run-in period with placebo. After 4 weeks run-in patients were randomized for treatment with either Rosiglitazone (4-8mg daily) or placebo for a double-blinded trial with a total duration of 16 weeks.

At baseline MRI, ^{1}H MRS and PET studies were performed and these measurements were repeated after 16 weeks of intervention with either Rosiglitazone or placebo. MRI and ^{1}H MRS were performed after a 2 hour fasting period, and the PET studies after overnight fast. Study I was a cross-sectional study based on baseline data, study II was a double-blind, placebo-controlled, parallel group study including treatment with either Rosiglitazone or placebo. And outline of the study design of study II is shown in Figure 9. The technical study IV was based on MRI and ^{1}H MRS data from patients involved in the intervention study, without taking into account the intervention as such but focusing on numerical data.

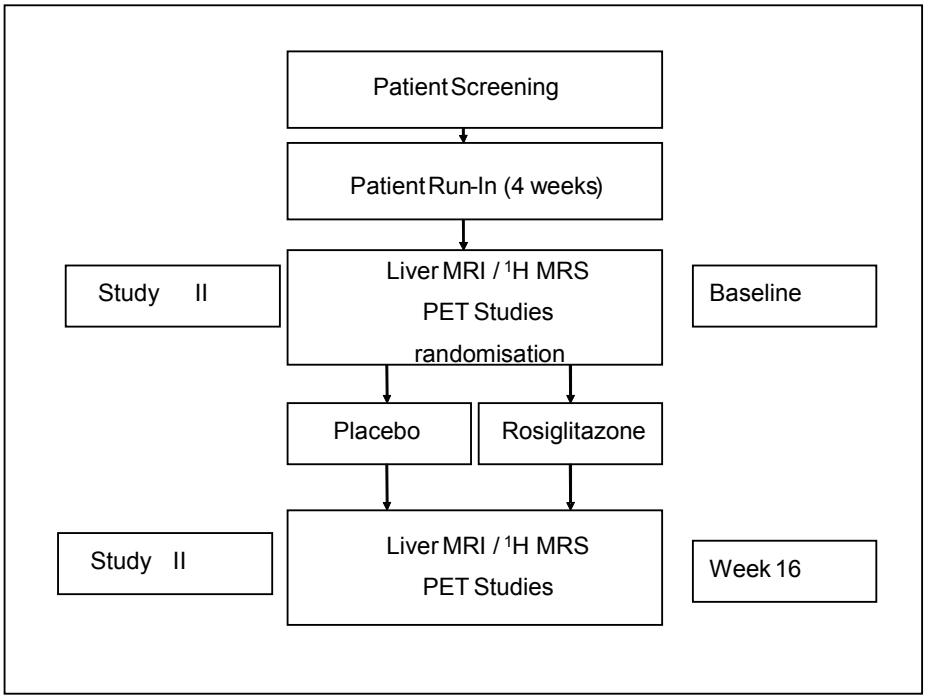

Figure 9. Outline of the study design (II).

8.2.2 Design of substudy III

All subjects underwent a general health screening before entering the study. During this first of in total four visits, also an oral glucose tolerance test was performed to reveal possible undiagnosed impaired glucose tolerance or diabetes mellitus. Additionally, diet counseling was provided to standardize the caloric intake during the study and to instruct patients to maintain their current lifestyle. Furthermore blood samples were drawn. During the second visit, abdominal MRI and ^{1}H MRS of the liver was performed, after an overnight fasting period to standardize possible nutritional effects on liver fat content. After this second (baseline) visit, a four-week treatment with Trimetazidine (35 mg, Vastarel®, Servier, once daily) was started. During the third visit, two weeks after onset of treatment, patient compliance was confirmed, a clinical examination performed and blood samples were drawn. During the fourth visit, one month after onset of the treatment, the measurements of the first and second visit were repeated. And outline of the study design is shown inFigure 10.

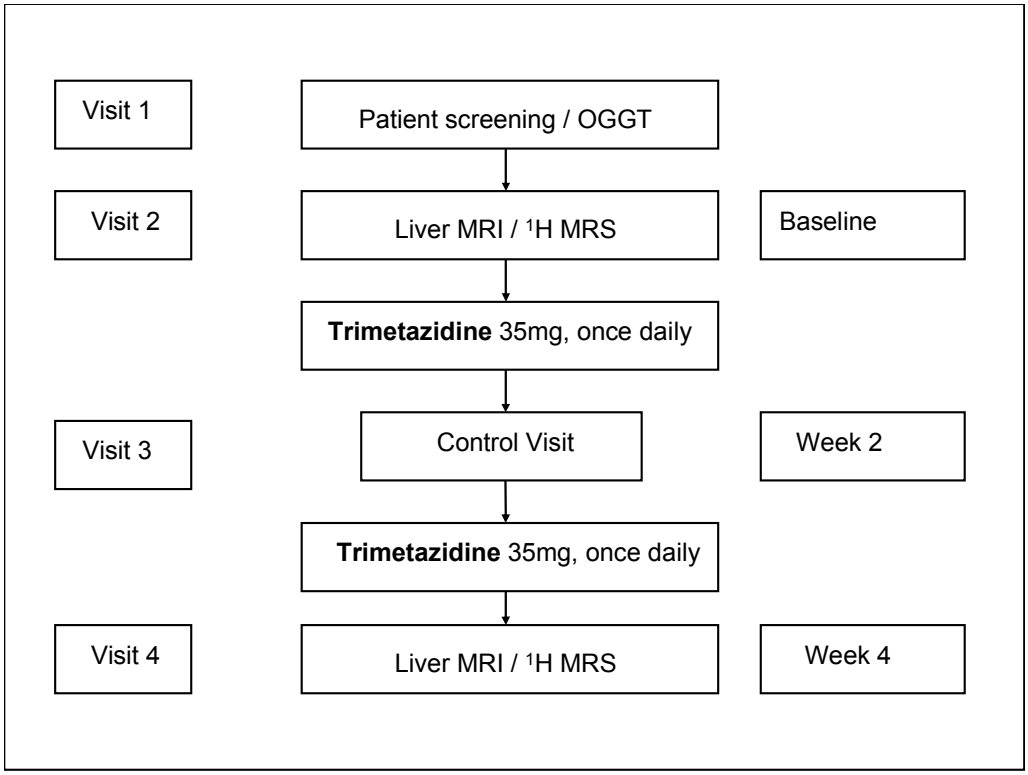

Figure 10. Design outline of study III.

9. METHODS

9.1 MAGNETIC RESONANCE SPECTROSCOPY OF THE LIVER

9.1.1 Hardware equipment

Study I, II and IV were conducted with a 1.5 Tesla Signa Horizon LX system, manufactured by GE Medical Systems, Milwaukee, Wisconsin, USA. The system was equipped with an internal body coil and general-purpose-flex surface coil which were used for MRI and MRS studies. This device was installed at the Medical Imaging Centre of Southwest Finland.

Study III was conducted using a 1.5 Tesla Gyroscan Intera CV Nova Dual system, manufactured by Philips Medical Systems, Best, the Netherlands. The system was equipped with an internal body coil and a flexible E1 surface coil for the MRI and MRS studies. This device was installed at the Turku PET Centre.

9.1.2 Software

Two different software packages, named jMRUI and LCModel, were used in this study to analyze the ^{1}H MRS data. The commercial LCModel software was purchased at a later stage during the studies and was therefore only available for analysis of the data of study III. Both software packages have specific advantages and disadvantages. Since an accurate analysis process and knowledge of important steps is essential in obtaining high-quality data, both software packages are discussed in more detail below.

9.1.2.1 Java Magnetic Resonance User Interface (jMRUI) (I,II & IV)

The java Magnetic Resonance User Interface (jMRUI) is a software package which was developed with EU support. This program is provided free of charge to scientific centers by the participants of the EU Network programmes: Human Capital and Mobility, CHRX-CT94-0432 and Training and Mobility of Researchers, ERB-FMRX-CT970160 (http://www.mrui.uab.es/mrui).

Since the program is java based, it can be used on a wide variety of computer platforms. Furthermore, it supports data input from a wide range of manufacturers. The software has possibilities for preprocessing and quantification of spectra. All preprocessing steps and input for final quantification are performed manually.

In this study the following processing steps were performed with jMRUI v. 1.2 in order to obtain the final amplitudes of water and fat:

1. Summation: Spectroscopy data is acquired in different frames, each consisting of 8 individual measurements. To cancel out noise and obtain a higher quality

spectrum, selected frames of the same acquisition were summed together with this function.

2. Apodization: Spectra with a visually estimate high amount of noise were multiplied by a Lorentzian or Gaussian lineshape (15Hz). This "smoothes" the looks of the spectrum and helps in the correct quantification of peaks. However, since apodization also broadens the original spectrum it was used with care.

3. Phase correction: Spectra acquired are usually "out of phase". For purposes of quantification a so-called pure absorption spectrum is obtained trough phase correction of the spectrum or individual frames. Phase correction can be done either automatically or manually. In this study each frame was phased individually, which is more reliable than the (blind) automated method, but also very time-consuming.

4. Frequency shift: The water signal in the spectra was centered at 0 Hz at this stage in the data processing. Small drifts in center frequency occur and need to be corrected before applying filters (with default frequency boundaries, see step 5) in order to obtain consistent results.

5. Hankel Lanczos Singular Values Decomposition (HLSVD) filtering (Pijnappel et al., 1992): At first the data from the frames without suppression was analyzed. The two frames were summed and a HLSVD filter was used to remove the unwanted (fat) signals in the area of 100 – 300 Hz to improve the analysis of water signal. The frames without the suppressed water peak were treated in the same manner, but the HLSVD filter was applied at the region of –100 to +100 Hz to remove residual water and improve the analysis of the fat signal.

6. Quantification using the Advanced Method for Accurate, Robust, and Efficient Spectral fitting (AMARES) algorithm (Vanhamme et al., 1997): In case of the water spectrum (sum of unsuppressed frames) the water peak and the resonance resulting from protons bound to double-bound carbon (frequency difference of 50Hz) were in principle marked separately for analysis. In the fat spectrum the methylene and the methyl peak were in general marked separately for analysis, but in most spectra analyzed together for at 1.5 T their separation and individual analysis is not reliable. In case of two visits by the same patient an identical routine was followed for the first and second visit.

As a final result the amplitudes in the output of the AMARES analysis were recorded and the correct peak location (number) confirmed using the graphical representation. As a general measure for the quality of the spectral analysis, the residue was studied for each individual analysis. In case of a large residue, step 6 was repeated.

For the calculation of final liver fat content the above-mentioned amplitudes were corrected for differences in relaxation times, proton density and liver dry weight (see 9.1.5)

As can be judged from the above, since the jMRUI the software demands quite much user intervention, analysis of each spectrum is a time consuming task. We have thoroughly investigated and tested the options of the software package for more automated processing (Batch Processing) of both in vivo and in vitro MRS data. However, the software version available to us did not support reliable batch processing for our data. For this reason all spectra analyzed in this study with jMRUI (substudy I, II and IV) were analyzed manually in order to obtain reliable and consistent results.

9.1.2.2 Linear Combination of Model spectra (LCModel) (III)

The second software package used for liver ^{1}H MRS data analysis in study III, LCModel, was originally developed for analysis of brain spectra (http://www.s-provencher.com/). In contrast to the jMRUI software, LCModel is a commercial product and we were able to purchase the program only during the later phase of the current study. The program has been developed for over 15 years at current, but functionality to analyze spectra from the liver was added more recently.

The main idea of the program is to analyze an in vivo spectrum as a linear combination of model spectra of metabolite solutions in vitro (Provencher, 1993). The great advantage of this method is that in vivo proton MR spectra can be quantified (almost) fully automatically, in a non-interactive, operator-independent fashion. In short, time-domain data is imported to the program and upon analysis a one-page summary output of the analysis is obtained. We used the program's graphical user interface (LCMgui, version 2.1-4) to control the UNIX based LCModel program (version 6.1-4). The software was running on a Sun Ultra 10 computer with SunOS 5.8.

For analysis of the spectra in our study, the special spectra type input command [SPTYPE ='liver-1'] was used, as instructed by the program developer. In this particular case the spectrum analysis is not based on model spectra ("basis-set") of metabolite solutions in vitro but on a basis-set simulated within the program.

In substudy III for every ^{1}H MRS examination each data-frame was first referenced, phased and analyzed using the [LCORAW = 10] command. This allowed for removal of data frames not fulfilling the criteria posed by the software (fit SD $\leq$ 20%), before summation of individual frames by an in-house written program and final analysis of the spectrum.

Below an example of the summed analysis of a patient participating in substudy III, showing the LCModel analysis and peaks which were recorded: Methylene and Methyl (Lip09+Lip31) and Water. Protons bound to double-bound carbon (Lip53) were separated from the water resonance (Figure 11).

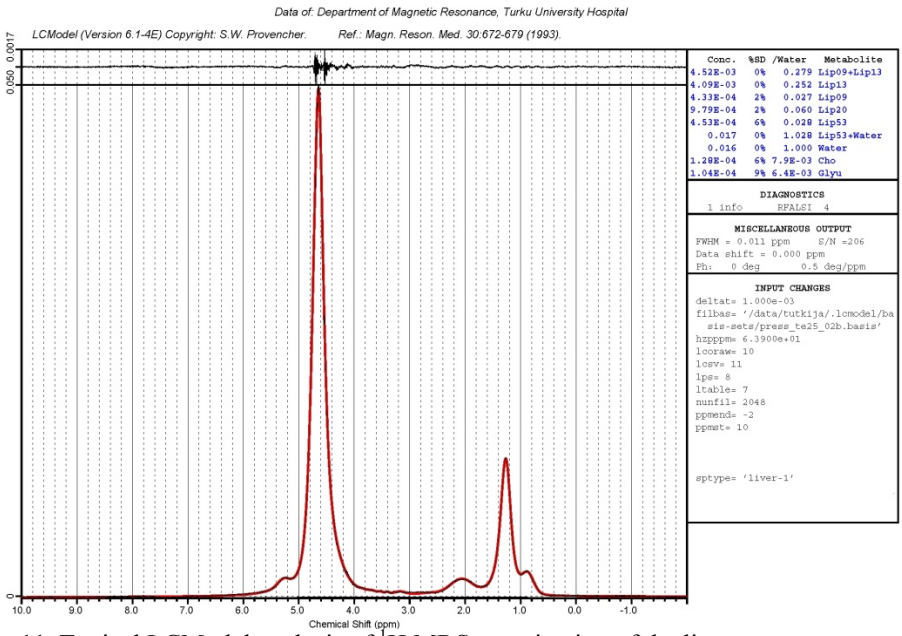

Figure 11. Typical LCModel analysis of ^{1}H MRS examination of the liver.

For the calculation of final liver fat content the concentrations in the LCModel output were corrected for differences in relaxation times, proton density and liver dry weight (see 9.1.5).

9.1.3 Validation of the method

9.1.3.1 ^{1}H MRS data acquisition

^{1}H MRS data was acquired on our GE 1.5 Tesla Signa Horizon LX system (substudy I, II and IV) using the automated single-voxel Proton Brain Exam (PROBE/SV). The PROBE/SV protocol, as mentioned in the name, was originally developed to enhance automation of ^{1}H MRS examinations of the brain. It consists of several routines which are combined to produce an optimal ^{1}H MRS examination in the shortest amount of time. The main steps regulated by PROBE/SV are shown in Figure 12.

The preparational steps involve the graphical selection of the ROI (voxel area) on an underlying MR image followed by automatic transmitter and receiver gain adjustment, determination of the center frequency, the highly importantly adjustment of the homogeneity of the magnetic field (shimming) for the x-, y- and z-axis direction and finally optimization of the water signal suppression.

During the following step of data acquisition ^{1}H MRS spectra are acquired using a Point Resolved Spectroscopy (PRESS) sequence with desired TR and TE. Finally, PROBE/SV saves the data, phases the spectrum according to the water peak and provides a preview of the Fourier transformed spectrum to the operator, allowing for assessment of the need to repeat the measurement.

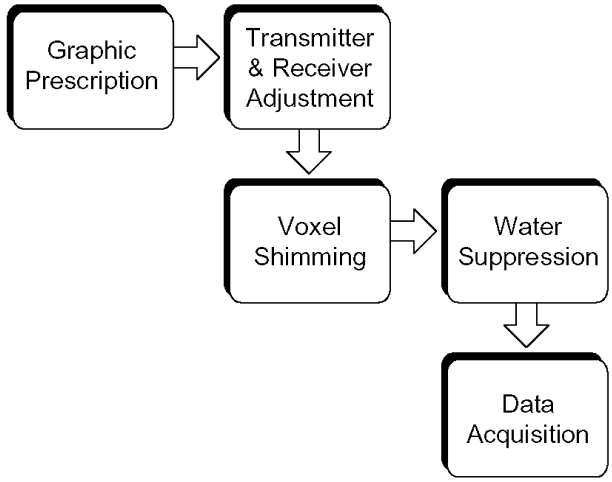

Figure 12. The main steps in the automated proton examination routine for single voxel ^{1}H MRS (PROBE/SV). (Adapted from: Kohler S, Signa Advantage PROBE/SV: Single-voxel Proton Brain Exam Applications Guide, Vol 5, General Electric Medical Systems, 1993)

We decided to use the PROBE/SV examination routine for obtaining ^{1}H MRS spectra of the liver, mainly for it contains time-saving automated steps and thus reduces patient examination time.

In substudy III, where ^{1}H MRS data was obtained with a 1.5 Tesla Philips system, a comparable PROBE/SV routine was not available and all above-mentioned steps were performed manually.

9.1.3.2 Validation experiments I – in vitro measurements

In order to assess the quality, linearity and sensitivity of the ^{1}H MRS measurements observed using PROBE/SV, the following two phantom and in vitro experiments were performed:

Experiment 1:

A ^{1}H MRS calibration-curve of different dilutions of sodium acetate.

Introduction

Sodium acetate solutions produce a very simple (single peak) spectrum and analysis of different dilutions provides information on both the sensitivity as well as the linearity of the ^{1}H MRS measurements.

Methods

Highly accurate solutions of sodium acetate (NaAc) were made by precise weighing of NaAc salt (Merck, Darmstadt, Germany) using a laboratory balance (Sartorius 2432, accuracy of 100 μg). In total 9 solutions ranging from 2.0% to 39.8% were created in acryl containers. The solution was doped with 0.17 mM $MnCl_2$ to reduce water T_1 relaxation times and to resemble liver T_1 as much as possible (approximately 600 ms).

From each solution ^{1}H MRS spectra using the PRESS PROBE/SV were obtained. Imaging parameters were the following: TR 3000 ms in all measurements and multiple TE's were used for each solution: 25 ms, 50 ms, 85 ms and 130 ms. An example of a spectrum acquired of sodium acetate is shown in Figure 13.

All spectra (water suppressed and unsuppressed) were analyzed with jMRUI, T_2 values and corrections for relaxation time and proton density were calculated.

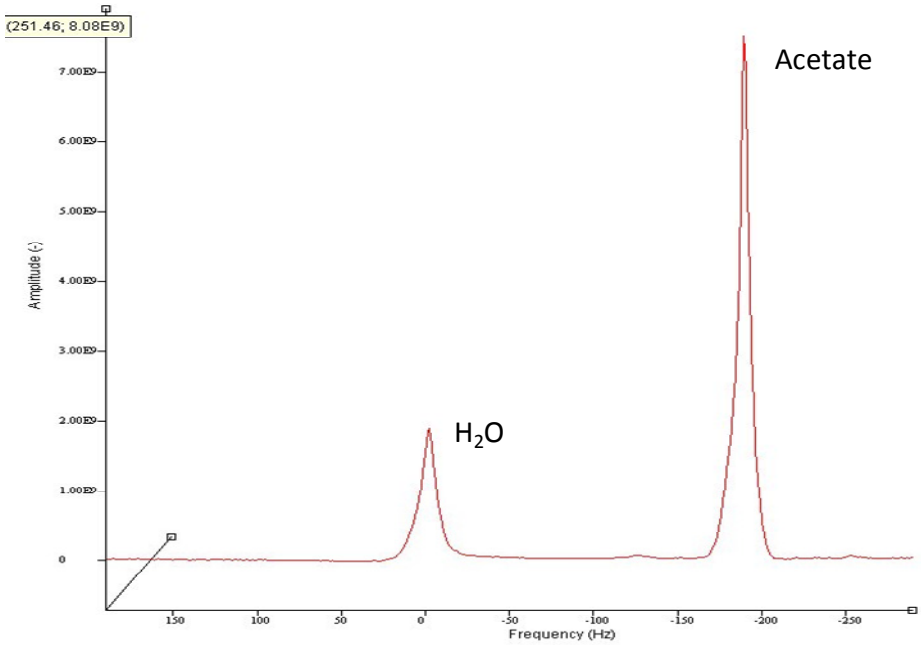

Figure 13. Typical spectrum of sodium acetate. Note the partially suppressed water peak.

Results

The ^{1}H MRS results correlated extremely well in a linear fashion, without detectible offset, with the measured mass-ratio's (r = 0.9995), as shown in Figure 14.

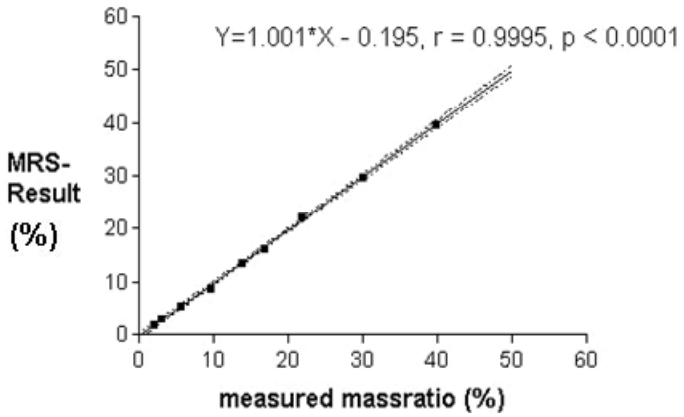

Figure 14. Correlation of measured NaAc massratios with MRS measurements.

Experiment 2:

Correlation of the fat percentage measured by ^{1}H MRS and chemical analysis in isolated pig-livers.

Introduction

This experiment aimed to provide information on the sensitivity of the PROBE/SV ^{1}H MRS method to detect liver fat content and to study the correlation of ^{1}H MRS findings with the actual fat content. In this way the in vivo situation was simulated as closely as possible.

Methods

A fresh pig-liver was obtained from a local shop and placed in a protective cup of polyethylene (PE) and covered by a thin plastic film. During positioning within the MR scanner, the build-in laser pin-pint cross was used as an aid to locate and mark the exact (isocenter) location on the plastic film covering the liver. The head coil and flexible coil was used as the receiving coil. Axial MR images were obtained and used to plan a single voxel ^{1}H MRS examination (Figure 15).

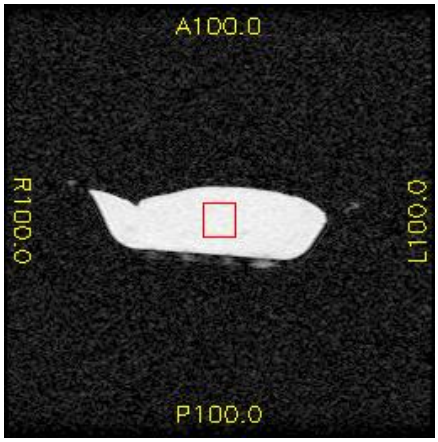

Figure 15. MR image of an isolated pig liver showing the ^{1}H MRS voxel position.

Imaging parameters were the following: TR 3000 ms, TE 25 ms, NOS 128, NEX 8 and voxel dimensions 20 x 14.8 x 15.2 mm (4.5 cm^3). In total this measurement was obtained for 8 individual locations / voxels within 4 individual livers. In addition, for each liver the identical measurement was performed, but with a variable TE of 35, 50, 70 and 100 ms in order to measure T2 of water and fat, respectively. Spectra were analyzed with jMRUI and the corrected liver fat content was calculated from the measured amplitudes as described in 9.1.5.

After the ^{1}H MRS experiment, markings on the liver, MR images and voxel dimensions were used to locate the original voxel location within the liver tissue. A tissue volume from the exact location of the ^{1}H MRS measurement was then removed and sent for laboratory analysis.

In the laboratory, water was removed from the tissue samples using a Hetosicc CD 52 Freeze Drier. From the remaining dry tissue, lipids were removed using petroleum ether (Analytical Reagent, 40-60ºC, Lab-Scan ltd.). The exact weight of the samples was registered between all steps using a Salter ER-182A electronic balance with an accuracy of 100 µg. Using the changes in weight between the individual steps, the water, fat and dry tissue masses were calculated for each sample.

Results

As expected, no statistical difference was observed (paired t-test, p=0.78) between the laboratory measurements of fat content (mean: 1.05 % ± 0.50) and the fat content measured by ^{1}H MRS (mean 1.10 % ± 0.24), thus showing (1) the functionality of the PRESS PROBE/SV protocol for ^{1}H MRS of the liver and (2) that the observed (corrected) values well reflect true liver fat content, even at very low lipid levels.

9.1.3.3 Validation experiments II – effects of breathing induced motion

To evaluate the possible effects of breathing motion on spectroscopy data acquired with our particular ^{1}H MRS sequence, a highly simplified phantom was constructed simulating breathing induced liver motion. A similar setup to experiment 2 (9.1.3.2) with the isolated pig-liver was chosen, but this time using the general purpose flex (GP-Flex) coil. An inflatable latex bag was placed under a pig liver placed in a protective cup of PE. The latex bag was connected to a long flexible plastic a tube, fed through an opening in the RF-cabin (Figure 16).

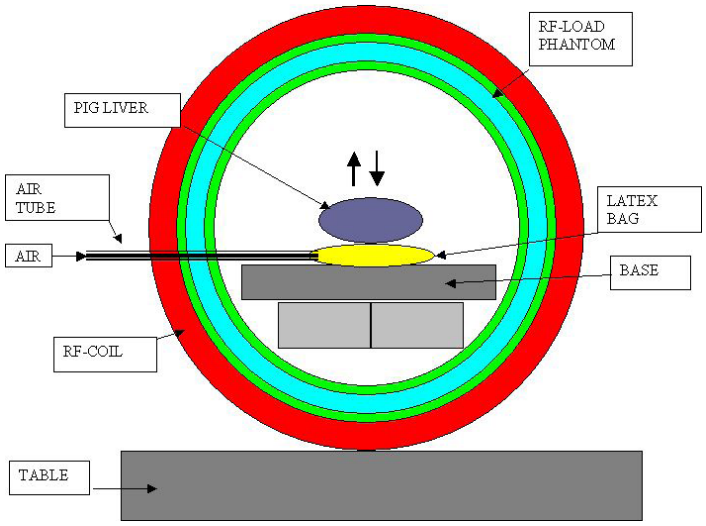

Figure 16. Schematic representation of a phantom to study the effects of breathing induced liver motion on ^{1}H MRS spectra.

This setup allowed for highly controlled and correctly timed motion of the liver phantom during spectroscopy data acquisition, by inflation and deflation of the latex bag.

The ^{1}H MRS voxel was placed in the liver identical to experiment 2 (9.1.3.2) and the following imaging parameters were used: TR 3000 ms, TE 25 ms, NOS 48, NEX 8 and voxel dimensions 25 x 20 x 19.9 mm (10 cm^{3}).

After baseline ^{1}H MRS acquisition (in rest), several scans were obtained with the liver phantom moving during water suppressed frames or water unsuppressed frames. The induced motion (approx 1-3 cm) was mostly in the anterior-posterior direction, and less in the other directions.

Comparison of the spectra acquired in rest and during motion showed no significant effect of (small amounts of) breathing motion on spectral quality or induced phase errors.

To gain further insight in the effects of possible breathing motion in vivo, the current validation experiment was expanded to an ^{1}H MRS examination of a healthy volunteer using identical imaging parameters. The effects of regular breathing, irregular breathing and breath hold on ^{1}H MRS spectral data were evaluated.

Severely (deep) irregular breathing induced phase errors and artifacts in both the water suppressed and unsuppressed frames, as expected, most likely due mechanical distortion of the (flexible) coil geometry (Star-Lack et al., 2000). However, also regular breathing motion was shown to affect spectral quality (Figure 17).

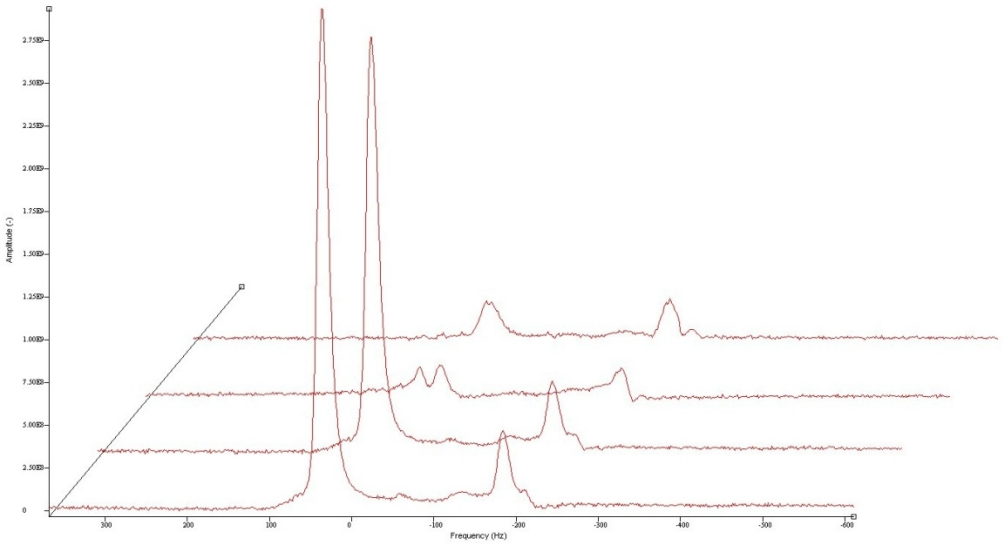

Figure 17. In vivo liver spectrum obtained in a healthy volunteer during breathing (first two frames) and breath hold (last two frames).

The level of water suppression was shown to be less powerful during breathing motion. In addition ^{1}H MRS spectra obtained during breathing motion showed slightly higher levels of fat, most likely due to increased spillover of subcutaneous and visceral fat signals outside of the voxel.

9.1.4 Development of in vivo protocol

The information obtained of the validation experiments was used to develop an optimal in vivo protocol. The main goal for the in vivo protocols was to obtain high quality liver spectra during an acceptable acquisition time. In addition, the protocol had to be applicable to all study subjects, including patients with a moderate to severe impaired physical condition (T2DM, obesity, coronary artery disease).

We decided to image all subjects by default in hospital garment to avoid any interference of possible metal within patient clothing with the magnetic field homogeneity, and thus spectral quality.

The linear general purpose flex (GP-Flex) coil used in the validation experiments was used as the receiving coil, mainly due to superior SNR compared to the internal body coil. The GP-Flex coil contains integrated Velcro straps, allowing for rigid positioning of the coil over the liver in patients with different abdominal circumference, without causing discomfort (Figure 18). In addition, a compression belt was used to reduce abdominal motion. The body coil was chosen as the transmitting coil for all acquired data.

Figure 18. GP-Flex linear surface coil. (© GE Medical Systems)

Since the validation experiments showed a clear effect of liver motion on spectral quality, we decided to incorporate two breath hold sessions during the ^{1}H MRS PROBE/SV data acquisition: one session during acquisition of a water unsuppressed signal and one during a water-suppressed signal. Simple breath hold techniques have previously proven highly effective in conventional MRI of the liver (Earls et al., 1999). Patients were asked to breathe in, breathe out and then breathe in halfway to obtain a long lasting and stable breath-hold without (undesirable) fluctuations in breath-hold level.

In order to give the patients enough time to recover after each breath-hold we constructed a sequence of in total 6 frames, thus resembling partly a multiple breath-hold averaging (MBA) method as used for liver imaging, resulting in improved data quality (Feinberg et

al., 1995;Star-Lack et al., 2000). The main advantage of acquisition of both water suppressed and unsuppressed data within a single acquisition is that shim settings and voxel location are identical, thus optimizing spectral data quality.

The number of scans (NOS) was set to 32, for the PROBE/SV sequence uses standard two unsuppressed water frames (NOS=16 when NEX=8), resulting in 32+16=48 signal acquisitions which are by default preceded by 4 dummy signals. The TR was set to 3000 ms as in the validation experiments, resulting in an imaging sequence of 52 x 3s = 156 seconds (2 minutes and 36 seconds, Figure 19). Only data acquired during breathold was used for analysis, all other data was disregarded in the final jMRUI analysis.

1	**2**	**3**	**4**	**5**	**6**	**7**	**8**	**9**	**10**	**11**	**12**	13
2:36	**2:33**	**2:30**	**2:27**	**2:24**	**2:21**	**2:18**	**2:15**	**2:12**	**2:09**	**2:06**	**2:03**	2:00
14	15	16	17	18	19	20	21	22	23	24	25	26
1:57	1:54	1:51	1:48	1:45	1:42	1:39	1:36	1:33	1:30	1:27	1:24	1:21
27	28	29	30	31	32	33	34	35	36	37	38	39
1:18	1:15	1:12	1:09	1:06	1:03	1:00	0:57	0:54	0:51	0:48	0:45	0:42
40	**41**	**42**	**43**	**44**	**45**	**46**	**47**	**48**	**49**	**50**	**51**	**52**
0:39	**0:36**	**0:33**	**0:30**	**0:27**	**0:24**	**0:21**	**0:18**	**0:15**	**0:12**	**0:09**	**0:06**	**0:03**

Figure 19. Overview of data acquisition timing. A total of 52 signals were obtained and patient breathold was ensured during the acquisition of a water suppressed spectrum (signal 5-12) and unsuppressed spectrum (signal 45-52).

The ^{1}H MRS voxel was positioned using axial in-out-phase images as described in detail in 9.2.1. In short, a voxel was placed in the right liver lobe carefully avoiding the area of the large vessels.

Before onset of research data acquisition, the above in vivo protocol for liver ^{1}H MRS was evaluated in ten healthy volunteers recruited from the local hospital staff (age 35±11 years). The protocol was found to be functional and to provide high quality spectra in all studied volunteers. ^{1}H MRS data was analyzed by jMRUI and corrected as described in 9.1.5.

In healthy subjects an average value of LFC of 1.65 % was observed, well below the upper limit for normal liver fat content of 5.56% (Szczepaniak et al., 2005). In addition to the developed breath-hold sequence, ^{1}H MRS was performed also without breath-hold using the body coil as both receiving and transmitting coil combined with longer data acquisition, since spectra obtained with the internal body coil were shown to be less sensitive to breathing induced liver motion in preliminary experiments. Surprisingly, body coil spectra were shown to be of fairly high quality and to provide results comparable to measurements performed with the GP-Flex coil (Borra et al.,

2003). Our preliminary findings were confirmed one year later by Schirmer et al. who showed, using an adapted breath-hold protocol, that on a GE Signa 3T MR-system ^{1}H MRS of the liver can be reliably performed by use of the internal body coil alone (Schirmer et al., 2004).

Final in vivo protocol

All subjects in the current study were studied using the breath-hold liver ^{1}H MRS protocol (TR 3000 ms, TE 25 ms) and surface coil as described above, since this combination was shown to provide high quality spectra in the shortest possible acquisition time on our MR-system.

9.1.5 Calculation of final liver fat content

In order for the ^{1}H MRS result to reflect true liver fat content the following three major corrections are needed:

1. Correction for (differences in) relaxation times.
   (Thomsen et al., 1994)
2. Correction for (differences in) proton density.
   (Szczepaniak et al., 1999)
3. Correction for liver (non-fat, non-water containing) dry weight.
   (Thomsen et al., 1994)

These corrections are discussed in detail below.

9.1.5.1 Correction for (differences in) relaxation times

The general formula for an observed MR-signal (magnetization) is the following:

$$M_{(TE,TR)} = M_0\left(1 - e^{-\frac{TR}{T_1}}\right)e^{-\frac{TE}{T_2}}$$

$M_{(TE,TR)}$ is the observed magnetization as a function of TE and TR, M_0 is the magnetization at time point t=0, TR is the used repetition time, TE the used echo time, and T_1 and T_2 the spin-lattice and spin-spin relaxation time of the substance observed. In the case of liver spectroscopy the above formula for both the water and fat signal have to be taken into account.

The following relaxation times were used in the present study (Table 2):

Table 2. Typical relaxation times for human liver tissue (Thomsen et al., 1994)

	T_1 relaxation time (ms)	T_2 relaxation time (ms)
Water	663	49
Fat	236	71

For the correction of spectroscopy data it is important to know for each component what the magnetization at time point t=0 (M_0) was, which reflects the true amount of protons (and in this way true total amount of water or fat).

As can be easily judged from the formula above, in case TR is very much longer than T_1 the formula can be reduced to:

$$M_{(TE)} = M_0 \cdot e^{-\frac{TE}{T_2}}$$

As TR is a parameter which can be set during imaging, a sufficiently long TR should be chosen in order to prevent T1 relaxation effects.

The function mentioned above was used as the fitting function and programmed in GraphPad Prism version 3.00 as Y=A*EXP-(X/B). M_o is obtained by extrapolation of the fitting curve. By fitting this function the T_2, and M_0 by extrapolation were obtained. An example of this method can be seen in Figure 20. The data is shown with the $M_{(TE)}$ extrapolated backwards from TE = 25 ms towards TE = 0 to obtain M_0.

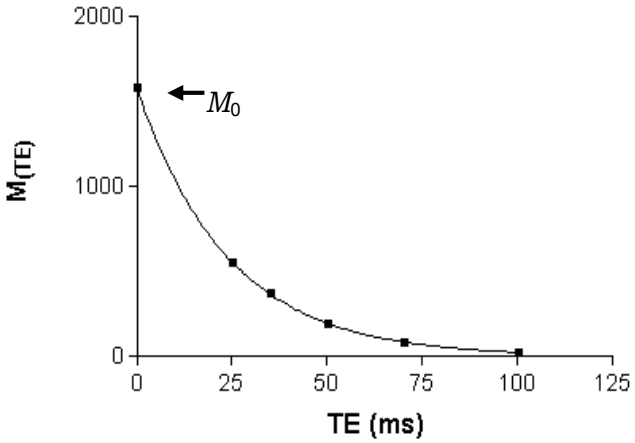

Figure 20. Fit of measured magnetization at different echo times (TE) to obtain the magnetization at timepoint 0 (M_0) by extrapolation.

For the calculation of the fat / water signal ratio, at a sufficiently long TR, the following formula can easily be deduced:

$$Fat_{(\%)} = \frac{S_{f(TE)}}{S_{w(TE)}} \cdot e^{TE\left(\frac{1}{T_2 f} - \frac{1}{T_2 w}\right)}$$

S_f and S_w are the observed MR signals amplitudes for fat and water at a certain TE and T_2f and T_2w the T_2 relaxation times for fat and water, respectively. When using the liver T_2 values from table 2, and TE = 25 ms as used in our study, a correction factor of 0.854 is found for the ratio of S_f and S_w.

9.1.5.2 Correction for (differences in) proton density

The signal observed in ^{1}H MRS originated from the protons (^{1}H) in the water and fat molecules. As can be easily observed from the illustration of a single water and fat molecule, the amount of protons (depicted by white hemispheres) within a single molecule is significantly larger in fat compared to water.

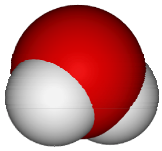

Water

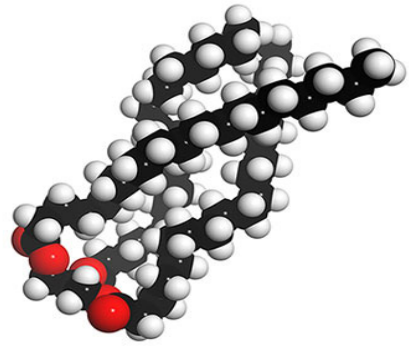

Triglyceride

Since our goal is to quantify the correct amount of water and fat *molecules* present within the tissue, correction of the raw signal is needed. Each water molecule always consist of two protons, the amount of protons within the triglyceride molecule depends on the lipid composition and the lengths of the individual fatty acid chains. In the current study the data obtained from the lipid composition of analysis of rabbits and dog livers was used (Szczepaniak et al., 1999). Using the average data on the lipid composition of rabbits and dogs an average correction term for the methylene (CH_2 including β-CH_2) and methyl (CH_3) resonances to water ratio of 1.26 was calculated.

9.1.5.3 Correction for liver (non-fat) dry weight

It is important to remember that the lipids observed with ^{1}H MRS solely involve the intracellular lipid droplets, so called “mobile lipids” (Szczepaniak et al., 1999)

In practice it is desirable for liver fat content measurement by ^{1}H MRS (fat / water ratio) to be comparable to liver fat content obtained by histological biopsy, which contains complete liver tissue. Therefore a correction for the non-fat containing and non-water containing (dry) tissue within the voxel volume has to be made. For a schematic illustration of this issue, please see below (Figure 21), showing the lipid droplets within the hepatocytes and the surrounding tissue containing mainly water and in addition (non-lipid) containing tissue.

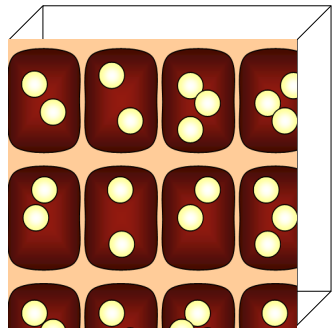

Figure 21. Schematic representation of voxel content, showing triglyceride lipid droplets within the hepatocytes.

To obtain an accurate estimate of fat per liver volume (fat % in this thesis) all matter contained within the voxel has to be accounted for. Taking into account the additional component of non-fat dry tissue, naturally decreases the liver fat % compared to the original value. Thomsen et al. have shown that the mean ratio of (non-fat dry weight)/(water) is 30/70**,** independent of the degree of fatty infiltration (Thomsen et al., 1994). Therefore, given that the non-fat dry weight of the liver relative to the water content is 0.30/0.70. This results in the following formula for total liver fat content (LFC) and thus fat percentage:

$$LFC_{(\%)} = \frac{(S_f)}{\left(S_f + S_w / 0.7\right)} \times 100$$

Where S_f and S_w are the observed MR signals amplitudes for fat and water respectively, each corrected for differences in relaxation time and proton density.

9.1.5.4 Combined correction factor for liver fat calculation

When combining the above formulae, final LFC (%) can be concisely calculated by multiplying the fat / water signal ratio (FW) in the ^{1}H MRS spectrum by 1.076 (relaxation time correction 0.854 times proton density correction 1.26) and substituting this result (FWcor) in the formula below:

$$LFC_{(\%)} = \frac{(FW_{Cor})}{(FW_{Cor} + 1.43)} \times 100$$

9.2. MAGNETIC RESONANCE IMAGING

9.2.1 In-Out-Phase Imaging (I-IV)

MR imaging of the liver was performed in all studies, in order to visualize the liver anatomy for spectroscopy planning and to evaluate the possibilities for assessment of liver fat content by imaging based methods.

Study I, II and IV

First a coronal scout image of the abdomen was obtained followed by transverse T1W dual-echo FSPGR (in-and-out-of-phase) imaging of the entire liver area during breath-hold using the internal body coil. Imaging parameters were: TR 150 ms, TE 2.1 ms (out-of-phase) and 4.4 ms (in-phase), flip angle 75°, slice thickness of 10 mm, intersection gap of 2 mm; matrix size 256 x 256, FOV 48 cm, acquisition time 23 seconds.

Study III

T1-weighted coronal, axial and saggital dual fast field echo (FFE) images were obtained covering the entire liver area using the internal quadrature body coil. Imaging parameters were the following: TR 120 ms, TE 2.3 ms (out-of-phase) and 4.6 ms (in-phase), flip angle 80°, slice thickness 10 mm without gap, matrix size 256 x 256, FOV 45 cm, acquisition time 22 seconds.

The obtained images were used to graphically indicate the (three dimensional) voxel location for the ^{1}H MRS examination (see 9.1.4) in the liver parenchyma outside the area of the great vessels. Nominal voxel dimensions were 30 x 30 x 30 mm (27 cm^{3}), but voxel dimensions were adjusted to avoid any visible vascular structures, also taking into account the effects of the chemical shift artifact on true voxel location. A typical location for the voxel is displayed in the T1W (out-of-phase) image with the corresponding spectrum of a patient with T2DM (Figure 22).

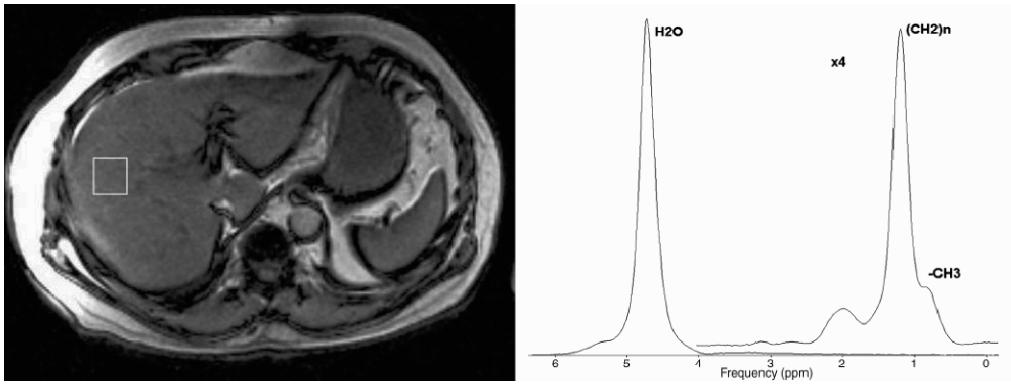

Figure 22. Typical voxel location for ^{1}H MRS and the corresponding spectrum. © Copyright RSNA, reproduced with permission.

In order to allow for reliable voxel re-positioning during a second visit exact voxel location (slice level) and dimensions were recorded numerically and graphically (screen capture). In addition this allowed for matched analysis of signal intensity (SI) of the entire voxel volume (see 9.2.2).

9.2.2 Analysis of in-and-out-of-phase images (IV)

Signal-intensity (SI) measurements of the in-phase and out-of-phase images were performed with a GE standard workstation (AW 3.1, GE Medical Systems, Milwaukee,

WI, USA). Regions of interest (ROI) were placed on the images to match the original size and location of the ^{1}H MRS voxel on three consecutive in-and-out-of-phase images, by using the recorded numerical and graphical information. Since the spectroscopy voxel dimension in the cranio-caudal direction was set to 30 mm, a voxel spanned approximately the 34 mm thickness of three in-and-out-of-phase images (3 x 10 mm slice and 2 x 2 mm intersection gap).

The SI for each ROI was recorded separately and in order to gather information from the entire ^{1}H MRS voxel volume an additional average SI was later calculated from the values of all three images. Furthermore, for the determination of image noise a standardized ROI (sized 62 x 62 mm) was placed outside the body area and the corresponding SI recorded (Figure 23).

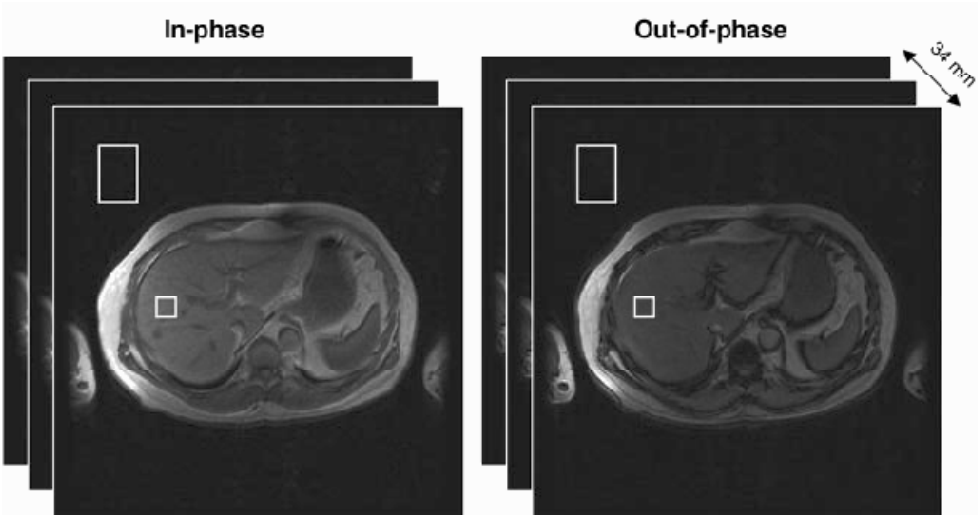

Figure 23. A typical in-phase and out-of-phase image of the liver and location of ROIs for SI measurements. © Copyright RSNA, reproduced with permission.

In addition to the SI measurements, the SI of liver tissue in ROI-areas of in-and-out-of-phase images was visually estimated by two experienced abdominal radiologists, without knowledge of the results of liver ^{1}H MRS measurements, SI measurements or patient information. Images were presented to the radiologists in a random order and the estimated SI difference between in-phase and out-of-phase-images was graded on a 5 point scale (Table 3).

Table 3. Grading system used by the radiologists.

Score	Description of *visually* observed signal intensities
-1	**In-phase** signal intensity **lower than out-of-phase**
0	**No difference** between in-phase and out-of-phase signal intensity
1	In-phase signal intensity mildly greater than out-of-phase signal intensity
2	In-phase signal intensity moderately greater than out-of-phase signal intensity
3	In-phase signal intensity markedly greater than out-of-phase signal intensity

Visual SI estimation and gradation was performed for each of all three consecutive slices for each subject. Final values were calculated as an average of the three estimated differences of in- and out-of-phase-images.

9.2.3 Calculation of fat indices from measured signal intensities (IV)

Using the measured SI of in-phase and out-of-phase images, fat indices (FI) were calculated using the following three formulas:

$$FI_1 = \frac{(SI_{in} - SI_{out})}{SI_{in}}$$ (Kawamitsu et al., 2003)

$$FI_2 = \frac{\left(SI_{in} / SI_{n-in} - SI_{out} / SI_{n-out} \right)}{SI_{in} / SI_{n-in}} \times 100$$ (Qayyum et al., 2005) *adapted*

$$FI_3 = SI_{in} - SI_{out}$$

SI_{in} represents the signal intensity measured from the in-phase and SI_{out} the signal intensity measured from the out-of-phase image. In the second formula $SI_{n\text{-}in}$ represents the measured signal intensity of the background noise in the in-phase image and $SI_{n\text{-}out}$ the noise in the out-of-phase image. The rationale behind this formula is to obtain a fat index independent of many sequence and image-embedded factors (e.g. receiver gain). In the third calculation the SI from the in-phase image is simply subtracted from the SI of the out-of-phase image.

9.2.4 Measurement of abdominal adipose tissue mass by MRI (I-III)

MR imaging was performed for the determination of abdominal tissue mass. An approach based on a single MR image was used at the level of the intervertebral disc L2-L3 (Abate et al., 1997).

Study I and II

First a saggital scout image of the spine was obtained to localize the intervertebral disc on the level of L2-L3. At this level a single axial T1W fast spin echo (FSE) image was obtained using the internal body coil. Imaging parameters were: TR 500 ms, TE 8.6 ms, echo train length (ETL) 4, slice thickness 10 mm, matrix size 256 x 256, FOV 48 cm, acquisition time 19 seconds. Images were analyzed using a GE standard workstation (AW 3.1, GE Medical Systems, Milwaukee, WI, USA).

Study III

At the level of the intervertebral disc L2-L3 a single axial T1W turbo spin echo (TSE) image was obtained using the internal quadrature body coil. Imaging parameters were: TR 500 ms, TE 13, ETL 4, slice thickness 10 mm, matrix size 256 x 256, FOV 53 cm,

acquisition time 16 seconds. Images were analyzed using a GE standard workstation (AW 4.3, GE Medical Systems, Milwaukee, WI, USA). On the workstation, using a free-hand drawing tool, the borders of the subcutaneous, retroperitoneal and visceral (or intraperitoneal) tissue compartments were outlined (Figure 24).

Figure 24. Typical analysis of abdominal adipose tissue compartments, showing the subcutaneous- (area 1 minus 2), retroperitoneal- (area 3 and 4) and visceral compartment (area 5).

In case of two individual visits identical (patient-specific) anatomical landmarks were used in the analysis and in this way a comparable analysis of the tissue compartments before and after intervention was ensured. Using the measured surface areas, slice thickness and adipose tissue density of 0.9196 g/ml (Abate et al., 1994) the weight of each individual compartment within the single slice was calculated. These masses were used to calculate the contribution to total abdominal tissue mass of each compartment, using the following formulas validated both in patients with and without T2DM (Abate et al., 1997):

Total subcutaneous abdominal adipose tissue mass (kg):
= 0.427 + 21 × subcutaneous abdominal adipose tissue mass at L2-L3

Total visceral (intraperitoneal) adipose tissue mass (kg):
= 0.181 + 16 × intraperitoneal adipose tissue mass at L2-L3

Total retroperitoneal adipose tissue mass (kg):
= 0.256 + 13 × retroperitoneal adipose tissue mass at L2-L3

9.3 POSITRON EMISSON TOMOGRAPY

9.3.1 Production of [^{15}O]H_2O (I)

For the production of [^{15}O], with a half life of 123 s, a low-energy deuteron accelerator Cyclone 3 (Ion Beam Application Inc., Louvain-la-Neuve, Belgium) was used. Using a dialysis technique [^{15}O]-water ([^{15}O]H_2O) was produced in a continuously working water module (Sipilä et al., 2001). To verify the purity of the product sterility and pyrogenity tests were performed. An approx. 97% radiochemical purity of the [^{15}O] was obtained.

9.3.2 Production of [^{18}F]FDG (I,II)

[^{18}F]FDG, with a half life of 110min, was synthesized using a modified method of Hamacher (Hamacher et al., 1986). The radiochemical purity exceeded 98%.

9.3.3 PET imaging and data corrections (I,II)

An eight-ring ECAT 931/08-12 scanner (Siemens/CTI Inc., Knoxville, TN, USA) with an axial resolution of 6.7 mm and in-plane resolution of 6.5 mm was used. All patients were imaged in a supine position. A rectilinear scan of both myocardium and liver was performed after a 5 minutes transmission scan for photon attenuation correction with a removable ring source containing ^{68}Ge. Two catheters were inserted, both in the antecubital vein, one for blood sampling and the other for tracer injection ([^{18}F]FDG / [^{15}O]H_2O) and infusion of insulin and glucose. To arterialize the venous blood in the arm for blood sampling a heating pad was used. Hepatic glucose uptake was measured during a hyperinsulinemic euglycemic clamp (DeFronzo et al., 1979). Insulin (Actrapid; Novo Nordisk, Copenhagen, Denmark) was infused at a constant rate of 1 mU/Kg/min and euglycemia (5 mmol/l) maintained by variable infusion of 20% glucose, depending on the plasma glucose concentration which was determined every 5-10 minutes. In addition, the levels of insulin and FFA were determined every 30 minutes and every 60 minutes, respectively.

In order to measure myocardial blood flow, dynamic imaging was performed at rest and after 60s from starting adenosine infusion (140 µg/kg/min) with imaging frames of 6x5 s, 6x15 s and 8x30 s, after an intravenous infusion of [^{15}O]H2O (1.3-1.5 GBq) over 2 minutes.

After [^{18}F]FDG injection the liver and myocardium were imaged during a 40 minutes dynamic scan with frames of 8x15, 2x30, 2x120, 1x180 and 6x300 seconds after which the femoral region was imaged during 5x240 seconds (Nuutila et al., 1992). To measure plasma and whole-blood [^{18}F]FDG radioactivity over time blood samples were drawn during the scanning. All obtained data was corrected for tissue attenuation, dead time and decay and reconstructed in a 128x128 matrix by a Bayesian (coefficient of 0.3) iterative reconstruction algorithm (Alenius and Ruotsalainen, 1997).

9.3.4 Calculation of hepatic, skeletal muscle and myocardial glucose uptake (I,II)

Hepatic, skeletal muscle and myocardial glucose uptake were measured by using a three-compartment model of [^{18}F]FDG kinetics (Sokoloff et al., 1977). Plasma and tissue time-activity curves were graphically analyzed to quantitate the fractional phosphorylation rate (K_i) of the tracer (Patlak and Blasberg, 1985).

Our imaging duration was selected such that tracer outflow from the hepatocyte could be neglected, and in this way measure solely HGU (Bender et al., 2001).

The rate of hepatic glucose uptake (HGU) was calculated as follows:

$$HGU = K_i \times \frac{[Glc]_p}{LC}$$

Where K_i represents the fractional rate of [^{18}F]FDG uptake and $[Glc]_p$ represents the plasma glucose level. An lumped constant (LC) of 1.0 was used (Iozzo et al., 2007). For calculation of skeletal muscle and myocardial glucose uptake an identical formula was used, with a LC in case of skeletal muscle of 1.2 (Peltoniemi et al., 2000) and in case of myocardium 1.0 was used (Ng et al., 1998).

Myocardial glucose uptake was analyzed with the MunichHeart Software (Nuklearmedizinische Klinik und Poliklinik der Technischen Universität München, Munich, Germany).

9.3.5 Calculation of whole-body insulin sensitivity (I,II)

Whole-body insulin sensitivity was calculated as previously described (DeFronzo et al., 1979). The metabolized glucose (M-value) was calculated according to the infusion speed of 20% glucose needed to maintain euglycemia during a primed and continuous infusion of insulin (1mU/kg/min, Actrapid; Novo Nordisk, Copenhagen, Denmark)

During the euglycemic hyperinsulinemic clamp skeletal muscle accounts for about 80% of the whole body GU, whereas the contribution of hepatic GU is less than 10%. (DeFronzo and Mandarino, 2003)

9.3.6 Calculation of regional myocardial blood flow (I)

Large regions of interest (ROI) were placed on representative transaxial slices to cover ischemic the non-ischemic regions. The ROIs drawn in the rest images were copied to the images obtained during adenosine-induced hyperemia. Myocardial blood flow was calculated by using single-compartment model (Iida et al., 1988;Iida et al., 1995). The arterial input function was obtained from the left ventricular time activity curve (Iida et al., 1992). This method corrects for the limited recovery of the left ventricular ROI and also for spillover from the signals originating from the myocardium. For calculation of coronary flow reserve (II) the hyperemic flow was divided by the flow at rest.

9.4 OTHER METHODS

9.4.1 Single-photon emission computed tomography (I)

Before the single-photon emission computed tomography (SPECT) study patients refrained from β-blockers, Ca-blockers and long-acting nitrates for 48 hours. A rest and stress SPECT study using ^{99m}Tc-Myoview®-tetrofosmin (Amersham plc, UK) were performed with an injection of 250MBq (1.5mSv) and 900MBq (5.36mSv), respectively. A VertexPlus EPIC^{TM} gamma camera (ADAC laboratories, Milpitas, CA, USA) was used for data acquisition 15-30 minutes after the injection.

9.4.2 Coronary angiography and echocardiography (I)

Coronary angiography was performed via the femoral artery, using a 5-Fr catheter (Cordis, Johnson & Johnson), after an intravenous injection of 3,750 IU of heparin and 0.5 mg of sublingual nitroglycerin. Images were calibrated with the catheter and coronary artery diameters were analyzed by a single operator using the QCA software (Quantcor stenosis evaluation software, Siemens, Munich, Germany).

Echocardiographic examination was performed at rest during insulin stimulation, after the completion of PET imaging, using an Acuson 128XP/10 ultrasound scanner (Acuson, Mountain View, CA). During this examination cardiac dimensions were measured and standard echocardiographic views of the left ventricle were obtained.

9.4.3 Classification of myocardial regions (I)

Using the SPECT, coronary angiography and echocardiography results ischemic and non-ischemic regions were determined in all subjects. Segments were classified as normal in case of normal wall motion on echocardiography, no reversible perfusion defect in SPECT and were associated with non-stenotic coronary artery. Segments were classified as ischemic in case of a wall motion abnormality (if any) in the area of the reversible perfusion defect in SPECT.

9.4.4 Biochemical analyses (I-IV)

Studies I,II and IV

Plasma glucose concentration was measured in the laboratory of the Turku PET Centre in duplicate using the glucose oxidase method (Analox GM7 or GM9 Analox Instruments Ltd., London, UK). All other laboratory samples of study I,II and IV, except the samples for the analysis of lipoprotein particles and inflammation, were sent by courier to a central laboratory (Quest Diagnostics UK Ltd, UK), where the concentration of total cholesterol, HDL cholesterol, triglycerides, HbA1c, fasting plasma glucose, fasting C-peptide, insulin and FFA were measured. Standard methods and quality control were performed at this laboratory. The LDL cholesterol concentration was calculated with the Friedewald formula (Friedewald et al., 1972). The concentrations of hsCRP, PAI-1 and soluble adhesion molecules were measured as

previously described (Laaksonen et al., 2002;Jarvisalo et al., 2002;Salmi et al., 2002;Metso et al., 2004). Serum adiponectin levels were measured using radioimmunoassay (Human adiponectin RIA Kit, Linco Research, St. Charles, Missouri, USA). Plasma radioactivity (I,II) was measured with an automatic gamma counter (Wizard 1480 3", Wallac, Turku, Finland).

Study III

All samples of study III were analyzed locally. Adipokine levels were determined by immunoassay using the LINCO*plex* kit (Luminex xMAP Technology). For measurement of hepatic growth factor Human Serum Adipokine Panel B was used. Human Serum Adipokine Panel A was used for analysis of adiponectin and total PAI-1 levels. Serum free fatty acid concentrations were measured fluorometrically (NEFA C, ACS-ACOD, Wako Chemicals GmbH, Neuss, Germany) and analyzed with a Roche Modular P800 automatic analyzer (Roche Diagnostics GmbH, Mannheim, Germany). Serum insulin was determined by an automated time-resolved immunofluorometric assay (AutoDELFIA, PerkinElmer Life and Analytical Sciences, Wallac Oy, Turku, Finland). Serum high-sensitivity C-reactive protein was analyzed with sandwich immunoassay method using an Innotrac Aio1 immunoanalyzer (Innotrac Diagnostic, Turku, Finland).

9.4.5 Statistical analysis

All data are reported as mean ± SD (study I, II and IV) or as mean ± SEM (Study III). In all studies two-tailed p-values were used and a p-value of < 0.05 was considered statistically significant.

In study I, to compare the variables between the groups an unpaired t-test was used in case of normally distributed data. Log-transformation or non-parametric Mann-Whitney-U test was performed in case of skewed variables. For proportion analysis in groups the Chi-square test was used. In case of normally distributed variables Pearson's correlation coefficient was calculated. For other selected variables Spearman's nonparametric rank correlation coefficients were calculated. Multiple linear regression analysis was performed in order to study the relationship between the liver fat content and the metabolic parameters.

In study II one-way ANOVA, and Kruskal-Wallis test in case of non-normal distributed variables, was used to compare LFC, HGU, glycemic control and metabolic characteristics between the healthy subjects and the patients with T2DM, and then between the Rosiglitazone and placebo groups. Unpaired t-tests were used to compare the other variables between the treatment groups. Student's paired t-test was used to compare the values between baseline and week 16 in each group. Pearson's correlation coefficients, or Spearman's correlation coefficients in case of non-normal distributed variables, were calculated for correlation analysis. In order to determine the role LFC in HGU values stepwise linear regression analysis was performed. To evaluate the differences in LFC and HGU between patients with T2DM and healthy controls a general linear model adjusting for BMI and age was used. A mixed model was used to

assess possible effects of gender on the results. Statistical analyses in these studies were performed with the SAS statistical analysis system version 8.2 (Cary, NC, USA).

In study III differences in paired data were evaluated using the Student's paired *t* test and the nonparametric Wilcoxon signed rank test. Regression analyses were carried out according to standard techniques. Statistical analysis in this study were performed using the StatView version 5.0 software (SAS institute inc. Cary, NC, USA)

In study IV Pearson's correlation was used to study the relationship between calculated fat indices from in-and-out-of-phase images, average radiologist estimates of SI changes and liver fat content measured by ^{1}H MRS. Differences between individual correlations were assessed using the statistical method suggested by Cohen & Cohen (Cohen and Cohen, 1983). Fisher r-to-Z transformation was used to assess possible differences in the correlations between male and female patients. To study the ability of FI(3) to correctly identify normal or increased LFC, Fischer's exact test was used. Kappa statistics were used to study the inter-radiologist agreement of subjective LFC estimates. The following definition of kappa was used: < 0.20 poor agreement, 0.20 - 0.40 fair agreement, 0.40 - 0.60 moderate agreement, 0.60 - 0.80 good agreement and 0.80 - 1.00 very good agreement. The data in this study were analyzed using the software packages GraphPad Prism 5.00, GraphPad Instat 3.05 (GraphPad Software, Inc., San Diego, CA) and SAS Version 9.1.3 SP4 (SAS Institute Inc, Cary, NC, USA).

10. RESULTS

10.1 High liver fat content as an independent risk factor for impaired myocardial metabolism (I)

Patient physical characteristics, CAD and myocardial perfusion

The groups of low (4.6 ± 2.0%; range 1.4–7.8%) and high liver fat (17.4 ± 8.0%; range 9.0–41.8%) were similar with respect to sex, age, BMI, and waist-to-hip ratio. Abdominal subcutaneous fat masses were not significantly different between the groups, but the amount of intra-abdominal (visceral) fat was increased in the high liver fat group compared with the low liver fat group (P = 0.009). The median of the degree of the main stenotic lesion was 60% (range 9–100%) with no significant difference between the groups. No statistical difference was found between the groups in left ventricular ejection fraction (66 ± 6 vs. 62 ± 7%, low liver fat and high liver fat group, respectively). With coronary flow reserve (CFR) used as an indicator of endothelial function, in patients with fatty liver it was found to be 28% lower, thus indicating more severe coronary dysfunction in these patients. In the pooled population, liver fat content was correlated negatively with CFR (r = –0.38, P = 0.020).

Glucose and lipid metabolism

Fasting plasma glucose and insulin levels were similar between the groups, but Hb A_{1c} (P = 0.08) tended to be, and fasting serum C-peptide levels (P = 0.001) were higher in the high liver fat group compared with the low liver fat group.

Serum insulin levels and steady-state plasma glucose did not differ between the groups during intravenously maintained hyperinsulinemia, (426.3 ± 58.0 vs. 449.1 ± 67.3 pmol/l, P = NS) and (5.1 ± 0.3 vs. 5.4 ± 0.5 mmol/l, P = NS), respectively. However, whole body insulin sensitivity was 24% (10.2 ± 3.8 vs. 13.4 ± 5.3 $\mu mol \cdot kg^{-1} \cdot min^{-1}$, P = 0.012) and skeletal muscle glucose uptake was 37% (15.2+7.4 vs. 24.3+11.9 $\mu mol \cdot kg^{-1} \cdot min^{-1}$, P = 0.002) lower in the high fat group compared with the low fat group. Also myocardial glucose uptake was significantly impaired in patients with fatty liver (P = 0.040). Furthermore, myocardial glucose extraction rate was significantly impaired in the high-fat group compared with the low-fat group (P = 0.0006). In the whole population, there was a significant inverse correlation between myocardial glucose uptake and FFA concentration during clamp (r = –0.39, P = 0.003).

Serum total cholesterol, triglycerides, and LDL and HDL cholesterol did not differ between the groups. Fasting FFA concentrations were similar in both groups, but patients with fatty liver showed a significantly higher level of circulating FFA during the clamp than patients with low liver fat content (0.12 ± 0.06 vs. 0.18 ± 0.07 mmol/l, P = 0.001).

Liver enzymes and inflammation markers

In both groups, the liver enzymes were within normal range (serum alanine transaminase <42 U/liter and serum γ-glutamyltransferase <65 U/liter); however, they were slightly but significantly higher in the high liver fat group compared with the low liver fat group. Patients with high liver fat content had significantly increased hsCRP level compared with the patients with low liver fat content. Homocysteine and plasminogen activator inhibitor-1 (PAI-1) tended to be higher in the high liver fat group. The levels of soluble intercellular adhesion molecule-1 (ICAM-1) and E-selectin, as well as soluble vascular adhesion protein-1 (VAP-1) molecules, were increased in patients with fatty liver.

Relation between hepatic fat content and myocardial metabolic mediators

Liver fat content was inversely associated with whole body glucose uptake ($r = –0.50$, $P < 0.0001$), skeletal muscle glucose uptake ($r = –0.36$, $P = 0.007$), myocardial glucose uptake ($r = –0.47$, $P = 0.0003$) (Figure 25) and positively correlated with FFA levels during clamp ($r = 0.45$, $P = 0.0007$).

To examine the relation between liver fat, myocardial insulin resistance, and measurements of obesity, simple and multiple linear regression analyses were employed. In simple regression analyses, liver fat content was correlated with BMI ($r = 0.38$, $P = 0.005$), waist circumference ($r = 0.38$, $P = 0.005$), and visceral fat mass ($r = 0.31$, $P = 0.021$), but no association was found between liver fat and HbA_{1c}, fasting plasma glucose, subcutaneous fat mass, or waist-to-hip ratio.

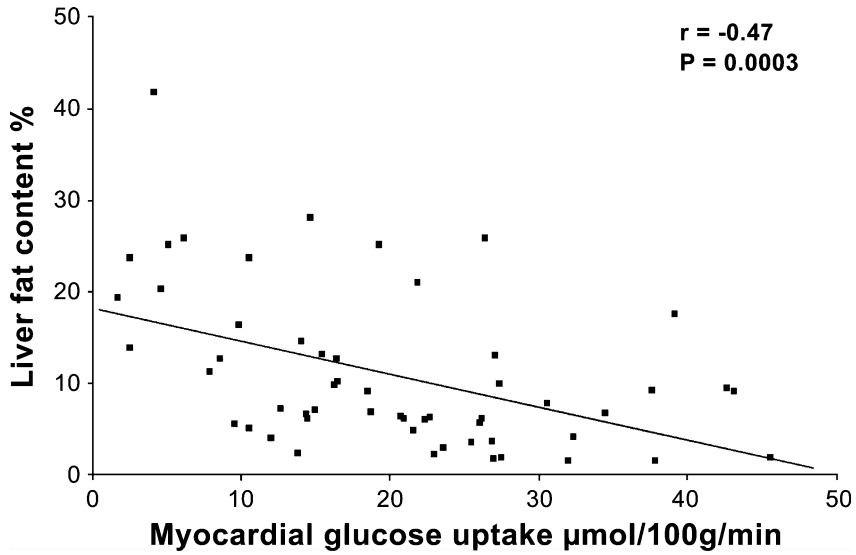

Figure 25. Liver fat content is strongly inversely correlated with myocardial glucose uptake.

To determine the role of liver fat content in myocardial metabolism, multiple regression analysis controlling for variables that showed significant correlation with

myocardial metabolism was performed. Only liver fat content ($P = 0.016$) and whole body glucose uptake ($P = 0.006$) were significant determinants of myocardial glucose uptake. Whole body glucose uptake was significantly correlated with myocardial glucose uptake ($r = 0.41$, $P = 0.002$); however, when liver fat content was used as a covariate, the association was no longer significant ($P = 0.06$). Finally, only liver fat remained a significant factor in a more specific multiple regression analysis model, with independent variables that directly affect myocardial metabolism.

10.2 Association between liver fat content and hepatic glucose uptake (II)

Liver fat content and hepatic glucose uptake in healthy subjects and patients with T2DM

Diabetic patients had poorer glycemic control compared to healthy subjects (Table 4). Whole body insulin sensitivity (p=0.012) was significantly lower in diabetic patients as compared to healthy subjects. LFC was significantly higher in patients with T2DM than in healthy subjects (p=0.0005, Table 4). Hepatic glucose uptake was significantly decreased in diabetic patients compared to controls (p=0.008). These differences in LFC (p=0.012) but not in hepatic glucose uptake (p=0.11) remained significant when correcting for differences in age and BMI between patients with T2DM and controls.

Table 4. Study subjects characteristics (II).

	Diabetic patients (n=54)	Healthy subjects (n=8)	P-Value
Demography			
Gender (M/F)	38/16	8/0	
Age (yr)	63.6±7.5	54.0±9.6	0.002
Metabolic characteristics			
BMI (kg/m^2)	29.6±4.1	26.4±2.6	0.037
HbA_{1c} (%)	7.2±0.9	5.2±0.3	< 0.0001
C-peptide (nmol/L)	0.84±0.32	0.59±0.14	0.012
F-NEFA (mmol/L)	0.77±0.3	0.24±0.3	< 0.0001
Total Cholesterol (mmol/L)	4.43±0.77	5.68±0.97	< 0.0001
Triglycerides (mmol/L)	1.8±0.9	1.3±0.5	0.15
LDL-Cholesterol (mmol/L)	2.51±0.68	3.85±0.95	< 0.0001
HDL-Cholesterol (mmol/L)	1.12±0.29	1.23±0.21	0.32
F-Insulin (pmol/L)	51.0±30.0	38.3±18.7	0.25
Alanine aminotransferase (ALAT) (U/l)	25.6±11.8	42.3±28.6	0.10
γ-glutamyl transferase (GT) (U/l)	36.6±35.13	49.4±38	0.14
Liver fat (%)	10.9±9.2	2.5±1.4	0.0005
Hepatic Glucose Uptake ($\mu mol \cdot kg^{-1} \cdot min^{-1}$)	24.5±14.2	35.6±9.7	0.008
Whole Body Glucose Uptake ($\mu mol \cdot kg^{-1} \cdot min^{-1}$)	11.9±5.1	16.0±4.1	0.037
Subcutaneous fat mass (kg)	3.9±1.4	3.1±0.9	0.12
Visceral fat mass (kg)	2.4±0.9	1.6±0.6	0.019
Retroperitoneal fat mass (kg)	1.4±0.6	1.0±0.2	0.002

Associations between liver fat content and hepatic glucose uptake

Liver fat content was significantly and inversely associated with hepatic glucose uptake in diabetic patients (r=-0.31, p=0.025, Figure 26) but not significantly in the smaller group of healthy subjects (r=-0.6460, p=0.08).

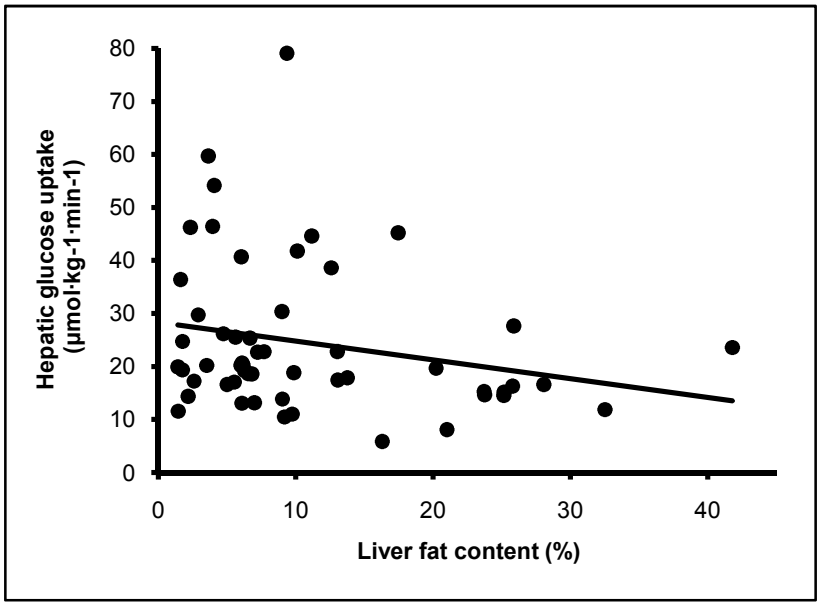

Figure 26. Liver fat content was significantly correlated with hepatic insulin stimulated glucose uptake.

In concert with that, LFC showed highly significant inverse correlations with the whole body glucose uptake (r=-0.47, p=0.0004) in diabetic patients but not in healthy subjects. The observed relationship between LFC and hepatic glucose uptake was identical for both sexes (p=0.53). LFC was significantly correlated to visceral fat-mass measured by MRI in patients with T2DM (r=0.34, p=0.013) and in healthy controls (r=0.77, p=0.02). Furthermore LFC was significantly associated with retroperitoneal fat mass (r=0.30, p=0.032), BMI (r=0.36, p=0.008), triglyceride levels (r=0.36, p=0.009), non-esterified fatty acids (NEFA) levels during clamp (r=0.45, P=0.0008), adiponectin levels (r=-0.48, p= 0.0004), c-peptide levels (r=0.42, p=0.002) and age (r=-0.34, p=0.015) in T2DM patients. Finally LFC was significantly associated to alanine aminotransferase (r=0.37, p=0.007) and γ-glutamyl transferase (r=0.29, p=0.040) in patients with T2DM. By using stepwise linear regression with the model including all these parameters, LFC was best explained by whole body glucose uptake (M-value) (p=0.0009) and adiponectin levels (p=0.016).

HGU was inversely associated with fasting c-peptide (r=-0.31 p=0.026), fasting insulin level (r=-0.35, p=0.01), subcutaneous fat mass (r=-0.33, p=0.0140) and BMI (r=-0.27, p=0.045) in T2DM patients. Using stepwise multiple regression analysis of significantly associated parameters, fasting insulin level was the strongest contributing factor to hepatic glucose uptake in T2DM (p=0.017).

10.3 The effects of Rosiglitazone treatment on liver metabolism (II)

Effects of Rosiglitazone in T2DM patients

The groups were well matched for fasting plasma glucose, c-peptide and for insulin levels at the time of randomization (Table 5). Rosiglitazone significantly improved glycemic control compared to placebo. Effects of Rosiglitazone on lipid profile were published separately by our group (Lautamaki et al., 2006b) and are therefore not include here. During hyperinsulinemia steady state plasma glucose concentrations were similar between the groups at baseline and at week 16. Serum NEFA concentrations (p=0.04 vs. baseline, p=0.014 vs. placebo) and insulin levels decreased during the clamp in the Rosiglitazone group (p=0.004 vs. baseline, p=0.006 vs. placebo). The whole-body glucose uptake (p<0.0001) increased in the Rosiglitazone group as compared to the placebo group. Rosiglitazone increased hepatic glucose uptake by 29.2% (p=0.013 vs. placebo). No changes occurred in placebo group.

Table 5. Metabolic data of patients with T2DM and effects of Rosiglitazone (© Elsevier Inc., 2008).

	Baseline		After 16 wk		P^a
	Placebo	Rosiglitazone	Placebo	Rosiglitazone	
At fast					
Plasma glucose (mmol/L)	7.7 ± 1.7	7.3 ± 2.0	8.1 ± 2.3	6.0 ± 1.1	<.0001
HbA_{1c} (%)	7.1 ± 0.9	7.3 ± 0.9	7.3 ± 1.0	6.9 ± 0.6	<.0001
Serum insulin (pmol/L)	53 ± 26	49 ± 34	56 ± 36	34 ± 17	.003
Serum NEFAs (mmol/L)	0.81 ± 0.3	0.73 ± 0.2	0.80 ± 0.3	0.67 ± 0.2	NS
Total cholesterol (mmol/L)	4.68 ± 0.8	4.19 ± 0.67	4.70 ± 0.88	4.70 ± 0.88	.014
Triglycerides (mmol/L)	1.9 ± 1.0	1.7 ± 0.8	1.8 ± 1.0	1.7 ± 1.2	NS
LDL cholesterol (mmol/L)	2.67 ± 0.73	2.35 ± 0.61	2.68 ± 0.67	2.61 ± 1.0	.015
HDL cholesterol (mmol/L)	1.17 ± 0.35	1.07 ± 0.2	1.18 ± 0.35	1.14 ± 0.25	.051
Serum C-peptide (nmol/L)	0.87 ± 0.3	0.82 ± 0.3	0.85 ± 0.4	0.69 ± 0.2	NS
Adiponectin (μg/mL)	7.2 ± 4.4	7.2 ± 2.6	7.4 ± 3.9	19.0 ± 7.9	<.0001
During hyperinsulinemia					
Plasma glucose (mmol/L)	5.24 ± 0.53	5.28 ± 0.42	5.36 ± 0.75	5.23 ± 0.36	NS
Serum insulin (pmol/L)	439 ± 88	440 ± 78	441 ± 76	405 ± 66	.006
Serum NEFAs (mmol/L)	0.16 ± 0.08	0.14 ± 0.06	0.15 ± 0.06	0.10 ± 0.06	.014
Whole-body glucose uptake (μmol/[kg·min])	11.5 ± 4.2	12.3 ± 6.0	12.0 ± 5.5	17.8 ± 6.8	<.0001
HGU (μmol/[kg·min])	25.2 ± 11.2	23.8 ± 16.9	25.4 ± 11.2	33.6 ± 21.3	.013
^1H *MRS and MRI*					
Liver fat (%)	10.1 ± 8.0	11.7 ± 10.4	9.8 ± 8.2	8.8 ± 10.2	.010
Subcutaneous fat mass (kg)	3.92 ± 1.4	3.87 ± 1.4	3.94 ± 1.3	4.12 ± 1.4	NS
Visceral fat mass (kg)	2.42 ± 0.8	2.42 ± 1.0	2.46 ± 0.8	2.32 ± 1.0	NS
Retroperitoneal fat mass (kg)	1.39 ± 0.5	1.40 ± 0.7	1.39 ± 0.5	1.44 ± 0.7	NS

NS indicates not significant.

[a] Change in rosiglitazone group vs change in placebo group.

Rosiglitazone significantly reduced liver fat content by 24.8 % (p=0.010 vs. placebo, Table 5). Subcutaneous fat mass, visceral fat mass and retroperitoneal fat mass did not change versus placebo. However within the Rosiglitazone group a trend of increase in subcutaneous fat mass (p=0.068) and a decrease of visceral fat mass was observed (p=0.175). The overall response to treatment was identical for men and women concerning both the decrease in LFC (p=0.81) as the increase in HGU (p=0.83).

Stepwise multiple regression analysis, with the model including all significantly associated parameters, was used to explain the changes in LFC and hepatic glucose uptake in the Rosiglitazone group. The increase in suppression of NEFA levels during clamp (p=0.0002) and increase of HbA1c levels (p=0.034) best explained the decrease LFC. Improvement in hepatic glucose uptake was best correlated with increase in HDL levels (p=0.002).

10.4 Effects of Trimetazidine on metabolism and liver fat content (III)

The group included four male and five female subjects (age 54±3 years). By selection, all patients had body mass index in the obesity range (median 30±1, range 27-38 kg/m^2). Calorie intake was 2070±201 and 2560±406 kcal/day, at baseline and end of treatment, respectively (ns). Dietary composition in the whole group did not vary significantly, and consisted of 48±3% *vs.* 54±3% carbohydrates, 33±4% *vs.* 26±3% fats, and 18±2% *vs.* 17±2% proteins, before and after treatment, respectively (ns). Out of all, only one subject increased his dietary fat intake during the treatment period as to double circulating triglycerides, and to increase body weight by 1.5 kg, and this patient was the outlier in treatment responses (*see below*). The effects of Trimetazidine on metabolic variables are given in Table 6.

The drug selectively reduced liver related markers. Liver enzymes were significantly lowered by the treatment. No change in abdominal visceral and subcutaneous fat masses was observed. The assessment of adiponectin was not available in one subject after treatment, due to technical reasons; in eight patients, Trimetazidine did not affect circulating adiponectin levels. Hepatic triglyceride content and fibro-inflammatory scores (calculated using ASAT, adiponectin, age, sex and triglycerides (Cancello et al., 2006) were decreased in most, but one outlying subject, corresponding to the patient with a higher dietary fat intake, as described above (Table 6, Figure 27). A representative example of MRS spectra and MR images of abdominal fat masses in one study patient before and after Trimetazidine treatment is given in Figure 27A-B. Individual changes in liver fat content and fibro-inflammatory scores are shown in Figure 27C. According to a literature-based cutoff of 5.56%, (Szczepaniak et al., 2005) approximately half of the subjects had liver steatosis at inclusion, and a positive correlation was observed between baseline values and Trimetazidine-induced decrements in liver fat content (Figure 27C), indicating that a more favorable response in terms of liver triglyceride deposition could be obtained in patients with organ steatosis.

Table 6. Characteristics of subjects and effect of treatment.

	Baseline	Trimetazidine	*% Change*	*P value*
f-glucose (mmol/L)	5.2±0.1	5.4±0.2	+5%	0.17
f-Insulin (mmol/L)	49±9	48±9	-8%	0.79
HbA_{1c} (%) §	5.6±0.1	5.5±0.1	**-3%**	**0.064**
f-Tg (mmol/L)	1.8±0.3	2.0±0.6	-1%	0.57
f-FFA (mmol/L)	0.62±0.05	0.68±0.04	+10%	0.23
CRP §	1.44±0.37	1.30±0.21	-6%	0.56
ALAT (IU/L)	**28±3**	**23±2**	**-26%**	**0.018**
ASAT (IU/L)	**26±2**	**24±1**	**-10%**	**0.046**
γ-GT (IU/L)	**22±3**	**19±2**	**-17%**	**0.084**
Adiponectin (μg/L) §	22.0±3.0	20.9±3.7	-5%	0.48*
PAI-1 (μg/L)	56±4	47±3	-11%	0.19
Hepatic growth factor (μg/L)	0.54±0.10	0.54±0.10	+1%	0.80
Hepatic insulin sensitivity index	0.13±0.03	0.11±0.02	-6%	0.35
Liver triglyceride content (%)	**8.3±2.6**	**6.3±2.3**	**-44%**	**0.015***
Visceral fat mass (kg)	1.70±0.22	1.71±0.21	+1%	0.87
Retroperitoneal fat mass (kg)	0.95±0.14	0.94±0.13	+1%	0.73
Subcutaneous fat mass (kg)	4.77±0.54	4.77±0.52	0%	0.99

§Data available in eight paired examinations; *non-parametric paired testing

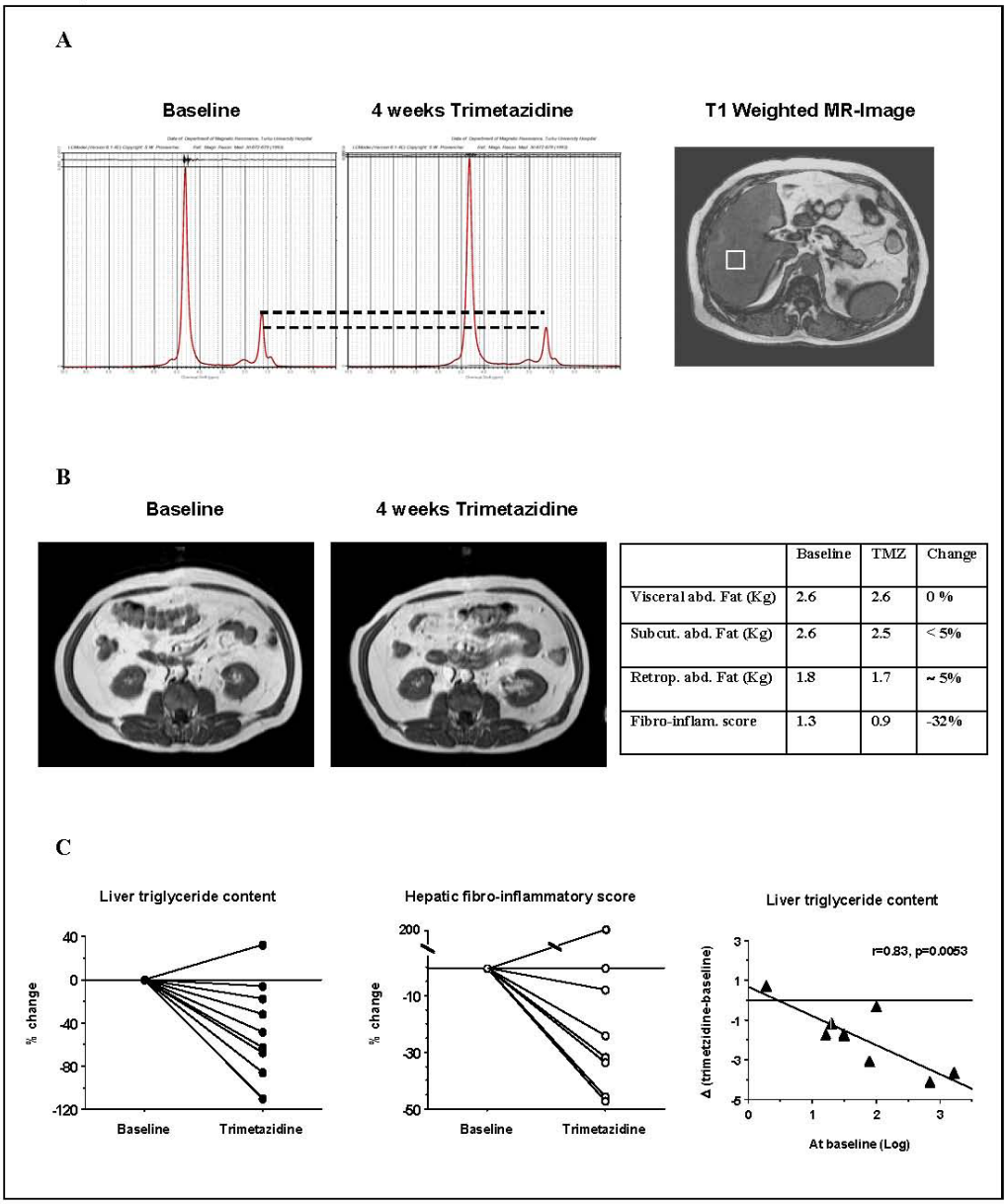

	Baseline	TMZ	Change
Visceral abd. Fat (Kg)	2.6	2.6	0 %
Subcut. abd. Fat (Kg)	2.6	2.5	< 5%
Retrop. abd. Fat (Kg)	1.8	1.7	~ 5%
Fibro-inflam. score	1.3	0.9	-32%

Figure 27. Typical results for a patient participating in substudy III showing A: Reduced LFC as measured by 1H MRS, B: No change in abdominal adipose tissue masses C: Trimetazidine reduces liver fat content (LFC) and fibroinflammatory score and the higher LFC at baseline, the larger the reduction in LFC during Trimetazidine treatment.

10.5 Association between ^{1}H MRS and in-and-out-phase imaging (IV)

Liver fat content measured by ^{1}H MRS ranged from 0.53 to 43.64%. A significant linear correlation was observed between liver fat % measured by ^{1}H MRS and all three fat indices calculated from the in-and-out-of-phase images. The correlation using FI(1)

was slightly stronger ($P<0.001$, $r=0.962$) compared to the correlations using FI(2) ($P<0.001$, $r=0.959$) and FI(3) ($P<0.001$, $r=0.943$) (Figure 28), however no statistical difference was observed (FI(1) vs. FI(2) $p=0.65$, FI(1) vs. FI(3) $p=0.09$, and FI(2) vs. FI(3) $p=0.17$). Similar statistical results were observed for separate correlations with only male or female patients ($p=0.30$). Fat indices calculated using measurements from a single (middle) slice or using an average value of all three slices also provided similar results.

10.6 Assessment of liver fat content by in-and-out-phase imaging (IV)

Using the simplest method to calculate the fat index, FI(3), an intercept of the regression line with the x-axis was observed at 5.1% (Figure 28), comparable to the upper limit for normal LFC measured by ^{1}H MRS or chemical analysis (Kwiterovich, Jr. et al., 1970;Szczepaniak et al., 2005). In other words, if SI_{in}-SI_{out} was negative, liver fat content was normal and if SI_{in}-SI_{out} was positive, liver fat was above the normal value. The contingency table (Table 7) shows the ability of in-and-out-of-phase imaging to correctly identify liver fat below or over 5.1%. Fischer's exact test was highly significant ($p<0.0001$) and a sensitivity of 95% and specificity of 98% was obtained.

A good degree of agreement between the estimates of SI changes by both radiologists was observed (weighted kappa=0.73). Despite displaying a significant relationship ($p<0.001$, $r=0.88$, Figure 28), the average estimates by the radiologists correlated significantly worse with liver fat % measured by ^{1}H MRS than all three fat indexes calculated from in-and-out-of-phase images ($p<0.0001$, $p<0.0001$ and $p=0.004$ for FI(1), FI(2) and FI(3), respectively).

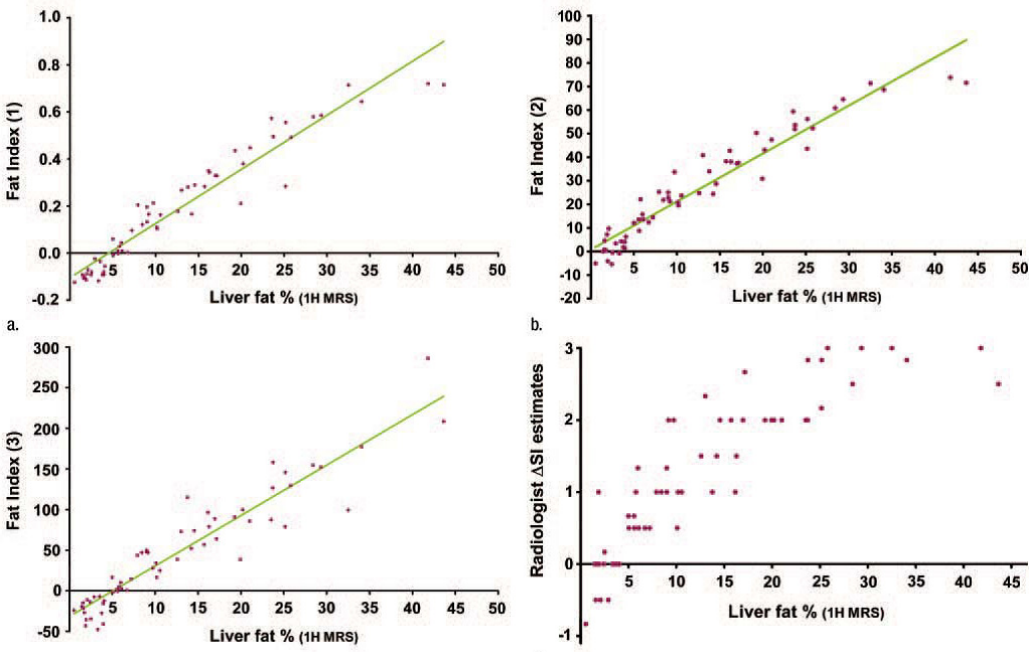

Figure 28. Correlations of liver fat measurements by ^{1}H MRS with fat indices (a) FI(1) (P<0.001, r=0.962), (b) FI(2) (P<0.001, r=0.959), (c) FI(3) (P<0.001, r=0.943) and (d) radiologist estimates of SI changes (p<0.001, r=0.88). © Copyright RSNA, Reproduced with permission.

Table 7. Contingency table for the ability of FI(3) to identify liver fat below or over 5.1%.

SI_{in}-SI_{out} (Total 61 examinations)	<0 (Negative)	>0 (Positive)	Total
Liver fat < 5.1%	18	1	19
Liver fat > 5.1%	1	41	42
Total	19	42	61

Fischer's exact test: P<0.0001
Sensitivity: = 94.7 %
Specificity: = 97.6 %

11. DISCUSSION

11.1 Role of magnetic resonance spectroscopy in the detection of NAFLD

In this study a fast ^{1}H MRS protocol for measurement of LFC was developed and applied in a study population of patients with T2DM and obesity. The safe, and robust measurement of LFC by ^{1}H MRS with our protocol proved to be well tolerated by the patient population and can therefore be regarded superior to other non-invasive methods such as CT and US (see: 6.3.1). Furthermore, due the robust protocol, it has the potential to be applied for the measurement of LFC in children.

This study emphasized that one of the additional benefits of ^{1}H MRS is the (almost obligatory) combination with MRI, allowing for simultaneous assessment of whole liver anatomy and an estimation of LFC using in-out-phase imaging (see 11.4). However, compared to imaging techniques, ^{1}H MRS has the benefit of producing absolute LFC values comparable to the traditional liver biopsy, making the measurements useful in the treatment of patients with NAFLD and their underlying diseases in an interdisciplinary team.

In addition, the previously mentioned technique of Magnetic Resonance Elastography (MRE) (Huwart and van Beers, 2008) providing information on the viscoelastic properties of the liver could extend the value of ^{1}H MRS. In case future studies show that MRE is a useful and reliable technique to estimate liver fibroses, the combination with ^{1}H MRS would even further strengthen the position of ^{1}H MRS and MRI as *the* non-invasive gold standard for LFC measurement.

Despite all the positive aspects of ^{1}H MRS, its use in clinical practice is currently likely to remain at a relatively low level due to high costs and low availability. Especially data-analysis using (free) software packages like jMRUI requires a certain level of skill and training, and this reduces the speed of clinical implementation of this technique. However, due to the increased demand for LFC measurements in the coming decade, implementation of automated routines by MR device manufactures is expected.

11.2 Liver fat content as a marker for whole body metabolic health (I)

The novel finding of the current study, that liver fat content is an independent mediator of myocardial glucose uptake in patients with type 2 diabetes, is well in line with a recent review suggesting that NAFLD is a major player in the development and progression of CVD (Loria et al., 2008). A new concept of “liver-vessel axis” was proposed, where it is hypothesized that atherosclerosis and NAFLD share similar biological precursors which effect the development and progression of both. This hypothesis of a common pathogenesis is supported by morphogenetic similarities in the

liver and vessels. The current study also showed that high LFC is related to increased visceral fat mass, impaired whole-body and skeletal muscle insulin sensitivity and coronary dysfunction, in addition to an increment in inflammation markers in patients with high LFC.

In the present study, visceral fat depots were 22% larger in patients with fatty liver, which may suggest enhanced delivery of FFAs into the liver. It was also found that liver enzymes were normal or only mildly elevated in patients with high liver fat content, which is in agreement with previous observations (Angulo, 2002). Thus, many patients with NAFLD remain undiagnosed until the progression to more severe liver disease occurs. Since silent high liver fat content may contribute to significant impairment in insulin sensitivity, coronary function and myocardial glucose uptake, the current study emphasizes that asymptomatic fatty liver cannot be considered as a benign condition.

CRP is a strong predictive biomarker of cardiovascular events as well as a direct participant in the pathogenesis of atherosclerosis (Yeh and Willerson, 2003). In the current study hsCRP is significantly higher in patients with high liver fat content suggesting low-grade inflammation in these patients. With respect to previous findings, it can be suggested that hepatic steatosis per se may cause low-grade inflammation, which may affect coronary vasculature as well as myocardial metabolism. Whole body insulin sensitivity, skeletal muscle glucose uptake, myocardial glucose uptake and myocardial glucose extraction rate were significantly lower in the high hepatic fat group. It has been suggested that whole-body insulin sensitivity is directly associated with myocardial insulin sensitivity (Iozzo et al., 2002), which is in agreement with the present study. This shows a close relationship between whole-body and myocardial glucose uptake, thus, the high-risk profile for cardiovascular events related to whole-body insulin resistance is in a close association with myocardial insulin resistance. Previously, it has been suggested that the underlying factor for hepatic steatosis could be insulin resistance itself (Bugianesi et al., 2005). The result of a multiple regression analysis in the current study showed that the association between insulin resistance at the whole-body level and myocardial glucose uptake (dependent variable) disappeared when liver fat content was taken into account as an additional independent variable, suggesting a more significant role of hepatic steatosis over the whole body insulin sensitivity. This supports the atherogenic role of NAFLD beyond the insulin resistance as has been previously suggested (Targher, 2005). However, the cellular mechanism behind this observation remains unclear. A possible underlying mechanism explaining the relationship between fatty liver and impaired myocardial metabolism may be an excessive FFA input into the myocardium due to the altered FFA metabolism (Taegtmeyer et al., 2002). Normally, FFAs are delivered into cells according to the requirement of fuel and little or no unoxidized FFA are left intracellularly (Unger and Orci, 2001). However, when the supply of FFAs exceeds the rate of mitochondrial β-oxidation, oxidative stress is induced (Listenberger et al., 2001) and intracellular triglycerides and fatty acid intermediates, ceramides, start to build up. In the current study, the patients were divided into two groups according to the median of the liver fat content. This division was also based on previous findings that liver triglyceride

content greater than 8% is a reliable sign of *pathological* fatty liver (Donhoffer, 1974), this in contrast to the upper border of normal liver fat (5.56 %) content mentioned previously (Szczepaniak et al., 2005).

Concluding, hepatic steatosis is a predictor of impaired myocardial metabolism and coronary dysfunction. Possible underlying mechanisms are lipotoxicity due to FFA accumulation and low-grade inflammation. More studies are needed to establish the relationship between (changes in) hepatic fat content and on myocardial metabolism in patients with type 2 diabetes. The current findings put the role of LFC as an indirect metabolic marker in a new context, and confirm the growing opinion that LFC can be seen as a whole-body barometer of metabolic health (Chitturi and Farrell, 2007).

11.3 Relation between liver fat content and hepatic glucose uptake (II)

The present study is the first to show a significant inverse relationship between liver fat content and hepatic glucose metabolism. LFC was significantly increased and hepatic glucose uptake was decreased in T2DM patients compared to healthy subjects suggesting impaired tissue specific metabolism and insulin resistance associated with tissue steatosis. The strong association of LFC to whole body glucose uptake ($p=0.0004$) observed in our study supports the important role of LFC in insulin resistance.

Although Rosiglitazone treatment had beneficial effects on both liver steatosis and hepatic glucose uptake, the individual changes were variable and no relationship of the changes was observed. However, changes in clamp NEFA levels were strongly associated with changes in LFC. The decrease in circulating NEFA levels indicates overall improvement of suppression of lipolysis. This might result in decreased portal NEFA load and thereby reduce liver fat content in patients treated with Rosiglitazone. Although hepatic glucose uptake has been shown to be dependent on plasma NEFA levels (Iozzo et al., 2004), suppression of lipolysis was not significantly associated with changes in hepatic glucose uptake in the Rosiglitazone group. This suggests that the increase in hepatic glucose uptake by Rosiglitazone action is only partly explained by reduced NEFA levels. Additional direct effects of Rosiglitazone on the liver possibly play an important role. PPAR-γ agonists have been shown to increase glycogen storage and decrease gluconeogenesis through direct effects on the hepatocyte in vitro (Ciaraldi et al., 1990;Fulgencio et al., 1996).

Previous studies have shown that thiazolidinediones promote redistribution of ectopic fat to subcutaneous fat depots. In the present study with Rosiglitazone only trends of increase in subcutaneous fat mass ($p=0.068$) and decrease of visceral fat mass were observed ($p=0.175$). This is in concert with previously observed borderline changes in studies by us (Iozzo et al., 2003b) and others (Tiikkainen et al., 2004) assessing the effects of Rosiglitazone on abdominal visceral and subcutaneous fat masses by MRI. The correlation between LFC and visceral fat mass in the current study supports the essential role of increased visceral fat mass in the development of NALFD in type 2 diabetes.

Liver fat content as assessed by ^{1}H MRS is presumably a very sensitive and early indirect marker of metabolic disregulation as even a small increase in LFC was associated with changes in hepatic glucose uptake and especially whole body glucose uptake. Judging from the data in this study, involving the observed positive correlation of LFC and ALAT, increased LFC seems to be mainly a marker for the inflammatory state of the liver and not as much a single factor directly impairing overall liver function.

The patients with type 2 diabetes included in this study had macrovascular complications. By taking into account the long pre-clinical period before diagnosis in T2DM, some degree of complications is often present even in early-onset T2DM patients. Therefore it is likely that the present findings apply to the general population of T2DM patients.

In conclusion, this study shows that increased liver fat content is associated with decreased hepatic insulin stimulated glucose uptake in patients with type 2 diabetes. Rosiglitazone therapy simultaneously decreases LFC and improves hepatic glucose uptake, but individual changes are not directly related. This suggest that the beneficial effects of Rosiglitazone on liver metabolism can be partly explained by improved suppression of lipolysis, leading to reduced LFC, in addition to more direct drug effects. Larger studies need to be conducted in order to understand the role of LFC in insulin resistance and pathways by which both LFC and HGU are regulated and modulated by Rosiglitazone to optimize treatment in patients with T2DM.

11.4 Effects of Trimetazidine on hepatic metabolism (III)

The present investigation is the first in which Trimetazidine was administered to obese, otherwise healthy subjects. Furthermore, no previous study has addressed the effects of Trimetazidine on organ steatosis. A significant decrease in liver triglyceride content was observed after four weeks of Trimetazidine treatment. This change was accompanied by a reduction in liver enzymes and hepatic fibro-inflammatory scores.

Animal studies, using radiolabeled glycerol, have shown that Trimetazidine lessens triacylglycerol synthesis, while stimulating the incorporation of glycerol in diacylglycerols, and redirecting the utilization of the latter in phosphatidyl-choline and phosphatidyl-ethanolamine synthesis (Sentex et al., 2001). Structural phospholipids are regarded as protective elements. Our findings extend the above observation by suggesting that this mechanism is operative in humans. In contrast to short-term animal experiments, the more sustained nature of the current treatment allowed for determination that this action results in an overall decrease in the liver triglyceride pool. Several recent studies, focused on the *ex-vivo* preservation of donor organs, have demonstrated that Trimetazidine reduces transaminase release by perfused livers, and promotes hepatocyte integrity by abating oxidative stress and hepatic vascular resistance, especially in steatotic livers (Ben, I et al., 2006;Ben, I et al., 2007). The level of oxidative stress is related with mitochondrial function and proportional to the oxidation rate of substrates, and to the content of triglycerides, serving as substrates for lipid peroxidation. In humans, the administration of Trimetazidine decreases the levels

of beta-hydroxybutyrate, (Monti et al., 2006) which is a specific marker of hepatic fatty acid oxidation. Our findings reflect the observations obtained *in vitro*, documenting a consistent reduction in liver enzymes and hepatic fibro-inflammatory scores in human subjects. These effects are likely to result from the summation of the events listed above. Notably, patients with higher liver triglyceride content were more responsive to the drug, suggesting that this agent would be effective in proportion with the severity of liver steatosis.

We controlled for major factors which have been implicated in the regulation of liver lipid deposition. Adipose depots located in the abdominal area release fatty acids to be directly conveyed to the liver, *via* the portal vein, and the fibro-inflammatory score was strongly associated with the abdominal visceral fat mass at baseline in this study. Adiponectin is a strong predictor of hepatic fat content, (Bajaj et al., 2004;Kotronen et al., 2007) and inversely parallels the grade of hepatic inflammation in patients with steatohepatitis(Aygun et al., 2006). In addition, circulating triglyceride and fatty acids constitute the substrate for ectopic fat, and also correlate with the deposition of fat in the liver. None of these factors changed in the current study to explain an indirectly mediated effect of the drug. On the contrary, our findings strongly suggest that the benefits of Trimetazidine depend on hepatocyte-specific targets. This interpretation is consistent with the evidence of at least two families of specific Trimetazidine binding sites, (Morin et al., 1998) located in the outer and inner membrane of purified rat liver mitochondria, as well as in other sub-cellular microsomal fractions, which have been implicated in the closure of mitochondrial pores, leading to a reduction in organelle swelling and damage, and enhanced efficiency in ATP production. Notably, the cytosol of liver cells contains an endogenous substance which is able to displace Trimetazidine from its binding sites, suggesting that this drug potentiates or restores a physiological mechanism (Morin et al., 2000).

The trends observed in the metabolic profile are supportive of the described effects of Trimetazidine on glucose control. Previous studies conducted in patients with diabetes and cardiovascular disease showed a decline in glycemia (Fragasso et al., 2003). Because the current investigation was meant as mechanistic, and focused on liver fat content, the confounding effects of the above disease conditions was purposely excluded. Therefore, gluco-metabolic changes were not expected to be as pronounced as in diabetic patients. Notwithstanding this, a decline in glycosylated hemoglobin was noted in spite of the limited duration of this study. Because fasting glycemia was not modified by the treatment, we may speculate that the drug modulates glucose metabolism especially during absorptive conditions, in accord with the observation that insulin-mediated, rather than fasting, skeletal muscleglucose disposal is significantly increased by Trimetazidine (Monti et al., 2006).

One limitation of the current study is that a placebo control group was not included. However, numerous studies have shown that the reproducibility of liver fat content determinations is satisfactory (Szczepaniak et al., 1999;Thomas et al., 2005), and that placebo treatment – even for a longer time period than the one in this study – does not change MRS-determined liver fat content to a significant extent (Belfort et al., 2006). In our hands, the repetition of measurement before and after 16 weeks of placebo in 25

subjects with type 2 diabetes (Borra et al., 2008) showed comparable numbers of LFC, 9.7±1.5% *vs.* 9.8±1.6% (p=ns), and the lack of significance was confirmed in both the low and high liver fat subgroups. Altogether, the available evidence indicates that the findings of the current study are not likely to be mediated by placebo effects or technique reproducibility.

Larger cohorts and placebo-controlled trials are needed to extend the current findings to patients with different grades of liver fibro-inflammatory disease. Our observations, together with the available literature, lead us to the theory represented in the diagram below (Figure 29), in which we suggest that Trimetazidine acts directly on human hepatocytes *in vivo*, to divert fatty acids away from triglyceride synthesis and to reduce oxidative damage in obese subjects, proving to be a promising agent for the treatment of liver steatosis and its complications.

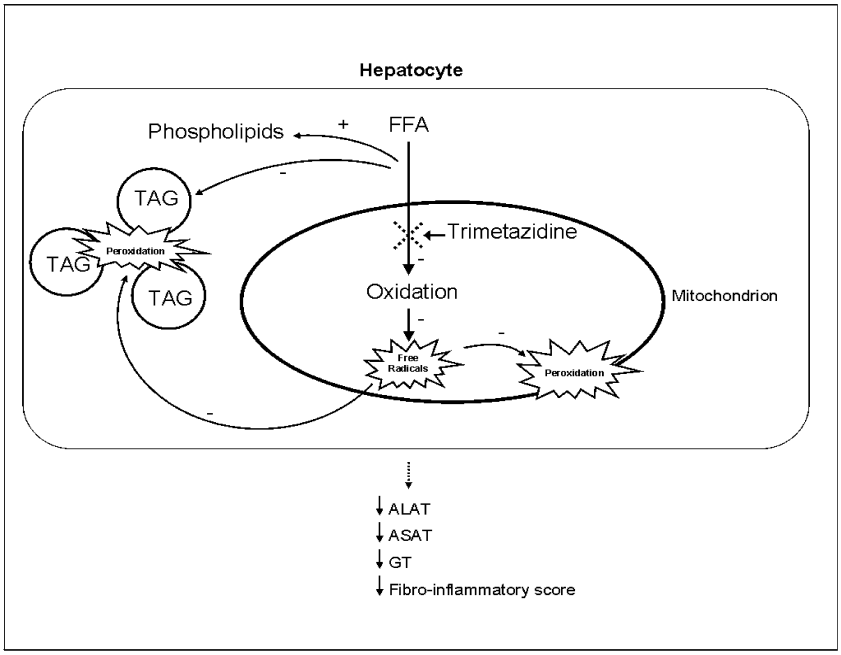

Figure 29. Proposed mechanism by which partial inhibition of fatty acid (FFA) beta-oxidation in the mitochondrion through Trimetazidine reduces liver inflammation and triacylglycerol (TAG) storage.

11.5 In-out-phase imaging for measurement of liver fat content (IV)

This study shows that in our study population, the measurement of SI from in-and-out-of-phase images provides useful information on liver fat content, consistent with ^{1}H MRS measurements. It also demonstrates the usefulness of a simple method to asses if liver fat content is within the normal range. We also showed a very high sensitivity and specificity in patients with type 2 diabetes and NAFLD, regardless of whether measurements from multiple or a single in-and-out-of-phase images are used. In our

view the simple SI_{in}-SI_{out} calculation provides a clinical tool for radiologists: liver fat content is over the normal level when the SI of the liver is higher in the in-phase than in the out-of-phase images.

In addition, estimation of liver fat content using SI measurements from in-and-out-of-phase images provided a more reliable approximation of the true liver fat content than subjective image interpretation, even if performed by an experienced radiologist. The advantage of this method in our view is that it can be a guideline for the less experienced radiologist and is valid throughout the large range of liver fat content, often observed in patients with type 2 diabetes and NAFLD.

These findings are consistent with results of a previous study (Kawamitsu et al., 2003) involving 17 healthy subjects in whom lower levels of LFC were observed by ^{1}H MRS than in the current study involving patients with type 2 diabetes. However, in a recent study by Westphalen et al. a weak correlation between SI changes in in-and-out-of-phase imaging versus fat content in liver biopsy samples was observed (Westphalen et al., 2007). This weak relationship was explained by the increased liver iron content in that patient group, which altered the T2* in the liver, and as a result, the in-and-out-of-phase imaging measurements. Since the study population consisted of patients with cirrhosis, an increased liver iron content was likely to be present. Subjects in our study did not have cirrhosis or other severe liver disease and therefore liver iron content was likely to be low, contributing to the significant relationship observed between the FI calculated from in-and-out-of-phase imaging and ^{1}H MRS. Additionally, the PRESS sequence used in our study for ^{1}H MRS is a spin-echo technique, which includes a second 180° pulse, making the observed signal less likely to be affected by dephasing due to increased liver iron content. Finally, liver biopsy suffers as a gold standard for LFC estimation due to the very small sample size compared to ^{1}H MRS and the resulting difficulty of precise lipid quantification in histological samples. Moreover, a *subjective* estimation by a pathologist is used in many studies to quantify lipid in histological samples, instead of chemical analysis, which also decreases the accuracy of the method (Petersen et al., 1996;Hussain et al., 2005;Thomas et al., 2005).

Clinical application and study limitations

Certain cautions on the application of the results of our study are appropriate. First, this study shows the utility of these techniques to be valid in patients with type 2 diabetes and NALFD without other liver abnormalities. As stated previously, iron accumulation in liver tissue is a pitfall in liver fat determination by in-and-out-of-phase imaging (Westphalen et al., 2007). Main causes for liver iron accumulation are cirrhosis, hemochromatosis and hemosiderosis. Repeated blood transfusions might also change liver SI on MR images (Siegelman et al., 1991;Gandon et al., 1994;Ludwig et al., 1997;Salo et al., 2002). Furthermore, NAFLD *itself* can progress to cirrhosis, associated with fibrosis and hemosiderosis (Ludwig et al., 1997). For the reasons mentioned above the rapid method for LFC quantification as proposed in this study should not be applied if the clinical data or when the MRI reveals clear signs of cirrhosis or if iron accumulation in the liver is suspected. Future research comparing ^{1}H

MRS to SI changes in in-and-out-of-phase is needed in patients with severe liver disease.

Another limitation in our study is the fact that both ^{1}H MRS and in-and-out-of-phase imaging solely measure liver lipid content and that other possible parameters, as inflammation in the case of nonalcoholic steatohepatitis (NASH), remain undetected. As NAFLD progresses in some patients towards cirrhosis total liver fat content might even decrease (Powell et al., 1990). Therefore it should be remembered that the level of liver fat content, although a good marker of primary NAFLD (Adams and Lindor, 2007), does not necessarily reflect the true state of the liver for all stages of NAFLD.

Finally, it should be noted that in our study, using a single voxel ^{1}H MRS technique, liver fat was assumed to be homogeneously distributed over the liver. A multivoxel ^{1}H MRS liver study by Sijens et al. (Sijens et al., 2006) showed an inter-voxel SD of 0.3-0.5%, indicating that in general liver fat heterogeneity is limited, but not necessarily negligible. On the other hand, a study by Thomas et al. suggested that there is a great variation in liver fat content heterogeneity between individuals: in certain individuals the variation of liver fat content within the liver is high (up to 50%) and in others very low (< 1%). (Thomas et al., 2005). Furthermore, also water content might differ over the liver area (Li et al., 2005), further increasing possible heterogeneity of LFC measurements. In this study we attempted to minimize the possible effects of liver heterogeneity on our final results by carefully matching the area and image-level of SI measurements and estimates with the original ^{1}H MRS voxel location and volume.

This study clearly shows the ability of in-and-out-of-phase imaging to assess liver fat content in patients with type 2 diabetes and NALFD. As a novel finding and clinical rule-of-thumb a cutoff value of 5.1% was chosen to allow for rapid discrimination between normal or increased liver fat content based on in-and-out-of-phase imaging alone. Increased use of in-and-out-of-phase imaging to assess liver fat content has the potential to promote early detection of NAFLD and to potentially improve treatment evaluation.

A possible source of error is that the fat composition (relative amount each fatty acids) of the diabetic patients might be different from healthy controls, which effects the interpretation of the spectra obtained. A second source of error is the possible variation in T1 and T2 values of liver tissue between patients. Furthermore, liver lipid composition and water content are assumed to be constant during intervention. This is not necessarily true, however most likely this has a negligible effect on the final results.

12. SUMMARY AND CONCLUSIONS

The results of the present study have led to following conclusions:

I

Patients with increased liver fat content (LFC) have decreased myocardial and whole-body insulin sensitivity. This finding stresses the importance of LFC as an indirect metabolic marker and confirms the growing opinion that LFC can be seen as a whole-body barometer of metabolic health. Furthermore, the relationship of increased liver fat content with impaired myocardial metabolism supports the existence of a recently proposed "liver-vessel axis" which hypothesizes that similar biological precursors effect the development of both atherosclerosis and non-alcoholic fatty liver disease (NAFLD).

II

A significant inverse relationship exists between LFC and hepatic glucose metabolism in patients with T2DM. Liver fat content is significantly increased and HGU decreased in T2DM patients compared to healthy subjects, suggesting impaired tissue specific metabolism and insulin resistance associated with tissue steatosis. Rosiglitazone treatment has beneficial effects on both liver steatosis and hepatic glucose uptake, but the individual changes are variable and no relationship among the changes is observed. This study provides a basis for future studies to increase our understanding of of LFC in insulin resistance and pathways by which both LFC and HGU are regulated and modulated by Rosiglitazone, in order to optimize treatment in patients with T2DM.

III

This pilot study showed that a one-month treatment with Trimetazidine reduces liver fat content, transaminase levels, and hepatic fibro-inflammatory scores in obese patients. A direct drug effect on the organ is supported by an absence of change in extra-hepatic factors known to regulate liver lipid metabolism. These observations suggest that Trimetazidine is a promising agent for the treatment of liver steatosis and its complications and therefore provides a platform for larger studies on the effects of Trimetazidine on liver fat content.

IV

In-and-out-of-phase imaging can accurately estimate liver fat content (LFC) up to high degrees of LFC and is more reliable than a visual inspection of images by an experienced radiologist. The proposed novel rapid diagnostic method for discrimination between normal or increased liver fat content based on in-and-out-of-phase imaging alone has the potential to promote early detection and treatment of NAFLD in large patient populations and thus reduce the risk of NAFLD progression to more severe liver disease.

13. ACKNOWLEDGEMENTS

This study was carried out at the Medical Imaging Centre of Southwest Finland, Turku University Central Hospital, the Turku PET Centre, and the Department of Diagnostic Radiology, University of Turku during the years 2002-2008.

I thank Professor Hannu Aronen, Chair of Radiology, University of Turku, for his interest in the present study. I am also grateful for his support concerning my future research plans. I also express my gratitude to Professor Juhani Knuuti, Director of the Turku PET Centre, University of Turku, for his guidance which has helped make the Turku PET Centre such an outstanding research facility.

I am extremely grateful to my teacher, supervisor and friend, Physicist Markku Komu, who has introduced me to the secrets of magnetic resonance and spectroscopy over the past decade. Markku: It has been such an honor to be your student and colleague, thank you so much for all your time, effort and never-ending patience. You have always had a (correct) answer to all my questions. Your tremendous experience and knowledge have always given me great confidence and motivation to continue. I thank you for being there for me and for always explaining to me, in your modest and kind way, how I should proceed. I am well aware that I would have never been able to complete this thesis without your help and guidance, for which I am eternally grateful.

I owe my sincere gratitude to my supervisor Docent Riitta Parkkola. Dear Riitta: Thank you for encouraging me over and over again, and especially for your positive attitude. You are such a wonderful person and working with you has been a great privilege. Your vast knowledge and practical approach have helped me tremendously over and over again. Thank you for teaching me and for always supporting me in difficult times. We have worked and laughed a lot together: I will never forget your teaching sessions of “peculiar Finnish sayings” during the long and late afternoon imaging sessions together with Markku. Thank you for all your hard work on the collaboration between the Medical Imaging Centre and the PET Centre. This has made it possible for me to do these studies in an outstanding research environment.

I wish to thank Professor Pirjo Nuutila for her overall guidance and support making this dissertation possible. I was very fortunate to benefit from your enormous experience in supervising dissertations. Dear Pirjo: You have guided me through all the (bureaucratic) steps and provided me with funding when needed. Thanks to your hard work I was able to obtain the Marie Curie Fellowship, which marked the starting point of this project, which has now come to an end. The door of your room has always been open and you were always willing to help me out when I had a question or a problem, for which I am extremely grateful. Your very large research experience in the field of endocrinology and PET has been a tremendous help in interpreting and publishing our findings. I am very grateful to have been your PhD student and I am looking forward to many projects to come.

I thank Docent Riikka Lautamäki for helping me throughout the years. Dear Riikka: I will never forget your outstanding guidance, especially when I started as a (completely inexperienced) Marie Curie fellow back in 2003. Thank you for letting me be part of your study and for trusting me with your patients. I am extremely grateful for your time and patience in teaching me PET techniques and clamp studies. Thank you for performing the liver PET data analysis and especially for helping me in writing my first publication. Your active attitude towards research really has inspired me a lot.

I want to thank Docent Patricia Iozzo for her guidance and very helpful discussions, especially concerning the Trimetazidine study. Dear Patricia: It is always great to work with you; you are always full of original ideas and you are one of the most dedicated researchers I know. I greatly admire your skill of combining lots of complicated information into a compact and logical package. Thank you for the "vanilla coffee" breaks together with Marco, which were always one of the few relaxing moments during the day.

Professor Tommy Olsson and Professor Leena Kivisaari are greatly acknowledged for their outstanding and constructive comments during the review of this work. The professional help on the dissertation formalities by Outi Irjala and Riitta Paju of the Medical Faculty is greatly acknowledged. I also thank Heli Törmänen for introducing me to the University of Turku as an exchange student, already nine years ago.

I wish to thank all of my excellent co-authors, Sakari Salo and Kirsti Dean for their help, suggestions and excellent work in measuring and scoring the in-and-out-of-phase MR-images. I thank Romina Maggio, Marco Bucci, Helena Tuunanen, and Mikko Kankaanpää for their help in the Trimetazidine study. Dear Mikko: Your tragic accident in 2006 followed by your absence had a great impact both on me personally as well as on the speed of finalizing this PhD thesis. I'm so happy you are with us and it's great to see you recover, slowly but steadily. I also thank Paul E. Sijens, Kirsti Hällsten and Jörgen Bergman for their help and useful comments.

I wish to thank my fellow researchers and friends Jan Kiss and Alexandru Naum. Dear Jan and Allu: Thank you for being there for me as friends, it really meant a lot to me and unfortunately Turku really hasn't been the same after you both left. I wish you all the best in pursuing your dreams, and I sincerely hope we will always stay in touch. I also want to express my sincere thanks to Antti Viljanen and Mikko Järvisalo. Dear Antti and Mikko: Your advice, friendship and vision on how to work as a medical doctor in Finland really helped me a lot and I am very grateful for everything.

Other (present and former) researchers in the Turku PET Centre that I would like to thank for their support are Jarna Hannukainen (thank you for your help with the translation!), Virva Lepomäki, Markus Lindroos, Hanna-Riikka Lehto, Kirsi Virtanen, Saila Kauhanen, Gaber Komar, Iina Laitinen, Kari Kalliokoski, Riikka Kalliokoski, Ilkka Heinonen, Anna Karmi, Miika Honka, Heidi Leppänen, Noora Scheinin, Jere Virta, Tove Grönroos, Jussi Virtanen, Han "Hannu" Chunlei, Jukka Kemppainen, Nobu Kudomi, Lotfi Slimani, Kira Stolen, Tuula Janatuinen, Kaike Kaisti, Jussi Pärkkä, Sergey Nesterov, Marko Seppänen and Sami Kajander. I wish to

thank Irina Lisinen for her outstanding advice on statistical methods and for performing many essential statistical analyses in this work.

I wish to thank all patients and healthy volunteers who chose to participate in this study. Your participation has made this work possible and I am very grateful for your patience during the long PET and MR-scanning sessions.

I would like to thank Docent Anu Alanen for allowing me to perform research in the Medical Imaging Centre of Southwest Finland and for supporting me in general. I also sincerely want to thank Docent Kimmo Mattila for frequently checking on the progress of this dissertation. You really took your task of "supervising the supervisors" seriously and you made me feel I could count on your support if needed.

I was fortunate to have the following outstanding co-workers in the Turku PET Centre: Mika Teräs, Professor Heikki Minn, Professor Juha Rinne, Professor Olof Solin, Hannu Sipilä and Tuula Tolvanen. Rami Mikkola, Seppo Tyrväinen and Marko Tättäläinen are greatly acknowledge for their help on IT-matters. I also want to thank Mirja Jyrkinen in the PET Centre and Pirjo Helanko, Paula Saino, Anne Österman and Ritva Eklund in the Medical Imaging Centre of Southwest Finland for taking care of many secretary and other matters in an outstanding manner.

I would like to thank the laboratory technologists at the Turku PET Centre, especially Leena Ruohonen, Sanna Suominen and Heidi Lappalainen. I am also extremely grateful to all radiographers both at the Turku PET Centre and the Medical Imaging Centre of Southwest Finland, in particular Outi Numminen, Anne-Mari Jokinen, Minna Aatsinki, Hannele Lehtinen, Marjo Tähti, Tarja Keskitalo and Sari Hermonen. Thank you all for your outstanding work and your flexibility.

I am very grateful for the support and friendship of all my colleagues in the department of Radiology, especially Aarto Haapanen, Ilkka Manner, Johanna Virtanen, Timo Kurki, Pekka Niemi, Pirkko Sonninen, Teemu Paavilainen, Milja Holstila, Jussi Kankare, Tomi Pudas and Jani Saunavaara. Thank you all for always being interested in what the "flying Dutchman" was up to.

I also wish to thank Professor Peter B. Dean for giving me such a warm welcome and introducing me to the Department of Radiology back in 2000, when I was an exchange student at the University of Turku. Dear Peter: You have always supported me and believed in me, and you taught me never to give up. It has been great to collaborate more intensively with you lately. In addition I want to thank Emeritus Professor Martti Kormano for supporting me in the early days.

Above all, I want to thank my parents, my family and loved ones for giving me so much love and care, for always believing in me, and for dealing so well with all this time that I was (far) away from home and the moments that you had to share me with computers and large piles of articles. Without you I would not be where I am now. I also want to thank my Father, in my heart you are always with me, thank you for making this wonderful life possible.

This study was financially supported by a Marie Curie Fellowship of the European Community programme QOL 1.1.1 under contract number QKGA-1999-51330, the Instrumentarium Research Foundation, the Diabetes Research Foundation, the Ella and Georg Ehrnrooth Foundation, the National Graduate School of Clinical Investigation (CLIGS), the Turku University Hospital and the Turku University Foundation.

Turku, June 2009

Ronald Borra

14. REFERENCES

Abate N, Burns D, Peshock RM, Garg A and Grundy SM (1994) Estimation of Adipose Tissue Mass by Magnetic Resonance Imaging: Validation Against Dissection in Human Cadavers. *J Lipid Res* **35**:1490-1496.

Abate N, Garg A, Coleman R, Grundy SM and Peshock RM (1997) Prediction of Total Subcutaneous Abdominal, Intraperitoneal, and Retroperitoneal Adipose Tissue Masses in Men by a Single Axial Magnetic Resonance Imaging Slice. *Am J Clin Nutr* **65**:403-408.

Adams LA and Lindor KD (2007) Nonalcoholic Fatty Liver Disease. *Ann Epidemiol* **17**:863-869.

Alberti KG and Zimmet PZ (1998) Definition, Diagnosis and Classification of Diabetes Mellitus and Its Complications. Part 1: Diagnosis and Classification of Diabetes Mellitus Provisional Report of a WHO Consultation. *Diabet Med* **15**:539-553.

Alenius S and Ruotsalainen U (1997) Bayesian Image Reconstruction for Emission Tomography Based on Median Root Prior. *Eur J Nucl Med* **24**:258-265.

Angulo P (2002) Nonalcoholic Fatty Liver Disease. *N Engl J Med* **346**:1221-1231.

Angulo P (2007) GI Epidemiology: Nonalcoholic Fatty Liver Disease. *Aliment Pharmacol Ther* **25**:883-889.

Arun J, Jhala N, Lazenby AJ, Clements R and Abrams GA (2007) Influence of Liver Biopsy Heterogeneity and Diagnosis of Nonalcoholic Steatohepatitis in Subjects Undergoing Gastric Bypass. *Obes Surg* **17**:155-161.

Assy N, Kaita K, Mymin D, Levy C, Rosser B and Minuk G (2000) Fatty Infiltration of Liver in Hyperlipidemic Patients. *Dig Dis Sci* **45**:1929-1934.

Aygun C, Senturk O, Hulagu S, Uraz S, Celebi A, Konduk T, Mutlu B and Canturk Z (2006) Serum Levels of Hepatoprotective Peptide Adiponectin in Non-Alcoholic Fatty Liver Disease. *Eur J Gastroenterol Hepatol* **18**:175-180.

Bajaj M, Suraamornkul S, Piper P, Hardies LJ, Glass L, Cersosimo E, Pratipanawatr T, Miyazaki Y and DeFronzo RA (2004) Decreased Plasma Adiponectin Concentrations Are Closely Related to Hepatic Fat Content and Hepatic Insulin Resistance in Pioglitazone-Treated Type 2 Diabetic Patients. *J Clin Endocrinol Metab* **89**:200-206.

Barrows BR, Timlin MT and Parks EJ (2005) Spillover of Dietary Fatty Acids and Use of Serum Nonesterified Fatty Acids for the Synthesis of VLDL-Triacylglycerol Under Two Different Feeding Regimens. *Diabetes* **54**:2668-2673.

Belfort R, Harrison SA, Brown K, Darland C, Finch J, Hardies J, Balas B, Gastaldelli A, Tio F, Pulcini J, Berria R, Ma JZ, Dwivedi S, Havranek R, Fincke C, DeFronzo R, Bannayan GA, Schenker S and Cusi K (2006) A Placebo-Controlled Trial of Pioglitazone in Subjects With Nonalcoholic Steatohepatitis. *N Engl J Med* **355**:2297-2307.

Bellentani S, Saccoccio G, Masutti F, Croce LS, Brandi G, Sasso F, Cristanini G and Tiribelli C (2000) Prevalence of and Risk Factors for Hepatic Steatosis in Northern Italy. *Ann Intern Med* **132**:112-117.

Ben M, I, Casillas-Ramirez A, Xaus C, Serafin A, Rosello-Catafau J and Peralta C (2006) Trimetazidine: Is It a Promising Drug for Use in Steatotic Grafts? *World J Gastroenterol* **12**:908-914.

Ben M, I, Massip-Salcedo M, Fernandez-Monteiro I, Xaus C, Bartrons R, Boillot O, Rosello-Catafau J and Peralta C (2007) Addition of Adenosine Monophosphate-Activated Protein Kinase Activators to University of Wisconsin Solution: a Way of Protecting Rat Steatotic Livers. *Liver Transpl* **13**:410-425.

Bender D, Munk OL, Feng HQ and Keiding S (2001) Metabolites of (18)F-FDG and 3-O-(11)C-Methylglucose in Pig Liver. *J Nucl Med* **42**:1673-1678.

Bloch F (1946) Nuclear Induction. *Physical Review* **70**:460-474.

Bloch F, Hansen WW and Packard M (1946) Nuclear Induction. *Physical Review* **69**:127.

Bloembergen N, Purcell EM and Pound RV (1948) Relaxation Effects in Nuclear Magnetic Resonance Absorption. *Physical Review* **73**:679-712.

Borra R, Lautamaki R, Parkkola R, Komu M, Sijens PE, Hallsten K, Bergman J, Iozzo P and Nuutila P (2008) Inverse Association Between Liver Fat Content and Hepatic Glucose Uptake in Patients With Type 2 Diabetes Mellitus. *Metabolism* **57**:1445-1451.

Borra RJH, Parkkola R, Lautamaki R, Nuutila P and Komu M (2003) Liver Fat Content Determined by Proton Magnetic Resonance Spectroscopy Is Increased in Patients With Type 2 Diabetes. *MAGMA* **16 Suppl 7**:S266.

Browning JD, Szczepaniak LS, Dobbins R, Nuremberg P, Horton JD, Cohen JC, Grundy SM and Hobbs HH (2004) Prevalence of Hepatic Steatosis in an Urban Population in the United States: Impact of Ethnicity. *Hepatology* **40**:1387-1395.

Bugianesi E (2007) Non-Alcoholic Steatohepatitis and Cancer. *Clin Liver Dis* **11**:191-1xi.

Bugianesi E (2008) Nonalcoholic Fatty Liver Disease (NAFLD) and Cardiac Lipotoxicity: Another Piece of the Puzzle. *Hepatology* **47**:2-4.

Bugianesi E, McCullough AJ and Marchesini G (2005) Insulin Resistance: a Metabolic Pathway to Chronic Liver Disease. *Hepatology* **42**:987-1000.

Buxton RB, Wismer GL, Brady TJ and Rosen BR (1986) Quantitative Proton Chemical-Shift Imaging. *Magn Reson Med* **3**:881-900.

Cairns SR and Peters TJ (1984) Isolation of Micro- and Macro-Droplet Fractions From Needle Biopsy Specimens of Human Liver and Determination of the Subcellular Distribution of the Accumulating Liver Lipids in Alcoholic Fatty Liver. *Clin Sci (Lond)* **67**:337-345.

Cancello R, Tordjman J, Poitou C, Guilhem G, Bouillot JL, Hugol D, Coussieu C, Basdevant A, Bar HA, Bedossa P, Guerre-Millo M and Clement K (2006) Increased Infiltration of Macrophages in Omental Adipose Tissue Is Associated With Marked Hepatic Lesions in Morbid Human Obesity. *Diabetes* **55**:1554-1561.

Cano C, Bermudez VJ, Medina MT, Bermudez FA, Ambard MJ, Souki AJ, Escalona D, Contreras F and Velasco M (2003) Trimetazidine Diminishes Fasting Glucose in Rats With Fasting Hyperglycemia: a Preliminary Study. *Am J Ther* **10**:444-446.

Charatcharoenwitthaya P and Lindor KD (2007) Role of Radiologic Modalities in the Management of Non-Alcoholic Steatohepatitis. *Clin Liver Dis* **11**:37-54, viii.

Charlton M (2004) Nonalcoholic Fatty Liver Disease: a Review of Current Understanding and Future Impact. *Clin Gastroenterol Hepatol* **2**:1048-1058.

Chitturi S and Farrell GC (2007) Fatty Liver Now, Diabetes and Heart Attack Later? The Liver As a Barometer of Metabolic Health. *J Gastroenterol Hepatol* **22**:967-969.

Ciaraldi TP, Gilmore A, Olefsky JM, Goldberg M and Heidenreich KA (1990) In Vitro Studies on the Action of CS-045, a New Antidiabetic Agent. *Metabolism* **39**:1056-1062.

Cohen J and Cohen P (1983) *Applied Multiple Regression/Correlation Analysis for the Behavioral Sciences*. L. Erlbaum Associates, Hillsdale, N.J.

Davies RJ, Saverymuttu SH, Fallowfield M and Joseph AE (1991) Paradoxical Lack of Ultrasound Attenuation With Gross Fatty Change in the Liver. *Clin Radiol* **43**:393-396.

Day CP and James OF (1998) Steatohepatitis: a Tale of Two "Hits"? *Gastroenterology* **114**:842-845.

DeFronzo RA and Mandarino LJ (2003) Pathogenesis of type 2 diabetes mellitus, in www.endotext.org (Goldfine ID and Rushakoff RJ eds) mdtext.com, Inc, South Dartmouth, MA.

DeFronzo RA, Tobin JD and Andres R (1979) Glucose Clamp Technique: a Method for Quantifying Insulin Secretion and Resistance. *Am J Physiol* **237**:E214-E223.

Dixon WT (1984) Simple Proton Spectroscopic Imaging. *Radiology* **153**:189-194.

Donhoffer H (1974) Quantitative Estimation of Lipids in Needle Biopsy Sized Specimens of Cadaver Liver. *Acta Med Acad Sci Hung* **31**:47-49.

Donnelly KL, Smith CI, Schwarzenberg SJ, Jessurun J, Boldt MD and Parks EJ (2005) Sources of Fatty Acids Stored in Liver and Secreted Via Lipoproteins in Patients With Nonalcoholic Fatty Liver Disease. *J Clin Invest* **115**:1343-1351.

Earls JP, Rofsky NM, DeCorato DR, Krinsky GA and Weinreb JC (1999) Echo-Train STIR MRI of the Liver: Comparison of Breath-Hold and Non-Breath-Hold Imaging Strategies. *J Magn Reson Imaging* **9**:87-92.

Ekstedt M, Franzen LE, Mathiesen UL, Thorelius L, Holmqvist M, Bodemar G and Kechagias S (2006) Long-Term Follow-Up of Patients With NAFLD and Elevated Liver Enzymes. *Hepatology* **44**:865-873.

Ernst RR and Anderson WA (1966) Application of Fourier Transform Spectroscopy to Magnetic Resonance. *Review of Scientific Instruments* **37**:93-102.

Feinberg DA, Rofsky NM and Johnson G (1995) Multiple Breath-Hold Averaging (MBA) Method for Increased SNR in Abdominal MRI. *Magn Reson Med* **34**:905-909.

Fishbein M, Castro F, Cheruku S, Jain S, Webb B, Gleason T and Stevens WR (2005) Hepatic MRI for Fat Quantitation: Its Relationship to Fat Morphology, Diagnosis, and Ultrasound. *J Clin Gastroenterol* **39**:619-625.

Fragasso G, Piatti Md PM, Monti L, Palloshi A, Setola E, Puccetti P, Calori G, Lopaschuk GD and Margonato A (2003) Short- and Long-Term Beneficial Effects of Trimetazidine in Patients With Diabetes and Ischemic Cardiomyopathy. *Am Heart J* **146**:E18.

Franzen LE, Ekstedt M, Kechagias S and Bodin L (2005) Semiquantitative Evaluation Overestimates the Degree of Steatosis in Liver Biopsies: a Comparison to Stereological Point Counting. *Mod Pathol* **18**:912-916.

Friedewald WT, Levy RI and Fredrickson DS (1972) Estimation of the Concentration of Low-Density Lipoprotein Cholesterol in Plasma, Without Use of the Preparative Ultracentrifuge. *Clin Chem* **18**:499-502.

Fulgencio JP, Kohl C, Girard J and Pegorier JP (1996) Troglitazone Inhibits Fatty Acid Oxidation and Esterification, and Gluconeogenesis in Isolated Hepatocytes From Starved Rats. *Diabetes* **45**:1556-1562.

Gaidos JK, Hillner BE and Sanyal AJ (2008) A Decision Analysis Study of the Value of a Liver Biopsy in Nonalcoholic Steatohepatitis. *Liver Int*.

Gan SK, Adams LA and Watts GF (2008) The Trials and Tribulations of the Treatment of Nonalcoholic Fatty-Liver Disease. *Curr Opin Lipidol* **19**:592-599.

Gandon Y, Guyader D, Heautot JF, Reda MI, Yaouanq J, Buhe T, Brissot P, Carsin M and Deugnier Y (1994) Hemochromatosis: Diagnosis and Quantification of Liver Iron With Gradient-Echo MR Imaging. *Radiology* **193**:533-538.

Gibbons GF, Islam K and Pease RJ (2000) Mobilisation of Triacylglycerol Stores. *Biochim Biophys Acta* **1483**:37-57.

Gorter CJ (1936) Negative Result of an Attempt to Detect Nuclear Magnetic Spins. *Physica* **3**:995-998.

Gorter CJ and Broer LJF (1942) Negative Result of an Attempt to Observe Nuclear Magnetic Resonance in Solids. *Physica* **9**:591-596.

Guyton AC and Hall JE (1996) *Textbook of Medical Physiology*. W.B. Saunders, Philadelphia.

Hahn EL (1950) Spin Echoes. *Physical Review* **80**:580-594.

Hamacher K, Coenen HH and Stocklin G (1986) Efficient Stereospecific Synthesis of No-Carrier-Added 2-[18F]-Fluoro-2-Deoxy-D-Glucose Using Aminopolyether Supported Nucleophilic Substitution. *J Nucl Med* **27**:235-238.

Heiken JP, Lee JK and Dixon WT (1985) Fatty Infiltration of the Liver: Evaluation by Proton Spectroscopic Imaging. *Radiology* **157**:707-710.

Holm C, Langin D, Manganiello V, Belfrage P and Degerman E (1997) Regulation of Hormone-Sensitive Lipase Activity in Adipose Tissue. *Methods Enzymol* **286**:45-67.

Hoyumpa AM, Jr., Greene HL, Dunn GD and Schenker S (1975) Fatty Liver: Biochemical and Clinical Considerations. *Am J Dig Dis* **20**:1142-1170.

Hussain HK, Chenevert TL, Londy FJ, Gulani V, Swanson SD, McKenna BJ, Appelman HD, Adusumilli S, Greenson JK and Conjeevaram HS (2005) Hepatic Fat Fraction: MR Imaging for Quantitative Measurement and Display--Early Experience. *Radiology* **237**:1048-1055.

Huwart L and van Beers BE (2008) MR Elastography. *Gastroenterol Clin Biol* **32**:68-72.

Iida H, Kanno I, Takahashi A, Miura S, Murakami M, Takahashi K, Ono Y, Shishido F, Inugami A, Tomura N and . (1988) Measurement of Absolute Myocardial Blood Flow With H215O and Dynamic Positron-Emission Tomography. Strategy for Quantification in Relation to the Partial-Volume Effect. *Circulation* **78**:104-115.

Iida H, Rhodes CG, de Silva R, Araujo LI, Bloomfield PM, Lammertsma AA and Jones T (1992) Use of the Left Ventricular Time-Activity Curve As a Noninvasive Input Function in Dynamic Oxygen-15-Water Positron Emission Tomography. *J Nucl Med* **33**:1669-1677.

Iida H, Takahashi A, Tamura Y, Ono Y and Lammertsma AA (1995) Myocardial Blood Flow: Comparison of Oxygen-15-Water Bolus Injection, Slow Infusion and Oxygen-15-Carbon Dioxide Slow Inhalation. *J Nucl Med* **36**:78-85.

Imber CJ, St PS, Handa A and Friend PJ (2002) Hepatic Steatosis and Its Relationship to Transplantation. *Liver Transpl* **8**:415-423.

Iozzo P, Chareonthaitawee P, Dutka D, Betteridge DJ, Ferrannini E and Camici PG (2002) Independent Association of Type 2 Diabetes and Coronary Artery Disease With Myocardial Insulin Resistance. *Diabetes* **51**:3020-3024.

Iozzo P, Geisler F, Oikonen V, Maki M, Takala T, Solin O, Ferrannini E, Knuuti J and Nuutila P (2003a) Insulin Stimulates Liver Glucose

Uptake in Humans: an 18F-FDG PET Study. *J Nucl Med* **44**:682-689.

Iozzo P, Hallsten K, Oikonen V, Virtanen KA, Parkkola R, Kemppainen J, Solin O, Lonnqvist F, Ferrannini E, Knuuti J and Nuutila P (2003b) Effects of Metformin and Rosiglitazone Monotherapy on Insulin-Mediated Hepatic Glucose Uptake and Their Relation to Visceral Fat in Type 2 Diabetes. *Diabetes Care* **26**:2069-2074.

Iozzo P, Jarvisalo MJ, Kiss J, Borra R, Naum GA, Viljanen A, Viljanen T, Gastaldelli A, Buzzigoli E, Guiducci L, Barsotti E, Savunen T, Knuuti J, Haaparanta-Solin M, Ferrannini E and Nuutila P (2007) Quantification of Liver Glucose Metabolism by Positron Emission Tomography: Validation Study in Pigs. *Gastroenterology* **132**:531-542.

Iozzo P, Lautamaki R, Geisler F, Virtanen KA, Oikonen V, Haaparanta M, Yki-Jarvinen H, Ferrannini E, Knuuti J and Nuutila P (2004) Non-Esterified Fatty Acids Impair Insulin-Mediated Glucose Uptake and Disposition in the Liver. *Diabetologia* **47**:1149-1156.

Jarvisalo MJ, Harmoinen A, Hakanen M, Paakkunainen U, Viikari J, Hartiala J, Lehtimaki T, Simell O and Raitakari OT (2002) Elevated Serum C-Reactive Protein Levels and Early Arterial Changes in Healthy Children. *Arterioscler Thromb Vasc Biol* **22**:1323-1328.

Joseph AE, Saverymuttu SH, al-Sam S, Cook MG and Maxwell JD (1991) Comparison of Liver Histology With Ultrasonography in Assessing Diffuse Parenchymal Liver Disease. *Clin Radiol* **43**:26-31.

Kantor PF, Lucien A, Kozak R and Lopaschuk GD (2000) The Antianginal Drug Trimetazidine Shifts Cardiac Energy Metabolism From Fatty Acid Oxidation to Glucose Oxidation by Inhibiting Mitochondrial Long-Chain 3-Ketoacyl Coenzyme A Thiolase. *Circ Res* **86**:580-588.

Kawamitsu H, Kaji Y, Ohara T and Sugimura K (2003) Feasibility of Quantitative Intrahepatic Lipid Imaging Applied to the Magnetic Resonance Dual Gradient Echo Sequence. *Magn Reson Med Sci* **2**:47-50.

Konno K, Ishida H, Sato M, Komatsuda T, Ishida J, Naganuma H, Hamashima Y and Watanabe S (2001) Liver Tumors in Fatty Liver: Difficulty in Ultrasonographic Interpretation. *Abdom Imaging* **26**:487-491.

Kotronen A, Seppala-Lindroos A, Bergholm R and Yki-Jarvinen H (2007) Tissue Specificity of Insulin Resistance in Humans: Fat in the Liver Rather Than Muscle Is Associated With Features of the Metabolic Syndrome. *Diabetologia*.

Kwiterovich PO, Jr., Sloan HR and Fredrickson DS (1970) Glycolipids and Other Lipid Constituents of Normal Human Liver. *J Lipid Res* **11**:322-330.

Laaksonen R, Janatuinen T, Vesalainen R, Lehtimaki T, Elovaara I, Jaakkola O, Jokela H, Laakso J, Nuutila P, Punnonen K, Raitakari O, Saikku P, Salminen K and Knuuti J (2002) High Oxidized LDL and Elevated Plasma Homocysteine Contribute to the Early Reduction of Myocardial Flow Reserve in Healthy Adults. *Eur J Clin Invest* **32**:795-802.

Lautamaki R, Borra R, Iozzo P, Komu M, Lehtimaki T, Salmi M, Jalkanen S, Airaksinen KE, Knuuti J, Parkkola R and Nuutila P (2006a) Liver Steatosis Coexists With Myocardial Insulin Resistance and Coronary Dysfunction in Patients With Type 2 Diabetes. *Am J Physiol Endocrinol Metab* **291**:E282-E290.

Lautamaki R, Nuutila P, Airaksinen KE, Leino A, Hiekkanen H, Turiceanu M, Stewart M, Knuuti J and Ronnemaa T (2006b) The Effect of PPARgamma-Agonism on LDL Subclass Profile in Patients With Type 2 Diabetes and Coronary Artery Disease. *Rev Diabet Stud* **3**:31-38.

Lauterbur PC (1973) Image Formation by Induced Local Interactions - Examples Employing Nuclear Magnetic-Resonance. *Nature* **242**:190-191.

Levenson H, Greensite F, Hoefs J, Friloux L, Applegate G, Silva E, Kanel G and Buxton R (1991) Fatty Infiltration of the Liver: Quantification With Phase-Contrast MR Imaging at 1.5 T Vs Biopsy. *AJR Am J Roentgenol* **156**:307-312.

Lewis MC, Phillips ML, Slavotinek JP, Kow L, Thompson CH and Toouli J (2006) Change in Liver Size and Fat Content After Treatment With Optifast Very Low Calorie Diet. *Obes Surg* **16**:697-701.

Li CW, Kuo YC, Chen CY, Kuo YT, Chiu YY, She FO and Liu GC (2005) Quantification of Choline Compounds in Human Hepatic Tumors by Proton MR Spectroscopy at 3 T. *Magn Reson Med* **53**:770-776.

Limdi JK and Hyde GM (2003) Evaluation of Abnormal Liver Function Tests. *Postgrad Med J* **79**:307-312.

Listenberger LL, Ory DS and Schaffer JE (2001) Palmitate-Induced Apoptosis Can Occur Through a Ceramide-Independent Pathway. *J Biol Chem* **276**:14890-14895.

Longo R, Pollesello P, Ricci C, Masutti F, Kvam BJ, Bercich L, Croce LS, Grigolato P, Paoletti S, de Bernard B and . (1995) Proton MR Spectroscopy in Quantitative in Vivo Determination of Fat Content in Human Liver Steatosis. *J Magn Reson Imaging* **5**:281-285.

Loria P, Lonardo A and Targher G (2008) Is Liver Fat Detrimental to Vessels?: Intersections in the Pathogenesis of NAFLD and Atherosclerosis. *Clin Sci (Lond)* **115**:1-12.

Luciani A, Vignaud A, Cavet M, Nhieu JT, Mallat A, Ruel L, Laurent A, Deux JF, Brugieres P and Rahmouni A (2008) Liver Cirrhosis: Intravoxel Incoherent Motion MR Imaging--Pilot Study. *Radiology* **249**:891-899.

Ludwig J, Hashimoto E, Porayko MK, Moyer TP and Baldus WP (1997) Hemosiderosis in Cirrhosis: a Study of 447 Native Livers. *Gastroenterology* **112**:882-888.

Ludwig J, Viggiano TR, McGill DB and Oh BJ (1980) Nonalcoholic Steatohepatitis: Mayo Clinic Experiences With a Hitherto Unnamed Disease. *Mayo Clin Proc* **55**:434-438.

Machann J, Thamer C, Schnoedt B, Stefan N, Haring HU, Claussen CD, Fritsche A and Schick F (2006) Hepatic Lipid Accumulation in Healthy Subjects: a Comparative Study Using Spectral Fat-Selective MRI and Volume-Localized 1H-MR Spectroscopy. *Magn Reson Med* **55**:913-917.

Maharaj B, Maharaj RJ, Leary WP, Cooppan RM, Naran AD, Pirie D and Pudifin DJ (1986) Sampling Variability and Its Influence on the Diagnostic Yield of Percutaneous Needle Biopsy of the Liver. *Lancet* **1**:523-525.

Marchesini G, Brizi M, Morselli-Labate AM, Bianchi G, Bugianesi E, McCullough AJ, Forlani G and Melchionda N (1999) Association of Nonalcoholic Fatty Liver Disease With Insulin Resistance. *Am J Med* **107**:450-455.

Mathiesen UL, Franzen LE, Aselius H, Resjo M, Jacobsson L, Foberg U, Fryden A and Bodemar G (2002) Increased Liver Echogenicity at Ultrasound Examination Reflects Degree of Steatosis but Not of Fibrosis in Asymptomatic Patients With Mild/Moderate Abnormalities of Liver Transaminases. *Dig Liver Dis* **34**:516-522.

Mehta SR, Thomas EL, Bell JD, Johnston DG and Taylor-Robinson SD (2008) Non-Invasive Means of Measuring Hepatic Fat Content. *World J Gastroenterol* **14**:3476-3483.

Mendler MH, Bouillet P, Le SA, Lavoine E, Labrousse F, Sautereau D and Pillegand B (1998) Dual-Energy CT in the Diagnosis and Quantification of Fatty Liver: Limited Clinical Value in Comparison to Ultrasound Scan and Single-Energy CT, With Special Reference to Iron Overload. *J Hepatol* **28**:785-794.

Metso S, Loimaala A, Mercuri MF, Nenonen A, Vuori I, Oja P, Bond MG, Laine S, Rontu R and Lehtimaki T (2004) Circulating Oxidized Low-Density Lipoprotein and Common Carotid Artery Intima-Media Thickness in a Random Sample of Middle-Aged Men. *J Biomed Sci* **11**:356-361.

Mitchell DG, Kim I, Chang TS, Vinitski S, Consigny PM, Saponaro SA, Ehrlich SM, Rifkin MD and Rubin R (1991) Fatty Liver. Chemical Shift Phase-Difference and Suppression Magnetic Resonance Imaging Techniques in Animals, Phantoms, and Humans. *Invest Radiol* **26**:1041-1052.

Monti LD, Setola E, Fragasso G, Camisasca RP, Lucotti P, Galluccio E, Origgi A, Margonato A and Piatti P (2006) Metabolic and Endothelial Effects of Trimetazidine on Forearm Skeletal Muscle in Patients With Type 2 Diabetes and Ischemic Cardiomyopathy. *Am J Physiol Endocrinol Metab* **290**:E54-E59.

Morin D, Elimadi A, Sapena R, Crevat A, Carrupt PA, Testa B and Tillement JP (1998) Evidence for the Existence of [3H]-Trimetazidine Binding Sites Involved in the Regulation of the Mitochondrial Permeability Transition Pore. *Br J Pharmacol* **123**:1385-1394.

Morin D, Sapena R, Elimadi A, Testa B, Labidalle S, Le RA and Tillement JP (2000) [(3)H]-Trimetazidine Mitochondrial Binding Sites: Regulation by Cations, Effect of Trimetazidine Derivatives and Other Agents and Interaction With an Endogenous Substance. *Br J Pharmacol* **130**:655-663.

Mottin CC, Moretto M, Padoin AV, Swarowsky AM, Toneto MG, Glock L and Repetto G (2004) The Role of Ultrasound in the Diagnosis of Hepatic Steatosis in Morbidly Obese Patients. *Obes Surg* **14**:635-637.

Needleman L, Kurtz AB, Rifkin MD, Cooper HS, Pasto ME and Goldberg BB (1986) Sonography of Diffuse Benign Liver Disease: Accuracy of Pattern Recognition and Grading. *AJR Am J Roentgenol* **146**:1011-1015.

Neuschwander-Tetri BA and Caldwell SH (2003) Nonalcoholic Steatohepatitis: Summary of an AASLD Single Topic Conference. *Hepatology* **37**:1202-1219.

Ng CK, Soufer R and McNulty PH (1998) Effect of Hyperinsulinemia on Myocardial Fluorine-18-FDG Uptake. *J Nucl Med* **39**:379-383.

Nuutila P, Koivisto VA, Knuuti J, Ruotsalainen U, Teras M, Haaparanta M, Bergman J, Solin O, Voipio-Pulkki LM, Wegelius U and . (1992) Glucose-Free Fatty Acid Cycle Operates in Human Heart and Skeletal Muscle in Vivo. *J Clin Invest* **89**:1767-1774.

Park SH, Kim PN, Kim KW, Lee SW, Yoon SE, Park SW, Ha HK, Lee MG, Hwang S, Lee SG, Yu ES and Cho EY (2006) Macrovesicular Hepatic Steatosis in Living Liver Donors: Use of CT for Quantitative and Qualitative Assessment. *Radiology* **239**:105-112.

Parks EJ and Hellerstein MK (2006) Thematic Review Series: Patient-Oriented Research. Recent Advances in Liver Triacylglycerol and Fatty Acid Metabolism Using Stable Isotope Labeling Techniques. *J Lipid Res* **47**:1651-1660.

Patlak CS and Blasberg RG (1985) Graphical Evaluation of Blood-to-Brain Transfer Constants From Multiple-Time Uptake Data. Generalizations. *J Cereb Blood Flow Metab* **5**:584-590.

Pauli W (1924) Zur Frage Der Theoretischen Deutung Der Satelliten Einiger Spektrallinien Und Ihrer Beeinflussung Durch Magnetische Felder. *Naturwissenschaften* **12**:741-743.

Peltoniemi P, Lonnroth P, Laine H, Oikonen V, Tolvanen T, Gronroos T, Strindberg L, Knuuti J and Nuutila P (2000) Lumped Constant for [(18)F]Fluorodeoxyglucose in Skeletal Muscles of Obese and Nonobese Humans. *Am J Physiol Endocrinol Metab* **279**:E1122-E1130.

Petersen KF, West AB, Reuben A, Rothman DL and Shulman GI (1996) Noninvasive Assessment of Hepatic Triglyceride Content in Humans With 13C Nuclear Magnetic Resonance Spectroscopy. *Hepatology* **24**:114-117.

Piekarski J, Goldberg HI, Royal SA, Axel L and Moss AA (1980) Difference Between Liver and Spleen CT Numbers in the Normal Adult: Its Usefulness in Predicting the Presence of Diffuse Liver Disease. *Radiology* **137**:727-729.

Pijnappel WWF, van den Boogaart A, de Beer R and van Ormondt D (1992) SVD-Based Quantification of Magnetic Resonance Signals. *Journal of Magnetic Resonance (1969)* **97**:122-134.

Powell EE, Cooksley WG, Hanson R, Searle J, Halliday JW and Powell LW (1990) The Natural History of Nonalcoholic Steatohepatitis: a Follow-Up Study of Forty-Two Patients for Up to 21 Years. *Hepatology* **11**:74-80.

Prorok R and Sawyer A (1992) *Signa Advantage Application Guide, Vol 4: Fast Imaging Techniques, General Electric Medical Systems*.

Provencher SW (1993) Estimation of Metabolite Concentrations From Localized in Vivo Proton NMR Spectra. *Magn Reson Med* **30**:672-679.

Purcell EM, Torrey HC and Pound RV (1946) Resonance Absorption by Nuclear Magnetic Moments in A Solid. *Physical Review* **69**:37-38.

Qayyum A, Goh JS, Kakar S, Yeh BM, Merriman RB and Coakley FV (2005) Accuracy of Liver Fat Quantification at MR Imaging: Comparison of Out-of-Phase Gradient-Echo and Fat-Saturated Fast Spin-Echo Techniques--Initial Experience. *Radiology* **237**:507-511.

Ratziu V, Charlotte F, Heurtier A, Gombert S, Giral P, Bruckert E, Grimaldi A, Capron F and Poynard T (2005) Sampling Variability of Liver Biopsy in Nonalcoholic Fatty Liver Disease. *Gastroenterology* **128**:1898-1906.

Reaven GM, Chang H and Hoffman BB (1988) Additive Hypoglycemic Effects of Drugs That Modify Free-Fatty Acid Metabolism by Different Mechanisms in Rats With Streptozocin-Induced Diabetes. *Diabetes* **37**:28-32.

Ricci C, Longo R, Gioulis E, Bosco M, Pollesello P, Masutti F, Croce LS, Paoletti S, de BB, Tiribelli C and Dalla PL (1997) Noninvasive in Vivo Quantitative Assessment of Fat Content in Human Liver. *J Hepatol* **27**:108-113.

Rosman AS and Lieber CS (1994) Diagnostic Utility of Laboratory Tests in Alcoholic Liver Disease. *Clin Chem* **40**:1641-1651.

Ruderman N, Chisholm D, Pi-Sunyer X and Schneider S (1998) The Metabolically Obese, Normal-Weight Individual Revisited. *Diabetes* **47**:699-713.

Saadeh S, Younossi ZM, Remer EM, Gramlich T, Ong JP, Hurley M, Mullen KD, Cooper JN and Sheridan MJ (2002) The Utility of Radiological Imaging in Nonalcoholic Fatty Liver Disease. *Gastroenterology* **123**:745-750.

Saha GB (2005) PET Scanning Systems, in *Basics of PET Imaging; Physics, Chemistry and Regulations* pp 19-38, Springer Science+Business Media Inc..

Salibi N and Brown MA (1998) *Clinical MR Spectroscopy*
First Principles. Wiley-Liss, New York.

Salmi M, Stolen C, Jousilahti P, Yegutkin GG, Tapanainen P, Janatuinen T, Knip M, Jalkanen S and Salomaa V (2002) Insulin-Regulated Increase of Soluble Vascular Adhesion Protein-1 in Diabetes. *Am J Pathol* **161**:2255-2262.

Salo S, Alanen A, Leino R, Bondestam S and Komu M (2002) The Effect of Haemosiderosis and Blood Transfusions on the T2 Relaxation

Time and 1/T2 Relaxation Rate of Liver Tissue. *Br J Radiol* **75**:24-27.

Samuel VT, Liu ZX, Qu X, Elder BD, Bilz S, Befroy D, Romanelli AJ and Shulman GI (2004) Mechanism of Hepatic Insulin Resistance in Non-Alcoholic Fatty Liver Disease. *J Biol Chem* **279**:32345-32353.

Sastre J, Serviddio G, Pereda J, Minana JB, Arduini A, Vendemiale G, Poli G, Pallardo FV and Vina J (2007) Mitochondrial Function in Liver Disease. *Front Biosci* **12**:1200-1209.

Savage DB, Petersen KF and Shulman GI (2007) Disordered Lipid Metabolism and the Pathogenesis of Insulin Resistance. *Physiol Rev* **87**:507-520.

Schirmer T, Thormann M, Fischbach F, Winter L, Bruhn H and Ricke J (2004) Semi-Quantitative Liver Spectroscopy With a Transmit/Receive Body Resonator at 3 T. *Proc Int Soc Magn Reson* **1: 924**.

Schonfeld G, Patterson BW, Yablonskiy DA, Tanoli TS, Averna M, Elias N, Yue P and Ackerman J (2003) Fatty Liver in Familial Hypobetalipoproteinemia: Triglyceride Assembly into VLDL Particles Is Affected by the Extent of Hepatic Steatosis. *J Lipid Res* **44**:470-478.

Sentex E, Helies-Toussaint C, Rousseau D, Lucien A, Ferrary E and Grynberg A (2001) Influence of Trimetazidine on the Synthesis of Complex Lipids in the Heart and Other Target Organs. *Fundam Clin Pharmacol* **15**:255-264.

Seppala-Lindroos A, Vehkavaara S, Hakkinen AM, Goto T, Westerbacka J, Sovijarvi A, Halavaara J and Yki-Jarvinen H (2002) Fat Accumulation in the Liver Is Associated With Defects in Insulin Suppression of Glucose Production and Serum Free Fatty Acids Independent of Obesity in Normal Men. *J Clin Endocrinol Metab* **87**:3023-3028.

Shulman GI (2000) Cellular Mechanisms of Insulin Resistance. *J Clin Invest* **106**:171-176.

Siegelman ES, Mitchell DG, Rubin R, Hann HW, Kaplan KR, Steiner RM, Rao VM, Schuster SJ, Burk DL, Jr. and Rifkin MD (1991) Parenchymal Versus Reticuloendothelial Iron Overload in the Liver: Distinction With MR Imaging. *Radiology* **179**:361-366.

Sijens PE, Smit GP, Borgdorff MA, Kappert P and Oudkerk M (2006) Multiple Voxel 1H MR Spectroscopy of Phosphorylase-b Kinase Deficient Patients (GSD IXa) Showing an Accumulation of Fat in the Liver That Resolves With Aging. *J Hepatol* **45**:851-855.

Silverman JF, O'Brien KF, Long S, Leggett N, Khazanie PG, Pories WJ, Norris HT and Caro JF (1990) Liver Pathology in Morbidly Obese Patients With and Without Diabetes. *Am J Gastroenterol* **85**:1349-1355.

Silverman JF, Pories WJ and Caro JF (1989) Liver Pathology in Diabetes Mellitus and Morbid Obesity. Clinical, Pathological, and Biochemical Considerations. *Pathol Annu* **24 Pt 1**:275-302.

Sipilä H, Clark J, Peltola O and Teräs M (2001) An Automatic [15O]H2O Production System for Heart and Brain Studies (Abst). *J Labelled Cpd Radiopharm* **44**:1066-1068.

Sokoloff L, Reivich M, Kennedy C, Des Rosiers MH, Patlak CS, Pettigrew KD, Sakurada O and Shinohara M (1977) The [14C]Deoxyglucose Method for the Measurement of Local Cerebral Glucose Utilization: Theory, Procedure, and Normal Values in the Conscious and Anesthetized Albino Rat. *J Neurochem* **28**:897-916.

Souhami RL and Moxham J (1997) *Textbook of Medicine*. Churchill Livingstone, Edinburgh.

Star-Lack JM, Adalsteinsson E, Gold GE, Ikeda DM and Spielman DM (2000) Motion Correction and Lipid Suppression for 1H Magnetic Resonance Spectroscopy. *Magn Reson Med* **43**:325-330.

Stroud M (1993) Shadows on the Wasteland, Penguin.

Suzuki A, Angulo P, Lymp J, St SJ, Muto A, Okada T and Lindor K (2005) Chronological Development of Elevated Aminotransferases in a Nonalcoholic Population. *Hepatology* **41**:64-71.

Szczepaniak LS, Babcock EE, Schick F, Dobbins RL, Garg A, Burns DK, McGarry JD and Stein DT (1999) Measurement of Intracellular Triglyceride Stores by H Spectroscopy: Validation in Vivo. *Am J Physiol* **276**:E977-E989.

Szczepaniak LS, Nurenberg P, Leonard D, Browning JD, Reingold JS, Grundy S, Hobbs HH and Dobbins RL (2005) Magnetic Resonance Spectroscopy to Measure Hepatic Triglyceride Content: Prevalence of Hepatic Steatosis in the General Population. *Am J Physiol Endocrinol Metab* **288**:E462-E468.

Taegtmeyer H, McNulty P and Young ME (2002) Adaptation and Maladaptation of the Heart in Diabetes: Part I: General Concepts. *Circulation* **105**:1727-1733.

Targher G (2005) Associations Between Liver Histology and Early Carotid Atherosclerosis in

Subjects With Nonalcoholic Fatty Liver Disease. *Hepatology* **42**:974-975.

Thamer C, Machann J, Haap M, Stefan N, Heller E, Schnodt B, Stumvoll M, Claussen C, Fritsche A, Schick F and Haring H (2004) Intrahepatic Lipids Are Predicted by Visceral Adipose Tissue Mass in Healthy Subjects. *Diabetes Care* **27**:2726-2729.

Thomas EL, Hamilton G, Patel N, O'Dwyer R, Dore CJ, Goldin RD, Bell JD and Taylor-Robinson SD (2005) Hepatic Triglyceride Content and Its Relation to Body Adiposity: a Magnetic Resonance Imaging and Proton Magnetic Resonance Spectroscopy Study. *Gut* **54**:122-127.

Thomsen C, Becker U, Winkler K, Christoffersen P, Jensen M and Henriksen O (1994) Quantification of Liver Fat Using Magnetic Resonance Spectroscopy. *Magn Reson Imaging* **12**:487-495.

Tiikkainen M, Hakkinen AM, Korsheninnikova E, Nyman T, Makimattila S and Yki-Jarvinen H (2004) Effects of Rosiglitazone and Metformin on Liver Fat Content, Hepatic Insulin Resistance, Insulin Clearance, and Gene Expression in Adipose Tissue in Patients With Type 2 Diabetes. *Diabetes* **53**:2169-2176.

Tomita K, Tanimoto A, Irie R, Kikuchi M, Yokoyama H, Teratani T, Suzuki T, Taguchi T, Noguchi M, Ohkura T and Hibi T (2008) Evaluating the Severity of Nonalcoholic Steatohepatitis With Superparamagnetic Iron Oxide-Enhanced Magnetic Resonance Imaging. *J Magn Reson Imaging* **28**:1444-1450.

Unger RH (2002) Lipotoxic Diseases. *Annu Rev Med* **53**:319-336.

Unger RH and Orci L (2001) Diseases of Liporegulation: New Perspective on Obesity and Related Disorders. *FASEB J* **15**:312-321.

Unger RH and Orci L (2002) Lipoapoptosis: Its Mechanism and Its Diseases. *Biochim Biophys Acta* **1585**:202-212.

Valls C, Iannacconne R, Alba E, Murakami T, Hori M, Passariello R and Vilgrain V (2006) Fat in the Liver: Diagnosis and Characterization. *Eur Radiol* **16**:2292-2308.

van der Poorten D, Kwok A, Lam T, Ridley L, Jones DB, Ngu MC and Lee AU (2006) Twenty-Year Audit of Percutaneous Liver Biopsy in a Major Australian Teaching Hospital. *Intern Med J* **36**:692-699.

Vanhamme L, van den Boogaart A and Van Huffel S (1997) Improved Method for Accurate and Efficient Quantification of MRS Data With Use of Prior Knowledge. *Journal of Magnetic Resonance* **129**:35-43.

Vlaardingerbroek MT and Boer JA (2003) *Magnetic Resonance Imaging Theory and Practice*. Springer, Berlin.

Wanless IR and Lentz JS (1990) Fatty Liver Hepatitis (Steatohepatitis) and Obesity: an Autopsy Study With Analysis of Risk Factors. *Hepatology* **12**:1106-1110.

Westerbacka J, Lammi K, Hakkinen AM, Rissanen A, Salminen I, Aro A and Yki-Jarvinen H (2005) Dietary Fat Content Modifies Liver Fat in Overweight Nondiabetic Subjects. *J Clin Endocrinol Metab* **90**:2804-2809.

Westphalen AC, Qayyum A, Yeh BM, Merriman RB, Lee JA, Lamba A, Lu Y and Coakley FV (2007) Liver Fat: Effect of Hepatic Iron Deposition on Evaluation With Opposed-Phase MR Imaging. *Radiology* **242**:450-455.

Yeh ET and Willerson JT (2003) Coming of Age of C-Reactive Protein: Using Inflammation Markers in Cardiology. *Circulation* **107**:370-371.

Zimmet P, Shaw J and Alberti KG (2003) Preventing Type 2 Diabetes and the Dysmetabolic Syndrome in the Real World: a Realistic View. *Diabet Med* **20**:693-702.